الجمهـــــورية الـجـزائرية الديمـــــقراطية الشـعـبية
REPUBLIQUE ALGERIENNE DEMOCRATIQUE ET POPULAIRE

وزارة التعليـــم العالـــي والبحـــث العلمـــــــي
MINISTERE DE L'ENSEIGNEMENT SUPERIEUR ET DE LA RECHERCHE SCIENTIFIQUE



جامعـــة سطيـــف1 فرحـات عبـاس
UNIVERSITE SETIF 1- FERHAT ABBAS
FACULTE DE TECHNOLOGIE

THESE

Présentée au Département d'Automatique et Systèmes Intelligents

Pour l'obtention du diplôme de

DOCTORAT

Filière : Automatique et Systèmes Intelligents

Spécialité : Automatique et informatique industrielle

Par

M. DOUDOU Abdel Fateh

THEME

Décodage des activités cérébrales à partir des signaux électroencéphalographiques (EEG) pour les applications d'interface cerveau machine (BCI)

Soutenue le : 01/07/2026 devant un jury compose de :

Mr ABDELAZIZ Mourad	Professor	Setif 1 Ferhat Abbas University	Président
Ms REFFAD Aicha	Professor	Setif 1 Ferhat Abbas University	Directeur de thése
Mr MEBARKIA Kamel	Professor	Setif 1 Ferhat Abbas University	Co-Directeur
Mr BOUGUEZEL Saad	Professor	Setif 1 Ferhat Abbas University	Examinateur
Mr ROUABAH Khaled	Professor	Mohamed BOUDIAF University of M'sila	Examinateur
Mr HACINE-GHARBI Abdenour	MCA	Mohamed El Bachir El Ibrahimi University B.B.A	Examinateur

الجمهـــــورية الـجـزائرية الديمـــــقراطية الشـعـبية
PEOPLE'S DEMOCRATIC REPUBLIC OF ALGERIA

وزارة التعليـــم العالـــي والبحـــث العلمـــــــي
MINISTRY OF HIGHER EDUCATION AND SCIENTIFIC RESEARCH



جامعـــة سطيـــف1 فرحـات عبـاس
SETIF 1 UNIVERSITY-FERHAT ABBAS
FACULTY OF TECHNOLOGY

THESIS

Presented to the Department of Automation and Intelligent Systems

To obtain the title of

DOCTORATE

Field of study: Automation and Intelligent Systems **Specialty: Automation and Industrial Informatics**

Defended by

DOUDOU Abdel Fateh

THEME

Brain activity decoding using electroencephalography (EEG) signals for Brain-Computer Interface applications

Defended on: 01/07/2026 In front of a Jury composed of :

Mr ABDELAZIZ Mourad	Professor	Setif 1 Ferhat Abbas University	President
Ms REFFAD Aicha	Professor	Setif 1 Ferhat Abbas University	Supervisors
Mr MEBARKIA Kamel	Professor	Setif 1 Ferhat Abbas University	Co-supervisors
Mr BOUGUEZEL Saad	Professor	Setif 1 Ferhat Abbas University	Examiner
Mr ROUABAH Khaled	Professor	Mohamed BOUDIAF University of M'sila	Examiner
Mr HACINE-GHARBI Abdenour	MCA	Mohamed El Bachir El Ibrahimi University B.B.A	Examiner

Dedication

I dedicate this thesis to my beloved parents Doudou Saad and Kada Sassia for their unconditional love, sacrifices, prayers, and constant encouragement throughout my life. Their support has been my greatest source of strength.

To my sisters, brothers, and their families, for their patience, understanding, and motivation.

I also dedicate this thesis to Pr. REFFAD Aicha, whose trust, support, and guidance made my doctoral journey possible. Without her encouragement and belief in my potential, I would not have had the opportunity to pursue this PhD.

To all members of the DOUDOU and KADA families.

To all my friends with whom I shared moments of joy and happiness, and to all those who have supported me throughout this journey.

To all the honorable teachers who contributed to my education.

تصريح

أصرح أنا الطالب **دودو عبد الفتاح** أني كتبت هذه رسالة الدكتوراه دون أي مساعدة من الآخرين وبدون استخدام وثائق ومساعدة غير تلك المذكورة؛ وأنني ذكرت جميع المصادر المستخدمة وأني قد استشهدت بها بشكل صحيح وفقا لقواعد الاقتباس الأكاديمي المعمول بها."

Declaration of authorship

"I, **DOUDOU Abdel Fateh**, hereby declare that I have written this thesis without any help from others and without the use of documents and aids other than those stated; that I have mentioned all used sources and that I have cited them correctly according to established academic citation rules."

Déclaration d'auteur

"Je soussigné, **M. DOUDOU Abdel Fateh**, déclare par la présente que j'ai rédigé cette thèse sans l'aide d'autres personnes et sans l'aide de documents et d'aides autres que ceux mentionnés, que j'ai mentionné toutes les sources utilisées et que je les ai correctement citées.

Acknowledgements

I am deeply grateful to Almighty Allah for granting me the faith, courage, and patience necessary to complete this work.

I would like to express my deep gratitude to my supervisor, Pr. REFFAD Aicha and my co-supervisor, Pr. MEBARKIA Kamel of Setif 1 University Ferhat Abbas, for their invaluable guidance, time, support, and constructive feedback throughout this research. This thesis would not have been possible without their encouragement, motivation, and inspiration.

I am also deeply honored that Pr. ABDELAZIZ Mourad, Professor at Setif 1 University Ferhat Abbas, has kindly agreed to serve as the chair of my thesis defense committee.

I am also grateful to the members of my jury: Pr. BOUGUEZEL Saad (Ferhat Abbas University of Sétif 1), Pr. ROUABAH Khaled (Mohamed Boudiaf University of M'sila), and Dr. HACINE-GHARBI Abdenour (Mohamed El Bachir El Ibrahimi University, B.B.A), for their time, careful evaluation, and constructive suggestions, which contributed to enhancing the quality of this work.

I extend my appreciation to all professors and researchers who, directly or indirectly, provided support, guidance, or useful discussions that enriched this research.

I am deeply grateful to my family for their constant encouragement, prayers, and unwavering belief in my abilities, which have given me the strength to persevere.

Finally, I would like to express my sincere gratitude to all those who contributed, directly or indirectly, to the development and completion of this work. May Allah bless them all.

Setif, on 01 /07/2026

Mr. Doudou Abdel Fateh

Contents

General Introduction 1
Thesis Organization 3
List of Publications 5

Chapter 01 ..... *6*

INTRODUCTION TO NEUROPHYSIOLOGY, EEG, AND MOTOR IMAGERY BCIS 6

1.1. Introduction 6
1.2. Anatomy of the human brain 8
1.2.1. Human brain 8
1.2.2. Human brain parts and their functions 9
1.2.3. Protective layers for the head 10
1.2.4. Cerebral lobes and their functions 11
1.3. The Brain's essential operations 13
1.4. Neurons and synapses 13
1.4.1. Neuron structure and function 13
1.4.2. Action potentials: The foundation of neuronal communication 16
1.4.3. Synaptic transmission 17
1.5. Techniques for measuring neuronal activity 18
1.5.1. Non-invasive (EEG, MEG, fMRI, fNIRS) 18
1.5.2. Partially invasive 20
1.5.3. Invasive methods 20
1.6. Principles of electroencephalography 22
1.6.1. History of EEG 22
1.6.2. The biophysical basis of the EEG signal 23
1.6.3. Brain waves and neural oscillations 24
1.6.4. Electrodes 25
1.7. Fundamentals of Brain-Computer Interfaces 29
1.7.1. Origins and early foundations of BCIs 29
1.7.2. Classes of BCIS 30
1.7.3. Brain patterns used in BCI systems 31
1.7.4. Components of a MI-BCI system 34
1.8. Thesis objectives and scope 39
1.9. Conclusion 39

Chapter 02 ..... *41*

MACHINE LEARNING FRAMEWORKS FOR MI DECODING IN BCI 41

2.1. Introduction 41
2.2. Supervised paradigm for EEG-MI classification 42

2.3. Machine Learning vs. Deep Learning for MI-BCI 42
2.4. Feature extraction 43
2.5. Classification in MI-Based BCIs 46
2.5.1. Linear Discriminant Analysis (LDA) 47
2.5.2. Support Vector Machines (SVM) 48
2.5.3. Logistic Regression (LR) 50
2.5.4. k-Nearest Neighbors (KNN) 51
2.6. Feature selection for dimensionality reduction 53
2.6.1. Feature selection as an optimization problem 53
2.6.2. Feature selection using GA 54
2.7. Performance evaluation and benchmarking 55
2.7.1. Standard metrics for MI-BCI 56
2.7.2. Validation strategies 58
2.8. Conclusion 59

Chapter 03 61

EEG DATASETS FOR MI-BASED BCI 61

3.1. Introduction 61
3.2. General characteristics of MI EEG datasets 62
3.2.1. EEG recording setup 62
3.2.2. Common MI tasks 63
3.2.3. Experimental protocol and trial structure 64
3.2.4. Data annotation and labeling 65
3.2.5. Common preprocessing steps 66
3.3. Dataset 1: BCI Competition III Dataset IIIb 67
3.3.1. Source and description 67
3.3.2. Experimental protocol 67
3.3.3. Recording setup and preprocessing 68
3.4. Dataset 2: BCI Competition II Dataset III 69
3.4.1. Source and description 69
3.4.2. Experimental protocol 69
3.4.3. Recording setup and preprocessing 70
3.5. Dataset 3: BCI Competition IV Dataset 2b 71
3.5.1. Source and description 71
3.5.2. Experimental protocol 71
3.5.3. Recording setup and preprocessing 73
3.6. Dataset 4: OpenBMI dataset 73
3.6.1. Source and description 73
3.6.2. Experimental protocol 74
3.6.3. Recording setup and preprocessing 75
3.7. Dataset 5: BCI Competition IV Dataset 2a 76
3.7.1. Source and description 76
3.7.2. Experimental protocol 77
3.7.3. Recording setup and preprocessing 78
3.8. Summary of datasets 79
3.9. Conclusion 80

Chapter 04 ..... *82*

Results and Contributions 82

Part I 82

AN ADAPTIVE FEATURE ENGINEERING FRAMEWORK WITH WFF FOR MULTI-DATASET MI-BCI CLASSIFICATION 82

4.1. introduction 82

4.2. Data preprocessing pipeline 83

4.2.1. Handling of incomplete trials 83

4.2.2. Spectral filtering for feature enhancement 84

4.3. Proposed feature set 85

4.3.1. Wavelet Transform (WT) 85

4.3.2. Power Spectral Density (PSD) 87

4.3.3. Variance (var) 87

4.3.4. Kurtosis and Skewness 87

4.3.5. Root Mean Square (RMS) 88

4.3.6. Enhanced Wavelength (EWL) and Enhanced Mean Absolute Value (EMAV) 88

4.3.7. Mean Curve Length (MCL) 89

4.3.8. Mean Energy (ME) 89

4.3.9. First Difference (FD) 89

4.4. Initial classification performance and classifier selection 92

4.5. Subject-Specific optimization of processing duration 93

4.6. Dimensionality reduction and feature selection 94

4.6.1. Results of feature selection 95

4.7. Feature space transformation via the Weight Features Function (WFF) 98

4.7.1. Classification performance with Weight Features Function (WFF) 98

4.8. Comparison with state-of-the-art methods 103

4.9. Conclusion 104

Part II 106

Enhanced Decoding of Four-Class Motor Imagery through NDD and Personalized Temporal Optimization 106

4.10. introduction 106

4.11. Spatial filtering and channel reduction with NDD 107

4.12. Data preprocessing pipeline 108

4.12.1. Spectral filtering for mi-relevant rhythms 108

4.12.2. Task-Specific feature emphasis 110

4.13. Proposed feature set 110

4.13.1. The Log detector (LD) 111

4.13.2. Mean Absolute Deviation (MAD) and Standard Deviation (STD) 111

4.14. Optimization of temporal segmentation and feature classification results 113

4.14.1. Optimization framework 114

4.14.2. Firefly algorithm implementation 114

4.14.3. Classifier integration 114

4.14.4. Temporal optimization results 114

4.15. Feature selection via GA 116

4.15.1. Feature selection results 116

4.16. Analysis of inter-subject performance variability through topographic mapping 118

4.17. Comparison with state-of-the-art methods 120
4.18. Conclusion 120

General Conclusions and Perspectives *122*

Appendix A *124*

Appendix B *124*

Appendix C *124*

List of Figures

Figure 1.1. A Comprehensive Overview of Gray and White Matter in the Brain and Spinal Cord. 9
Figure 1.2. Illustration of Skin, Skull, and Meningeal Layers Enclosing the Brain. 11
Figure 1.3. Illustration of the Cerebral Cortex: Frontal, Parietal, Temporal, and Occipital Lobes [1]. 12
Figure 1.4. Structure of a Neuron. 14
Figure 1.5. Structural Classification of Neurons based on Number of Neurites and Dendritic Morphology 15
Figure 1.6. Action Potential Waveform and Phases. 17
Figure 1.7. Synaptic neurotransmission: Electrical-to-chemical-to-electrical signal conversion across the synaptic cleft. 18
Figure 1.8. Comparative Spatiotemporal Resolution of Major Neuroimaging Techniques [26]. 22
Figure 1.9. showcases Hans Berger's initial EEG recording from the skull of his son in 1924[1]. 23
Figure 1.10. EEG Electrode Placement Systems: (a) Measurement Basis for 10-20 configuration [26], (b) 10-20 configuration, and (c) 10-10 configuration. 27
Figure 1.11. General Architecture of a BCI System. 35
Figure 2.1. Feature Extraction. 45
Figure 2.2. General Framework of Supervised Machine Learning. 46
Figure 2.3. Illustration of the LDA principle. 48
Figure 2.4. Illustration of Linear and Non-Linear SVM Decision Boundaries. 49
Figure 2.5. The k-Nearest Neighbors classification principle. 52
Figure 2.6. Confusion Matrix for a Binary Classification. 56
Figure 2.7. Schematic Representation of both Holdout and K-Fold Cross-Validation. 59
Figure 3.1. Standard Timeline structure of a single MI trial (Fixation, Cue, MI, Rest). 65
Figure 3.2. Timing scheme of the MI paradigm. 67
Figure 3.3. The placement of electrode positions based on dataset 1. 68
Figure 3.4. Timing scheme of the MI paradigm. 70
Figure 3.5. Timing scheme of the MI paradigm. (a) Screening sessions without feedback. (b) Feedback sessions with the smiley paradigm. 72
Figure 3.6. Timing scheme of the MI paradigm. 75
Figure 3.7. EEG/EMG Electrode Layout According to the 10–20 System. 76
Figure 3.8. Timing preparation for a single session. 77
Figure 3.9. Paradigm for Four-Class Kinesthetic Motor Imagery. 78
Figure 3.10. Locations of EEG and EOG electrodes. 79
Figure 4.1. Example of a corrupted trial leading to NaN values. 84
Figure 4.2. DWT decomposition of the signal up to the third level. 86
Figure 4.3. Flowchart of the signal processing with feature extraction. 90
Figure 4.4. Feature Selection Using GA Optimization for High-Performing Subjects: (a) Subject O3, (b) Subject S1, (c) Subject B04, (d) Subject S35. 97

Figure 4.5. GA Optimization for WFF Across Subjects. (a) O3, (b) S1, (c) B04, (d) S35. 101

Figure 4.6. Comparison of CA Before and After WFF Application. 101

Figure 4.7. Confusion matrices of the proposed method for MI-EEG classification across four datasets. 102

Figure 4.8. Reduction of EEG Channels Using NDD: Electrode placement following the international 10–20 system. (b) Resulting 10 NDD derived from the original 22 electrodes. 108

Figure 4.9. Comparison of Normal and Zero-Phase Butterworth Filters on NDD1 Signals. 109

Figure 4.10. Subject-Specific Motor Imagery Onset and Duration. 113

Figure 4.11. GA Feature Selection: (a) Selected features for subject 4 and (b) Selected features for subject 9. 117

Figure 4.12. Comparative Topographic Maps of Cortical Activation During Four MI Tasks in Subjects 4 and 9. 119

List of Tables

Table 1.1. Characteristic EEG frequency bands 25
Table 3.1. Overview of the EEG MI datasets used in this study. 80
Table 4.1. Proposed Features and Their Mathematical Expressions 91
Table 4.2. CA of Different Classifiers Across All Datasets 92
Table 4.3. Subject-Specific Optimal Processing Durations and Corresponding CA 94
Table 4.4. GA Configuration Parameters 95
Table 4.5. CA (%) Before and After Feature Selection, with SF Count for Each Dataset 96
Table 4.6. Final CA (%) After WFF Transformation 99
Table 4.7. Comparative Summary of CA from Relevant Studies Across the Four Datasets 104
Table 4.8. Summary of the Proposed Features and Their Mathematical Expressions 112
Table 4.9. CA of the Proposed Feature Set with Firefly-Optimized Parameters vs. Fixed Window 115
Table 4.10. Classification Performance After GA-Based Feature Selection 118
Table 4.11. CA comparison on Dataset 5 120

List of Acronyms and Symbols

Acronyms

BCI	Brain-Computer Interface
CA	Classification Accuracy
CNN	Convolutional Neural Networks
CNS	Central Nervous System
CSP	Common Spatial Patterns
CWT	Continuous Wavelet Transform
DL	Deep Learning
DWT	Discrete Wavelet Transform
ECOG	Electrocorticography
EEG	Electroencephalogram
EMG	Electromyography
EOG	Electrooculography
ERD	Event-Related Desynchronization
ERS	Event-Related Synchronization
FA	Firefly Algorithm
FFT	Fast Fourier Transform
fMRI	Functional Magnetic Resonance Imaging
fNIRS	Functional Near-Infrared Spectroscopy
GA	Genetic Algorithm
KNN	K-Nearest Neighbors
LDA	Linear Discriminant Analysis
LR	Logistic Regression
LSVM	Linear Support Vector Machine
MEG	Magnetoencephalography
MI	Motor Imagery
NDD	Normal Double Difference
PCA	Principal Component Analysis
PSD	Power Spectral Density
RMS	Root Mean Square
RNN	Recurrent Neural Networks
SCPs	Slow Cortical Potentials
SF	Selected Features
SNR	Signal To Noise Ratio
SSVEP	Steady-State Visual Evoked Potentials
SVM	Support Vector Machine
WFF	Weight Features Function

General Introduction

Brain–computer interfaces (BCIs) have become an important and rapidly evolving research area in neural engineering and assistive technology. These systems decode brain activity to enable direct communication and control without relying on any muscles, thereby introducing new forms of human–machine interaction [1]. The decoded information is translated into commands, allowing users to interact with their environment using only their thoughts. Such systems offer substantial potential to support individuals with severe motor impairments, including those caused by ALS, stroke, and spinal cord injuries.

Among the various BCI paradigms, motor imagery (MI)–based BCIs are particularly promising, as they interpret neural patterns associated with imagined movements from electroencephalographic (EEG) signals through an intuitive and non-invasive approach well-suited for practical and daily-use applications.

Modern MI-BCI systems constitute complex hybrid signal-processing architectures, where raw neural data, feature extraction algorithms, and machine learning classifiers must operate in harmony. These systems are inherently complex due to the non-stationary nature of brain signals, the high dimensionality of EEG data, and the dynamic variability between individual users. The simultaneous presence of informative neural activity, noise, and subject-specific neurophysiological patterns creates significant challenges for achieving reliable real-world performance, ultimately affecting the robustness, accessibility, and clinical viability of BCI technologies.

The integration of machine learning, and more recently deep learning, into MI-BCI pipelines has encountered several fundamental technical obstacles. Unlike conventional pattern-recognition tasks, EEG-based MI decoding is characterized by extremely low signal-to-noise ratios, pronounced inter- and intra-subject variability, and a lack of standardized feature representations. These characteristics critically influence the three pillars of effective BCI design: classification accuracy, system adaptability, and operational transparency. In particular, the trend toward complex, data-hungry deep-learning models, while powerful, often reduces interpretability and increases computational cost, thereby limiting real-time deployment and clinical trust. This creates a pressing

need for intelligent, hybrid methodologies that balance algorithmic sophistication with practical constraints.

To address these challenges, this thesis entitled “Brain activity decoding using EEG signals for Brain-Computer Interface applications” proposes a structured, multi-stage approach aimed at enhancing the accuracy, adaptability, and interpretability of MI-BCI systems. This research develops two complementary contributions:

First, a comprehensive, multi-dataset adaptive framework is developed. This involves the creation of a rich feature set spanning time, frequency, and time-frequency domains, optimized per subject through dynamic window selection and refined via a novel Weighted Features Function (WFF) for enhanced class separability. This contribution targets generalizability across diverse experimental protocols and subject populations.

Second, a focused optimization pipeline is designed for a particularly challenging four-class MI benchmark. This approach employs the Normal Double Difference (NDD) method for spatial filtering and channel reduction, paired with optimization algorithms for finding the optimal temporal segmentation and Genetic Algorithms for feature selection to achieve high performance while maintaining computational efficiency and interpretability.

This research is positioned within the broader pursuit of human-centered, accessible BCI technology. It seeks to bridge the gap between experimental validation and practical deployment by developing transparent, efficient, and user-tailored processing pipelines. The outcomes of this thesis aim to contribute significantly to the scientific understanding of EEG-based MI decoding while providing tangible methodological advances for researchers, engineers, and clinicians working toward the next generation of reliable brain-computer interaction systems.

Thesis Organization

Chapter 1: Introduction to Neurophysiology, EEG, and MI BCIs

This chapter provides a foundational overview of brain physiology, neuronal communication, and the principles of EEG. It introduces the field of BCIs, with a particular focus on MI-based systems, outlining their potential, challenges, and the core objectives of this thesis.

Chapter 2: Machine Learning Frameworks for MI Decoding in BCI

This chapter presents a comprehensive review of the signal-processing pipeline for MI-BCIs. It covers the supervised learning paradigm, comparative analysis of machine learning versus DL approaches, and details key stages including feature extraction, classification algorithms, feature selection for dimensionality reduction, and performance evaluation metrics.

Chapter 3: EEG Datasets for MI-Based BCI

Here, we survey the landscape of publicly available MI-EEG datasets. The chapter details the general characteristics of these datasets and provides an in-depth analysis of five key benchmarks used in contemporary research, setting the stage for the experimental validation in subsequent chapters.

Chapter 4: Results and Contributions

This chapter presents the two core research contributions of this thesis, each corresponding to a published work. The chapter is divided into two integrated parts:

Part I: An Adaptive Feature Engineering Framework with WFF for Multi-Dataset MI-BCI Classification

This part details the first core contribution of this thesis, corresponding to a published journal article. It details the proposed comprehensive feature set, the subject-specific optimization of processing duration, the novel WFF, and the achieved classification performance across four different MI datasets.

Part II: Enhanced Decoding of Four-Class MI through NDD and Personalized Temporal Optimization

This part presents the second core contribution, which was published in the *International Journal of Electronics and Electrical Engineering Systems* following its presentation at a national conference. It focuses on the challenging Dataset 5, describing the pipeline that integrates NDD for spatial filtering, Firefly optimization for temporal window tuning, GA-based feature selection, and the resulting

state-of-the-art accuracy and interpretable insights into inter-subject variability via topographic performance mapping.

List of Publications

Journal Papers

Abdel Fateh Doudou, Aicha Reffad, Kamel Mebarkia, "Enhancing Motor Imagery EEG Classification Accuracy Using Weight Features Function", The International Arab Journal of Information Technology (IAJIT), Vol. 22, No. 06, pp. 1141-1154, November 2025, doi: 10.34028/iajit/22/6/8.

International Conferences

A. F. Doudou, A. Reffad, and K. Mebarkia, "Improving classification accuracy for motor imagery BCI using DWT based Features," 2023 International Conference on Electrical Engineering and Advanced Technology (ICEEAT), Batna, Algeria, pp. 1-5, 2023, doi: 10.1109/ICEEAT60471.2023.10426300.

National Conferences

Abdel Fateh Doudou, Aicha Reffad, Kamel Mebarkia, "Enhancing BCI System Performance through NDD Channel Configuration", International Journal of Electronics and Electrical Engineering Systems *(IJEES)*, Setif, Algeria, Vol. 7, PP.280-287, 2024.

Chapter 01

INTRODUCTION TO NEUROPHYSIOLOGY, EEG, AND MOTOR IMAGERY BCIS

1.1. Introduction

The development of a direct pathway of communication between the human brain and an external device stands as one of the most ambitious and transformative endeavors in modern science. This pursuit is driven by a profound human need: to restore agency to those who have lost it. The human capacity for intricate tasks from writing and typing to operating complex tools, is a faculty granted by our sophisticated motor system and the exceptional dexterity it affords. When this capability becomes unavailable because of injury, stroke, or disease, the resulting loss of independence becomes devastating. BCI technology emerges as a beacon of hope, offering a potential bridge across this physical disconnect.

This pursuit is fundamentally rooted in a core neurophysiological principle: the electrical activity of the brain is directly related to its underlying structural and functional organization. This concept was proven with the introduction of Electroencephalography (EEG), which Berger established in the 1920s as the first non-invasive tool for recording human electrical activity, thereby creating the foundational method for linking macroscopic brain signals to physiological and cognitive states [2]. After several decades of research, EEG has enabled a multitude of successful applications for probing brain function [3], [4]. It is a non-invasive and affordable approach for recording electrical activity from the human scalp with good temporal resolution. This principle forms the intellectual bedrock of BCI research, an interdisciplinary field converging neuroscience, engineering, and computer science. For any BCI to successfully translate a user's intention into action, it must first accurately decode command signals from measurable neural activity. However, the effective use of EEG remains a significant challenge because of its complex nature and the challenges that occur during the signal acquisition process [5]. Consequently, a rigorous understanding of the biological substrate generating these signals is not merely beneficial it is an absolute prerequisite for meaningful progress.

This chapter is designed to establish this essential foundation, with a specific focus on the principles underlying EEG-based MI BCIs. The exposition begins with a systematic exploration of the human brain, examining its fundamental anatomy and the intricate organization that underpins its complex functions. The discussion then delves into the brain's cellular machinery, emphasizing the unique electrophysiological properties of cortical pyramidal neurons. It is the synchronized postsynaptic potentials within these cells that generate the macroscopic rhythms detectable at the scalp. Of particular relevance stand the sensorimotor mu (μ, 8–13 Hz) and the beta (β, 13–30 Hz) rhythms, whose characteristic modulation during imagined movement forms the critical neural signature for MI-BCIs.

Building upon this neurophysiological foundation, the chapter provides a comparative survey of the primary methodologies for measuring neuronal activity. This review spans the spectrum from invasive intracortical recordings to non-invasive modalities, critically evaluating the inherent trade-offs in spatial resolution, temporal resolution, and practical applicability. Within this technological landscape, EEG is justified as the modality of choice for this thesis, owing to its non-invasiveness, mobility, excellent temporal resolution, and proven applicability for developing accessible real-time BCI systems.

Finally, the chapter concludes by situating MI within the broader taxonomy of BCI paradigms. A critical distinction is drawn between exogenous approaches, like the Steady-State Visual Evoked Potentials (SSVEP) and P300, which rely on the brain's response to external stimuli, and endogenous approaches like MI, which are driven by the user's internal, self-generated cognitive processes. MI specifically engages the cortical sensorimotor networks through the mental simulation of movement. This internal activation produces distinctive and quantifiable modulations in sensorimotor rhythms known as Event-Related Desynchronization (ERD) and Event-Related Synchronization (ERS) which serve as the primary neural correlates for decoding user intent. It is this foundation in the brain's intrinsic motor circuitry that renders MI a highly intuitive and user-centric paradigm, making it highly appropriate for applications that demand self-paced control and long-term user agency, thereby solidifying its selection as the central focus of this thesis.

Collectively, this chapter establishes the essential neuroanatomical, physiological, and methodological principles that underpin EEG-based MI-BCI research. The knowledge presented herein provides the necessary groundwork for the subsequent chapters, which will delve into the advanced signal processing, feature extraction, and machine learning methodologies required to translate the fundamental principles into functional and robust BCI systems.

1.2. Anatomy of the human brain

1.2.1. Human brain

The human brain is often described as among the most intricate biological structures in the human organism, likened to a potent and complex computer. Despite significant progress in neuroscience and artificial intelligence, no one has yet succeeded in fully replicating or simulating its entire structure. The brain's neural networks are so complex, with approximately 86 billion neurons firing in intricate networks and constantly changing connections [6]. This ongoing mystery fuels scientific inquiry and underscores the awe-inspiring nature of the human brain, reminding us of the vast depths yet to be explored in our understanding of cognition and consciousness.

The brain is a vital organ responsible for regulating higher cognitive functions, including thought, memory, emotion, and sensory processing, as well as autonomic processes such as respiration, thermoregulation, and hunger [7]. The typical mass of the adult human brain is approximately 1.4 kilograms [8]. According to [9], the human brain ranks among the most lipid-rich organs in the human organism on a dry-weight basis, with lipids comprising approximately 58% of its mass. These structural lipids form the membranes of neurons and the myelin sheaths that insulate axons, and should not be confused with energy-storing adipose tissue. The remaining dry mass consists primarily of proteins, carbohydrates, and inorganic salts.

Unlike muscular tissue, the brain lacks contractile properties but is highly vascularized and densely populated with neurons and glial cells, which form an intricate electrochemical network fundamental to neural signaling [10].

The central nervous system (CNS), which comprises the brain and spinal cord, serves as the primary command center for coordinating and integrating body functions. The CNS has a specialized division of labor between its two main parts: gray matter and white matter. Gray matter, mainly consisting of neuronal cell bodies, unmyelinated axons, and dendrites, acts as the CNS's processing center, responsible for information processing and integration [11]. In contrast, white matter, mostly composed of myelinated axonal tracts, serves as the communication network, allowing efficient signal transmission between distant parts of the CNS.

Anatomically, this structural dichotomy reveals distinct regional differences within the CNS. In both the cerebrum and cerebellum, gray matter primarily lines the outer cortical regions, while white matter is located deeper inside, see Figure 1.1. Unlike the brain, the spinal cord has the opposite arrangement, with white matter surrounding the central H-shaped gray matter core.

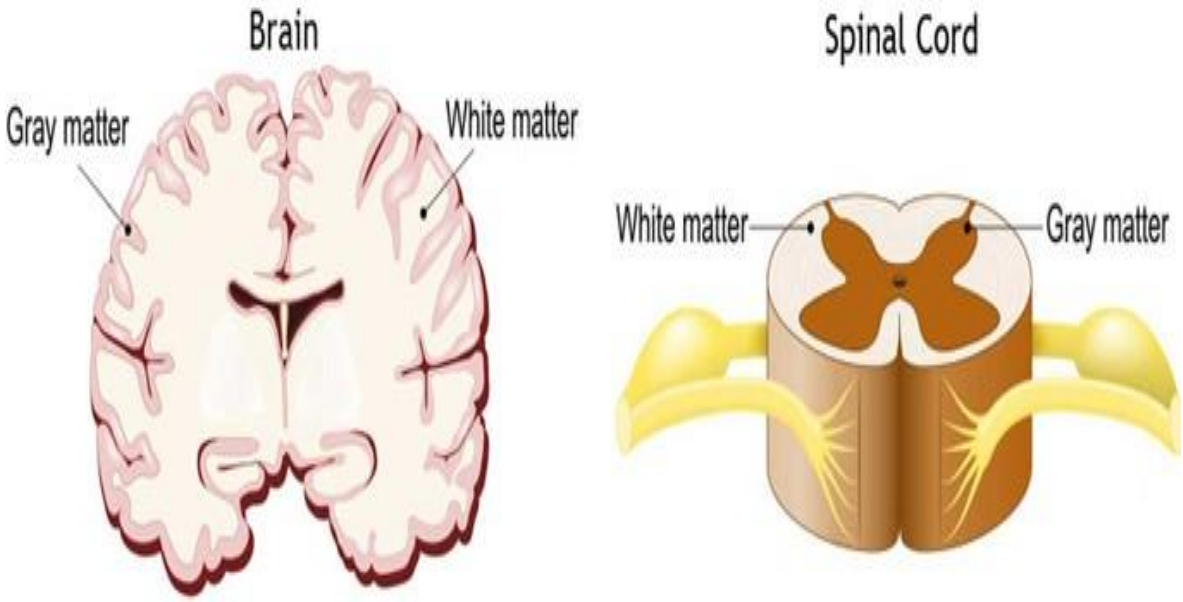

Figure 1.1. A Comprehensive Overview of Gray and White Matter in the Brain and Spinal Cord.

This spatial reversal corresponds with functional specialization: the superficial positioning of gray matter in the brain enables higher-order neural processing. In contrast, the peripheral distribution of white matter in the spinal cord improves long-range axonal transmission between the CNS and the peripheral nervous system. Gray matter primarily contains the main parts of nerve cells and their connections, whereas white matter consists of nerve fibers coated in a fatty layer that helps support rapid interneuronal signaling. These compositional differences explain the contrasting features seen in neuroimaging studies.

1.2.2. Human brain parts and their functions

The human brain consists of three primary parts that work together to control both conscious and unconscious functions. The cerebrum, the brain's largest and most prominent structure is divided into two hemispheres that manage higher cognitive processes, including sensory interpretation (touch, vision, and hearing), learning abilities, emotional regulation, language production, logical reasoning, and precise motor control [12], [13]. Beneath the cerebrum is the cerebellum, a small but essential structure responsible for coordinating voluntary muscle movements, maintaining posture, and ensuring physical balance. Connecting these upper brain regions to the rest of the body is the brainstem, which acts as both a neural pathway to the spinal cord and a control center for vital autonomic functions such as breathing rhythm, heart activity, temperature regulation, circadian cycles, and reflex actions like digestion, sneezing, coughing, vomiting, and swallowing.

1.2.3. Protective layers for the head

Our heads are protected by an ingenious, multi-layered security system that nature perfected over millennia[14], [15]. Picture it like an ancient fortress with concentric walls, each layer adding its own specialized protection for the precious brain inside (see Figure 1.2). Our scalp, that familiar layer of skin and hair that we wash every day, is our first line of protection. But this isn't just ordinary skin it's a living, breathing shield that does triple duty. Its smart design of sweat glands and hair follicles keeps our body temperature exactly perfect while keeping out hazardous bacteria and UV radiation. Under this protective blanket is a cushy layer of fat that makes life's bumps and jolts less painful. Underneath this soft armor comes our built-in helmet the skull. This remarkable bony structure isn't just one solid piece, but rather an intricate puzzle of fused bones that somehow remains both rock-solid and surprisingly resilient. Its secret lies in the sandwich-like construction: tough outer and inner layers with a shock-absorbing spongy core (called diploë) in between. This structure protects the sensitive brain, eyes, and hearing that are tucked inside our skull while enabling it to tolerate unexpectedly high forces. Beneath the skull lies another crucial layer of defense, the meninges, a trio of protective membranes that encase the brain and cerebrospinal fluid [16]. The outermost layer, the dura mater, feels like tough leather; it's actually two layers thick with channels for blood flow in between. Similar to the interhemispheric fissure that divides the brain’s left and right hemispheres, this membrane creates intelligent barriers that keep different parts of the brain from colliding.

The middle layer, known as the arachnoid mater, is composed of transparent, flexible tissue that resembles a spider's web. Between this spider's web layer and the inner membrane is a special fluid-filled region known as the brain's liquid shock absorber.

The deepest layer, the pia mater, attaches to the brain's surface like an additional skin, embracing all of its grooves and curves. Packed with tiny blood vessels, it nourishes the brain while forming the final protective barrier. The cerebrospinal fluid washing through these layers serves as both a cushion and a cleaning system, constantly bathing the brain in nutrients while flushing away waste.

Together, these layers form a masterclass in biological protection from the hair on our heads to the membranes deep inside, all working in perfect harmony to keep our most vital organ safe and sound.

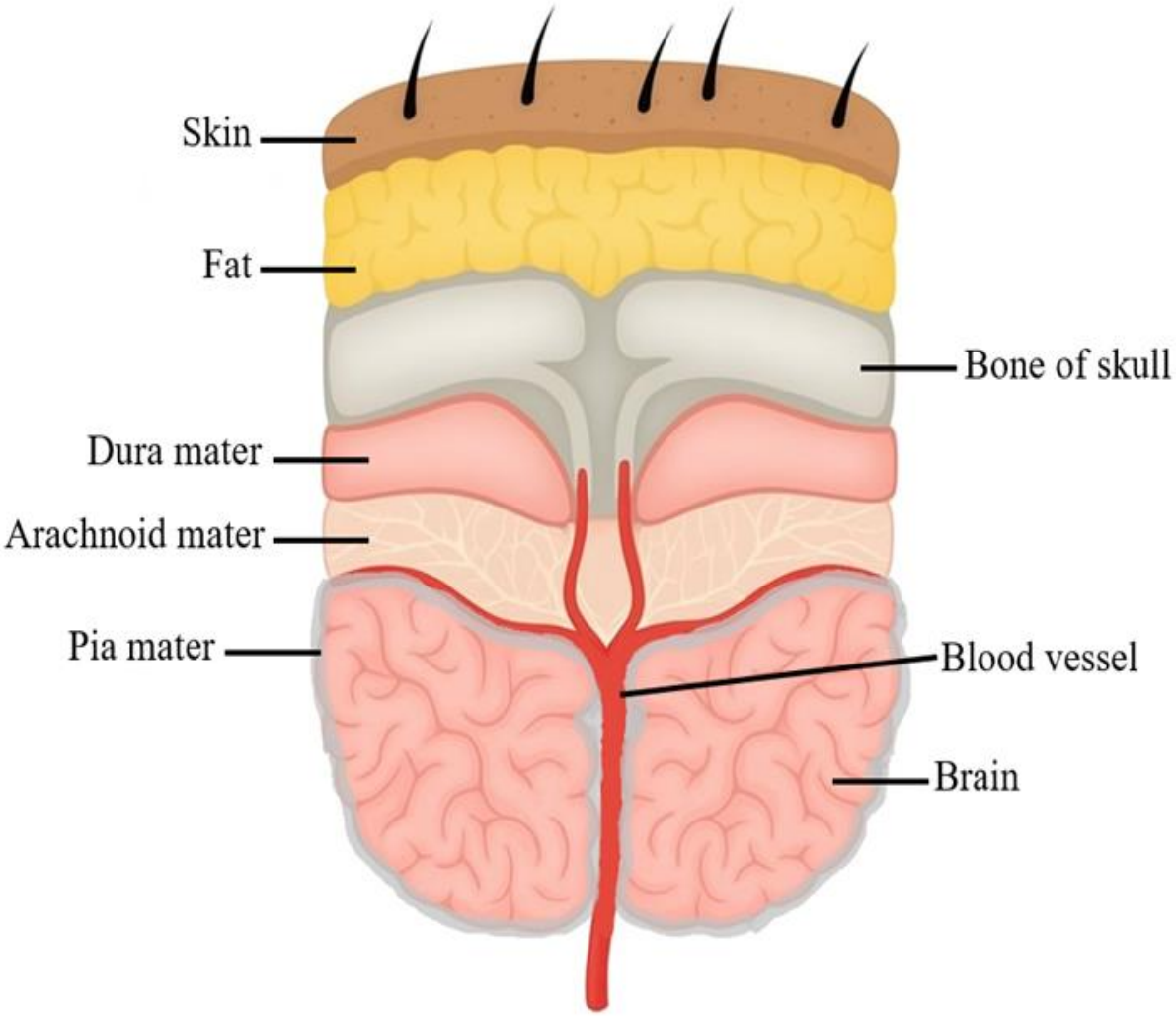

Figure 1.2. Illustration of Skin, Skull, and Meningeal Layers Enclosing the Brain.

1.2.4. Cerebral lobes and their functions

The cerebral cortex, a highly convoluted outer layer measuring 2–4 mm in thickness with multiple folds, serves as the foundation for higher cognitive functions through its specialized regional structure. It is composed of two cerebral hemispheres (right and left), which are linked by the corpus callosum, a thick nerve bundle that enables constant communication between both sides. Although these hemispheres appear symmetrical, they display a fascinating division of labor: each controls movement and sensation on the contralateral side of the body [7]. The cortex further divides into four paired lobes per hemisphere: frontal, parietal, temporal, and occipital, each designed for specific functions, see Figure 1.3. These anatomical features support three main cortical sub-groups that work together: sensory networks for environmental input, motor systems for behavioral output, and association areas that combine information for higher cognition [16]. This complex setup allows for the simultaneous

processing of multiple cognitive tasks, from recognizing a face to planning a response, all within milliseconds.

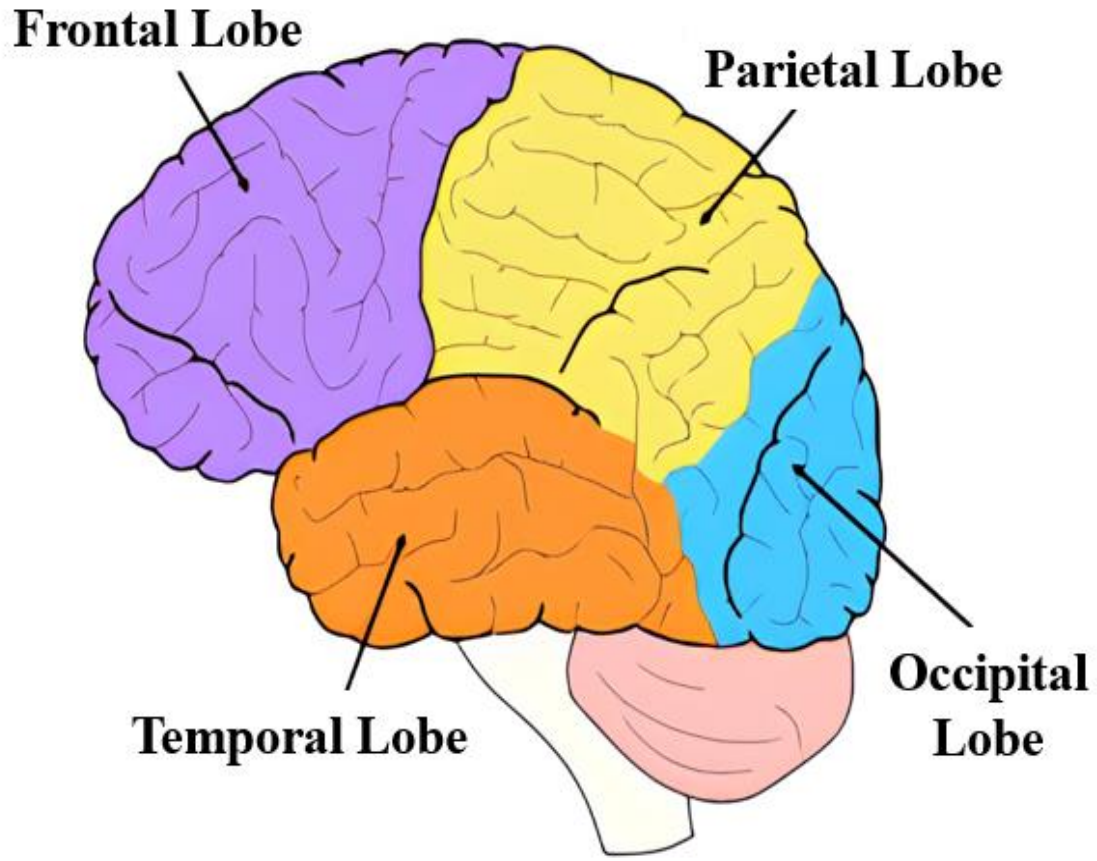

Figure 1.3. Illustration of the Cerebral Cortex: Frontal, Parietal, Temporal, and Occipital Lobes [1].

1.2.4.1. Frontal lobe

Located above the ocular orbits, integrate critical higher-order functions. These regions coordinate voluntary movement, speech production, memory, emotion, planning, reasoning, and decision making, as well as many aspects of personality.

1.2.4.2. Parietal lobe

Located posterior to the frontal lobe and above the temporal lobe, serving as the brain's center for sensory processing. It handles touch, temperature, and body position through the somatosensory cortex and is integral to spatial awareness, math skills, and object manipulation.

1.2.4.3. Temporal lobe

Located along the brain's lateral surfaces, just above and below eye level, the temporal lobes are responsible for hearing, visual recognition, and language comprehension. Their subcortical parts (the hippocampus and amygdala) work together to encode new memories and assign emotional importance to them.

1.2.4.4. Occipital lobe

occupies the posterior cranial area, serving as the main processing center for visual information. In addition to enabling object recognition, spatial navigation, and the seamless integration of visual information with other sensory systems, this specialized region enables accurate perception and interaction with our surroundings.

This modular yet integrated organization allows simultaneous processing across domains, with white matter tracts facilitating rapid communication between specialized areas. Such neuroanatomical design principles inform both advances in brain function comprehension and the evolution of targeted interventions like BCI.

1.3. The Brain's essential operations

As previously stated, the brain is a vital organ that serves as the control center for behavior and movement. It primarily serves three basic functions. First, it functions as a receptor, receiving information through neurons from many sections of the human body. Secondly, it is considered an interpreter that performs a response operation by combining the received electrical signals. As a result, the brain acts as a hub for signal transmission, which is then processed to produce reactions or responses to the surrounding environment. In conclusion, the brain's main activities are the integration, reception, and transmission of signal processes that include sensations, consciousness, memory, and movement all at the same time [17].

1.4. Neurons and synapses

1.4.1. Neuron structure and function

A neuron (or nerve cell) are the essential element of the brain and nervous system. Neurons connect to form various neural networks. These are special cells that transmit electrical signals rapidly. Unlike most cells, they don't regenerate [18], but are supported and maintained by glial cells [19]. As people age, their brains naturally lose about 50,000 neurons each day. This loss causes the brain volume to shrink gradually, but the remaining neurons compensate by forming more connections [20]. These

cells have unique structural and functional features for electrochemical communication, allowing them to integrate and transmit information across neural networks. A typical neuron is consists of three primary components: the axon, the cell body, and the dendrites.

The fundamental anatomical structure of a neuron is depicted in Figure 1.4. The axon is a singular, elongated process that transmits action potentials to different neurons, muscles, and glands. Some axons are covered in myelin, a fatty insulation that speeds up signal transmission. Their length varies based on connectivity: some may be very short or very long, such as those running from the spine to the toes. The cell body, known as the soma, contains the nucleus and organelles, serving as the metabolic and genetic control center where essential biomolecules for neuronal function are synthesized. Dendrites, which look like a tree's branches, extend from the cell body and enable the transfer of information from other neurons to the cell body. Dendrite branching lets one neuron get as many as 100,000 inputs [16].

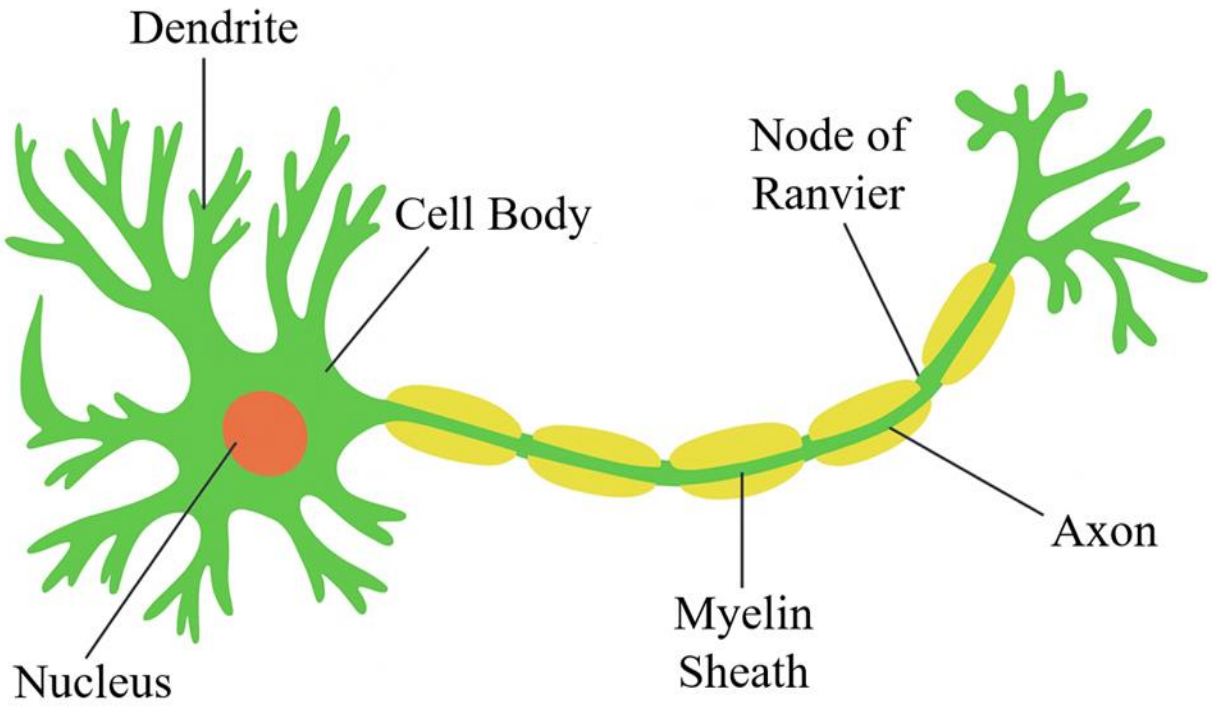

Figure 1.4. Structure of a Neuron.

Neuron classification in the brain is considerably more complex than in the spinal cord. While spinal neurons can be generally classified into sensory, motor, and interneurons with clearly defined roles, cortical neurons exhibit remarkable diversity even within a single region. Neuroscientists have developed several classification schemes to describe this diversity based on morphology, connectivity, axon length, and neurotransmitter type [16]. From a morphological standpoint and as shown in Figure 1.5, neurons can be distinguished by the number and structure of their neurites, for example, unipolar, bipolar, and multipolar neurons. The vast majority of cortical neurons are multipolar, possessing a

single axon and multiple dendrites that allow extensive synaptic integration. Within the cerebral cortex, two major morphological classes are commonly recognized: pyramidal neurons, which are spiny and excitatory, and stellate cells, which may be either spiny or aspinous and are typically inhibitory interneurons [7], [16].

By connectivity, neurons can also be categorized according to their connections such as primary sensory neurons, interneurons, and motor neurons, or by axon projection length, where Golgi type I neurons have long-range axons and Golgi type II neurons operate as local circuit cells. Furthermore, chemical classification distinguishes neurons by the neurotransmitters they release, such as glutamatergic, GABAergic, or cholinergic neurons, each contributing differently to neural communication and circuit dynamics.

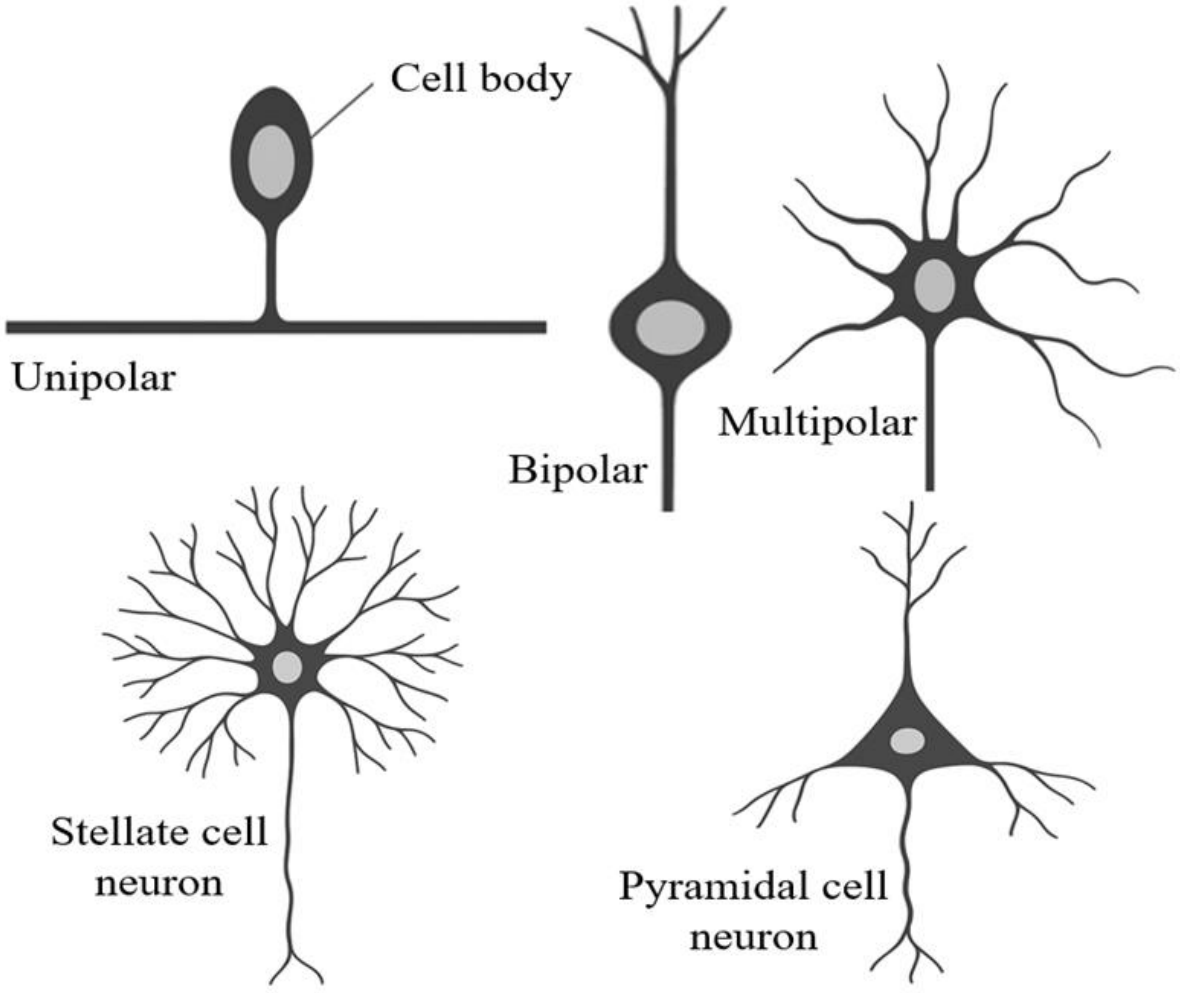

Figure 1.5. Structural Classification of Neurons based on Number of Neurites and Dendritic Morphology.

Among these types, pyramidal neurons are of particular importance in EEG research. They are densely distributed throughout the neocortex and exhibit a characteristic orientation with their apical

dendrites aligned perpendicular to the cortical surface. The synchronized postsynaptic firing of large ensembles of these excitatory neurons generates extracellular fields that summate to form the macroscopic potentials detected by EEG at the scalp [21]. In contrast, the more isotropic organization and limited synchrony of interneurons and Purkinje cells make their direct contributions to scalp EEG negligible.

1.4.2. Action potentials: The foundation of neuronal communication

Action potentials serve as the primary electrical signals that travel along neurons, enabling quick communication throughout the nervous system. Their generation depends on sequential changes in membrane permeability to sodium and potassium ions, creating a brief but powerful reversal of electrical polarity [22]. They represent a temporary, self-regenerating, millisecond-scale change in membrane potential that allows information to travel along neurons. The sequential phases of the action potential waveform are illustrated in Figure 1.6.

In the resting state, neurons keep a membrane potential of roughly –70 mV. When depolarization reaches a critical threshold (approximately –55 mV), voltage-gated sodium (Na^+) channels open, resulting in rapid Na^+ influx and a sharp depolarization known as the rising phase. The membrane potential briefly becomes positive (overshoot) before voltage-gated potassium (K^+) channels restore negativity through repolarization. This is followed by a brief period of hyperpolarization (undershoot) before returning to resting potential, and the entire event lasts about 1–2 milliseconds. Following the all-or-none law, action potentials fire completely once the membrane potential surpasses the depolarization threshold, producing a complete spike; subthreshold stimuli have no effect. Depolarization can result from mechanical stimulation in sensory neurons or synaptic excitation in interneurons. Once generated, the action potential travels through the axon without a decrement in amplitude. In myelinated fibers, saltatory conduction between nodes of Ranvier allows transmission speeds up to 120 m/s [10]. These mechanisms, driven by interactions between sodium and potassium channels, form the electrophysiological basis of the neural signals that, when summed across millions of synchronously active neurons, generate the macroscopic EEG activity measured in BCI research.

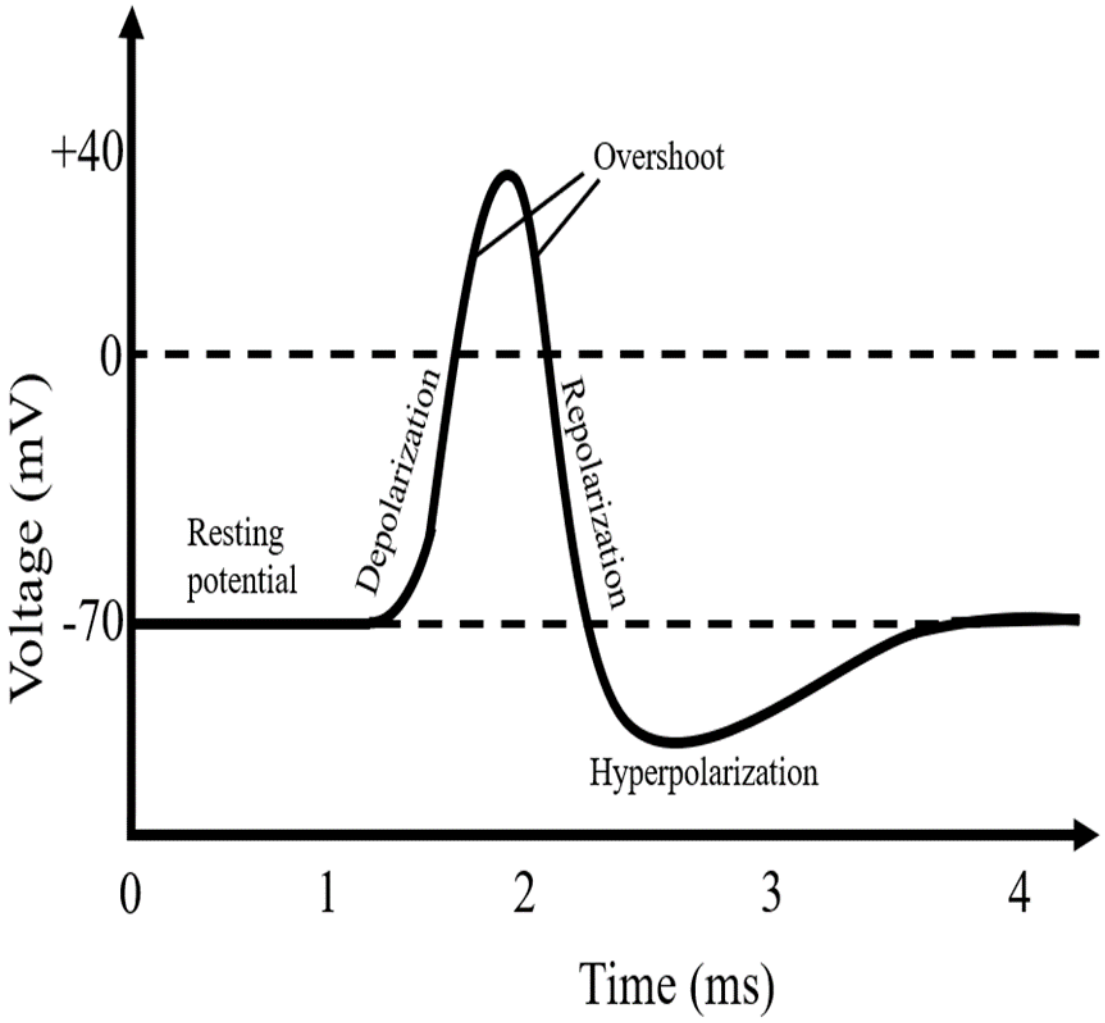

Figure 1.6. Action Potential Waveform and Phases.

1.4.3. Synaptic transmission

Neurons communicate through specialized junctions known as synapses, where electrical signals are transformed into chemical messages, as illustrated in Figure 1.7. When an action potential reaches the presynaptic terminal it induces the release of neurotransmitters within the synaptic cleft, a gap of exactly 20 to 40 nanometers between the postsynaptic dendrite and the presynaptic axon terminal [16]. After diffusing across the synaptic cleft, the neurotransmitter binds to receptors on the postsynaptic membrane. Depending on the releasing neuron type certain positive ions (like Na+, K+, and Ca+) or negative ions (like Cl-) will travel through channels that span the membrane. Synapses transform an electrical signal (the action potential) to a chemical signal via neurotransmitters release. Upon binding of the neurotransmitter to postsynaptic receptors, the signal is transformed back into an electrical response as ions move across of the postsynaptic neuron.

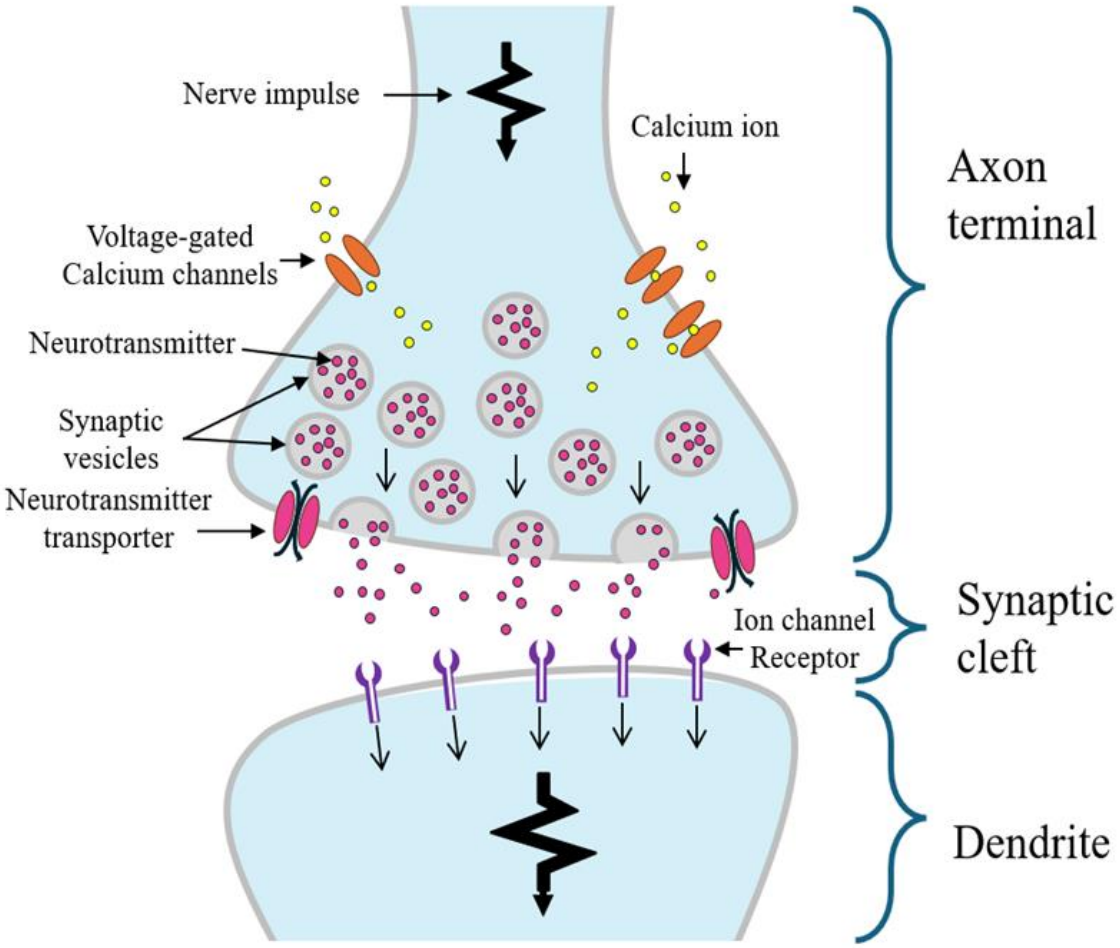

Figure 1.7. Synaptic neurotransmission: Electrical-to-chemical-to-electrical signal conversion across the synaptic cleft.

1.5. Techniques for measuring neuronal activity

Understanding the fundamental functions of the brain requires investigating the neuronal mechanisms and information processing that govern its operation. The action potential generated by neural activity (Section 1.4.2) can be recorded using a variety of techniques. Currently, invasive, partially invasive, and non-invasive modalities are employed to analyze neuronal activity, each offering distinct strengths and constraints regarding spatial resolution, temporal precision, and level of invasiveness [1]. This section outlines the primary technologies used to measure neuronal activity, from non-invasive scalp recordings to invasive cellular-level measurements.

1.5.1. Non-invasive (EEG, MEG, fMRI, fNIRS)

This approach avoids the need for penetrating or directly contacting brain tissue. Instead, it focuses on measuring neural activity from outside the skull or utilizing methods that circumvent the

necessity for surgery or electrode implantation. In comparison to partially invasive and invasive procedures, these approaches are less risky and easier to execute.

1.5.1.1. Magnetoencephalography (MEG)

Magnetoencephalography (MEG), invented in the 1960s, is a non-invasive method that record the brain activity by detecting the magnetic fields generated by neuronal currents. Researchers can examine brain function in great detail thanks to its high temporal and spatial resolution. MEG uses superconducting sensors to detect the tiny magnetic fields produced by electrical currents traveling within neurons [23]. These sensors are typically housed within a specialized helmet-like device, and the measurements are conducted in a place that is magnetically shielded to minimize interference from external magnetic fields. By analyzing the patterns of magnetic activity, MEG can pinpoint the precise timing and location of neural activity, providing insights into various cognitive processes, sensory perception, motor function, and neurological disorders.

1.5.1.2. Functional Magnetic Resonance Imaging (fMRI)

It was invented in the 1990s. fMRI is a powerful neuroimaging method that measures changes in blood flow and oxygenation levels in the brain, offering valuable insights into neural activity associated with various cognitive processes and behaviors [24]. Unlike traditional MRI, which primarily provides structural information about the brain, fMRI detects changes in blood oxygen level-dependent (BOLD) signals to infer neuronal activity. Researchers can examine processes like perception, attention, memory, language processing, and emotion regulation by using fMRI to map these changes in brain activity.

1.5.1.3. Functional Near-Infrared Spectroscopy (fNIRS)

Introduced in the 1990s, FNIRS is a non-invasive neuroimaging method that allows for the measurement of changes in brain tissue concentration of oxygenated (HbO2) and deoxygenated (HbR) hemoglobin following neuronal activation [4]. fNIRS measures hemodynamic reactions linked to cerebral cortex neuronal activation by using near-infrared light to enter the scalp and skull. Because of its portability and simplicity of use, this approach can be used to study brain function in a variety of contexts, such as naturalistic and clinical settings.

1.5.1.4. EEG

The evolution of digital technology has transformed our ability to investigate the workings of the brain, making it more accessible and affordable to employ efficient tools for this purpose. Notably,

EEG emerges as a standout among these methods, providing a non-invasive means to observe and analyze electrical activity in the brain [25]. Through sophisticated analytical techniques, researchers and medical professionals can decipher these electrical signals, unveiling insights into various states of brain function [26]. This capability not only facilitates the continuous monitoring of brain activity but also aids in the diagnosis and management of neurological disorders.

1.5.2. Partially invasive

Electrodes are implanted inside the skull, typically on the inner surface of the dura mater or within epidural space, without penetrating the delicate gray matter of the brain. By avoiding direct penetration into the gray matter, which includes the brain's neurons and sophisticated neural networks, this method avoids the dangers associated with invasive procedures such as tissue damage, inflammation, and infection. This strategic placement aims to minimize the invasiveness of the procedure while still enabling direct access to neural signals.

1.5.2.1. Electrocorticography (ECoG)

Electrocorticography (ECoG), pioneered in the early 1950s, is a neurophysiological method used to record electrical activity directly from the surface of the brain (the cerebral cortex), offering a more localized and higher-resolution measurement of neural activity compared to traditional EEG [25]. Typically, electrodes are implanted subdurally between the dura mater (the outer protective layer of the brain) and the brain tissue itself, allowing for direct access to cortical activity while minimizing the risk of brain damage [14].

1.5.3. Invasive methods

Electrodes are surgically inserted directly into gray matter to extract the necessary neural information. This invasive approach enables electrodes to interface closely with neurons, providing high-fidelity recordings of neural activity. By directly accessing the brain's gray matter, these electrodes can capture precise electrical signals generated by individual neurons or neuronal populations.

1.5.3.1. Intra-Cortical Recording

Intra-cortical recording entails the precise placement of a single electrode or sometimes an array of tiny electrodes that penetrate the brain tissue, specifically targeting the cerebral cortex [21]. This intricate procedure is typically conducted through surgical intervention by skilled neurosurgeons. Despite its invasiveness, intra-cortical recording offers unparalleled access to neural activity within

small local neuronal populations in the brain, providing researchers and clinicians with invaluable knowledge into the brain's complex functional architecture.

- Utah Arrays: Created in the early 2000s, Utah Arrays are multi-electrode arrays consisting of numerous microelectrodes arranged in a grid-like pattern, providing high spatial resolution for recording neural activity. This enables researchers to record complex patterns of brain activity accurately.
- Michigan Probes: Developed in the late 1990s, Michigan Probes are silicon-based microelectrode arrays that can be inserted into the brain tissue to record neural signals with high precision. These probes consist of tiny electrodes arranged in a specific pattern, allowing for simultaneous recording from multiple sites within the brain. Michigan Probes offer high spatial resolution, enabling researchers to capture detailed patterns of neural activity and decode complex brain signals.
- Neuropixels Probes: Developed in the mid-2010s, represent a significant advancement in intra-cortical recording technology. These probes are equipped with thousands of tiny electrodes, enabling simultaneous recording from multiple neurons across different brain regions with exceptional spatial resolution. The high density of electrodes allows researchers to capture detailed neural activity patterns with unprecedented precision. Additionally, Neuropixels Probes offer high temporal resolution, facilitating the real-time monitoring of neural dynamics.

In summary, the selection of a neural recording methodology is governed by a fundamental trade-off between temporal and spatial resolution [26], as illustrated in Figure 1.8. Invasive techniques, such as intra-cortical recording, provide exceptional spatial (μm) and temporal (ms) resolution, but their high degree of invasiveness and surgical risk render them unsuitable for most non-clinical applications. Partially invasive methods, like ECoG, offer a favorable compromise, capturing local field potentials (LFPs) with high fidelity but are still limited to clinical populations. Non-invasive methods prioritize participant safety and practical accessibility. FMRI provides detailed spatial maps (mm resolution) but is constrained by poor temporal resolution (seconds).

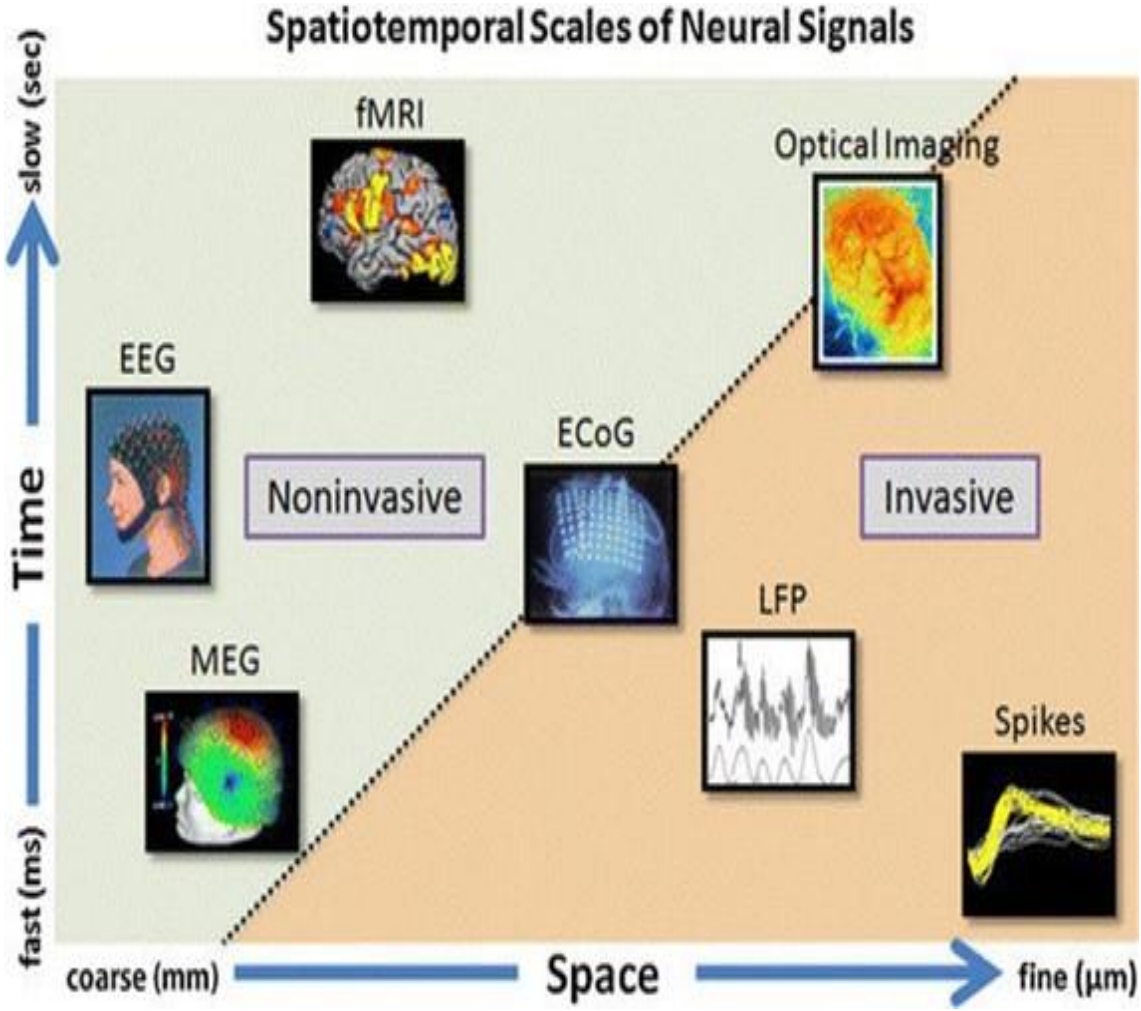

Figure 1.8. Comparative Spatiotemporal Resolution of Major Neuroimaging Techniques [26].

In this thesis, EEG is selected as the primary technique for recording and analyzing brain activity because it represents one of the most practical and widely adopted approaches for BCI. Its non-invasive nature, portability, affordability, and ability to capture neural dynamics with millisecond precision make it particularly well-suited for both research and real-world applications.

1.6. Principles of electroencephalography

1.6.1. History of EEG

In the 1920s, German physiologist and psychiatrist Hans Berger made the first recording of human brain electrical activity using EEG [2]. The recording, taken from the scalp of his son, revealed a rhythmic pattern that he later termed the “alpha rhythm” as illustrated in Figure 1.9.

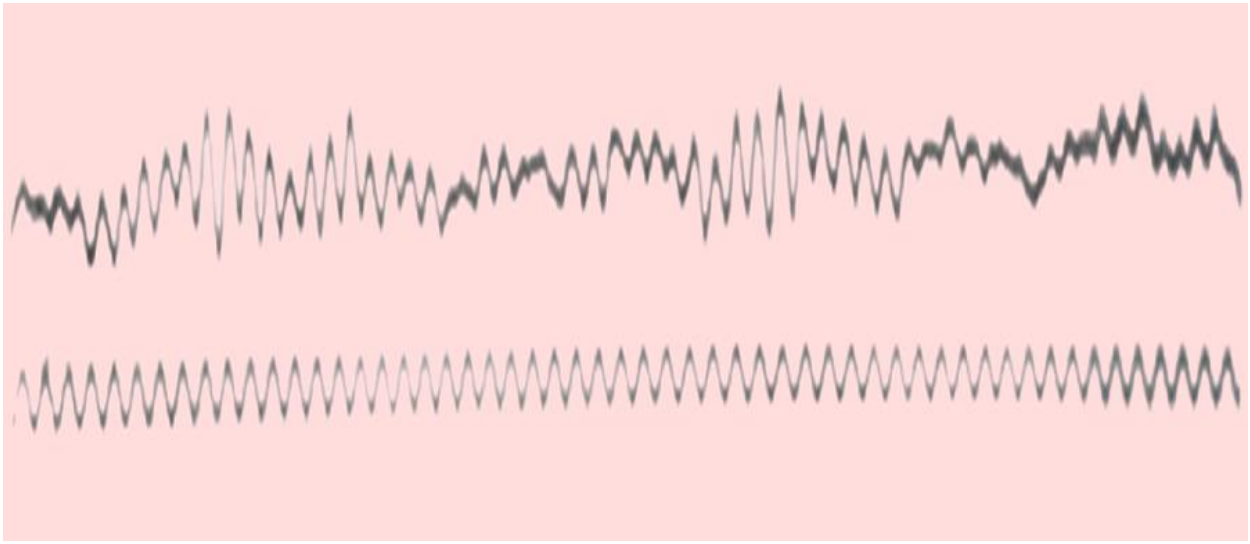

Figure 1.9. showcases Hans Berger's initial EEG recording from the skull of his son in 1924 **[2]**.

During that period, neurophysiologists presumed that the rhythmic "brain waves" observed by Berger were merely noise or artifacts, not indicative of genuine brain activity. However, over the following years, numerous other physiologists also began observing the human EEG signal, confirming the findings of Berger's studies. These validations confirmed EEG as a genuine scientific phenomenon. As a result, the term electroencephalogram was introduced, combining "electro" (electrical), "encephalon" (brain), and "gram" (recording), to describe the recording of brain's electrical activity [2].

1.6.2. The biophysical basis of the EEG signal

EEG primarily measures the voltage difference between at least two different locations, using a minimum of two electrodes, capturing the summed postsynaptic potentials of large, parallel-oriented pyramidal neurons in the cerebral cortex (see Section 1.4) [25]. Since the electrical charges generated at that scale are too tiny, scalp electrodes are unable to measure signals from individual neurons, even though they are able to detect this electrical activity, which is often referred to as brain waves because of their rhythmic patterns. Rather, EEG captures the activity of thousands of synchronized neurons in a specific region of the brain. Because these brain waves propagate efficiently through biological tissue, the delay between neural activity and its detection at the scalp is minimal, granting EEG its excellent temporal resolution [21]. Consequently, the electrical signals picked up by scalp electrodes, while originating from numerous neurons, are relatively weak and require substantial amplification before they can be displayed as waveforms on a computer screen.

1.6.3. Brain waves and neural oscillations

The electrical activity recorded by EEG, which results from the summation of local field potentials, often appears as rhythmic patterns similar to sine waves, known as neural oscillations. In humans, these oscillations typically range from 0.01 to over 100 Hz [26]. Although not always present, these synchronized patterns are expected to have an important part in enhancing communication between neuronal groups, thereby supporting the complex network interactions essential for brain function. The shape, amplitude, frequency, and spatial synchronization of these brain waves offer valuable insights into a person's level of wakefulness, cognitive state, and overall neurological health. In healthy adults, the features of these rhythms vary predictably between states like wakefulness and sleep, and they also change with age and in various clinical conditions.

The main rhythmic activities are divided into five characteristic frequency bands [27], as summarized in Table 1.1, these brain waves can be distinguished by their unique oscillatory patterns. Each band is linked to specific brain states and functions:

Delta (δ): These are the slowest, highest-amplitude waves. They are dominant during deep, dreamless sleep and are necessary for vital functions such as memory consolidation and physical recovery. Their presence in awake adults is unusual and often indicates a medical issue.

Theta (θ): Theta rhythms emerge during light sleep, deep meditation, and relaxation. Beyond aiding in memory processes, they are associated with fostering creativity, enhancing problem-solving abilities, and boosting cognitive flexibility.

Alpha (α): Alpha waves (8–13 Hz) are the dominant rhythm during relaxed wakefulness with eyes closed and are most prominent over occipital regions. They attenuate with eye opening and increased visual processing. Within this frequency range, the mu rhythm represents a functionally distinct sensorimotor variant localized over central regions (C3, Cz, C4). Unlike occipital alpha, mu rhythms are associated with motor processes and exhibit ERD during both actual and imagined movements, forming the neurophysiological foundation of EEG-based MI BCIs.

Beta (β): Beta waves are dominant during fully alert states characterized by active, focused thinking, decision-making, and problem-solving. They are primarily seen over the central and frontal regions. Higher frequencies within this band often signify increased alertness, anxiety, or mental effort.

Gamma (γ): The fastest EEG oscillations, gamma waves, underpin higher-order cognitive processes like sensory integration, attention, and conscious perception. They facilitate learning, memory consolidation, and information binding across neural networks. Their low amplitude makes them difficult to detect with scalp EEG due to contamination from muscle activity.

Table 1.1. Characteristic EEG frequency bands

Rhythm	Frequency Range	Amplitude (uV)	Brain Region	Associated State
Delta (δ)	0.5 - 4 Hz	20-200	Central region	Deep Sleep, Physical Recovery
Theta (θ)	4 - 8 Hz	10	Central region	Light Sleep, Meditation, Creativity
Alpha (α)	8 - 13 Hz	< 10	Posterior brain	Relaxed Wakefulness (eyes closed), calm but alert state; occipital dominant
Mu (μ)	8-13 Hz	< 50	Somatosensory cortex	active during rest, desynchronizes during actual or imagined movement, the basis for MI BCI
Beta (β)	13 - 30 Hz	5-10	Central region	Alertness, Active Thinking, Focus
Gamma (γ)	>30 Hz	5-10	Highly localized	Higher-order Cognition, Perception

1.6.4. Electrodes

The precise measurement of brain activity using EEG mainly depends on the electrodes and their standardized placement on the scalp. A clear naming system is used to identify electrode locations: each is labeled with a letter indicating the underlying brain region (Frontal, Frontopolar, Central, Temporal, Parietal, Occipital) and a number or second letter indicating its position [28]. Left-hemisphere electrodes are assigned odd numbers (1, 3, 5, 7), whereas right-hemisphere electrodes are assigned even numbers (2, 4, 6, 8), and the letter 'z' (zero) signifies positions along the midline (e.g., Cz, Pz), as shown in Figure 1.10. This naming system is used across several standardized international systems for electrode placement, which are essential for obtaining reliable and consistent data.

1.6.4.1. Electrode placement

Electrode placement in EEG recording is crucial for obtaining accurate and reliable data, and various systems are utilized for this purpose, each offering unique advantages and applications [29]. Some of the employee systems include:

- 10-20 system: Widely recognized and used, this system divides the scalp into regions based on percentages of specific cranial landmarks, as illustrated in Figure 1.10.a. A key part is the sagittal line, which runs from the nasion to the inion, passing through the vertex. This line is divided proportionally: the first 10% of its length above the nasion defines the frontal pole, and the first 10% above the inion defines the occipital pole. The remaining 80% of the line is divided into four equal segments, each representing 20% of the total length, to place the frontal, central, parietal, and occipital midline electrodes. The resulting standard configuration of 21 electrodes is shown in Figure 1.10.b. Importantly, this proportional method ensures perfect symmetry for the placement of lateral electrodes across the two hemispheres, making it a reliable tool for both research and clinical applications.
- 10-10 system: This system enhances the 10-20 system by increasing electrode coverage through the inclusion of supplementary locations. This extension enhances spatial resolution, enabling more detailed mapping of brain activity across the scalp.
- 10-5 system: A refinement of the 10-10 system, the 10-5 system introduces an even greater number of electrodes to achieve higher spatial resolution. This technique significantly enhances the accuracy of EEG recordings, particularly in research environments where precise localization of brain activity is crucial.
- Other custom systems: In addition to standardized systems like the 10-20, 10-10, and 10-5 systems, researchers and clinicians may develop custom electrode placement systems tailored to specific experimental or clinical requirements. These custom systems provide flexibility in electrode configuration, enabling optimized positioning tailored to the unique objectives of the study or treatment protocol.

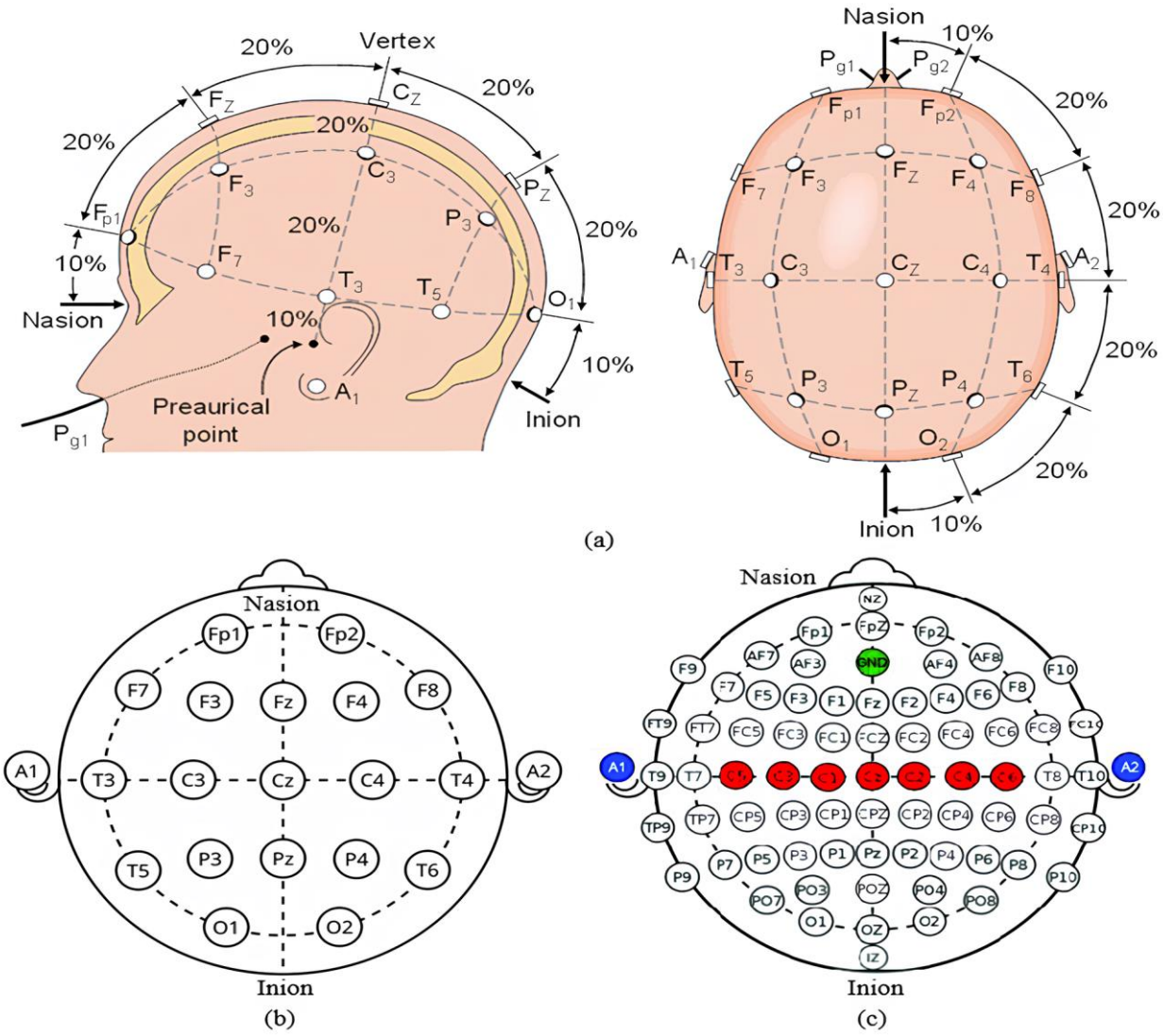

Figure 1.10. EEG Electrode Placement Systems: (a) Measurement Basis for 10-20 configuration [26], (b) 10-20 configuration, and (c) 10-10 configuration.

1.6.4.2. Types of electrodes

When it comes to EEG electrode types, two primary categories stand out: wet electrodes and dry electrodes [29]. Each has its own advantages and limitations, catering to different preferences and applications.

a. Wet electrodes

- Cost-effective and widely used in EEG recording.
- Exhibits low contact impedance, ensuring efficient signal transmission and high-quality EEG recordings.

- Requires skin preparation involving the removal of the outer skin layer and the use of conductive electrolyte gel.
- This process can lead to longer preparation times and may cause discomfort for some patients due to skin irritation.

b. Dry electrodes

- Offer a convenient alternative as they do not require the use of conductive gels, pastes, or skin preparation.
- Streamlines the electrode application process, reducing setup time and enhancing patient comfort during EEG recordings.
- lower signal quality compared to wet electrodes.
- Factors such as increased electrode-skin impedance and reduced signal-to-noise ratio may limit data acquisition and analysis.

The selection between wet and dry electrodes hinges on factors including the particular needs of the EEG setup and considerations regarding patient comfort and signal fidelity.

1.6.4.3. Montage configurations in EEG

As previously mentioned, EEG measures the voltage differences between pairs of electrode positions on the scalp. These recordings can be obtained using different types of montages, which determine how the electrodes are referenced and how brain activity is displayed. The most commonly used montages are described below[25]:

Referential Montage: Also known as a Unipolar Montage, in this configuration, each active scalp electrode's voltage is compared to a single, common reference point. This common reference is ideally placed in a location with minimal brain electrical activity, such as the linked mastoids (A1/A2), earlobe, or the vertex (Cz). This montage is useful for observing the absolute voltage and distribution of activity at each site.

Bipolar Montage: In this method, electrodes are connected in a sequential 'daisy-chain,' where the potential difference is measured between neighboring pairs (e.g., Fp1-F3, F3-C3, C3-P3). This configuration is highly effective for localizing focal abnormalities, such as epileptic spikes, as it emphasizes local activity and creates a specific pattern for pinpointing a source. A trade-off is that it decreases sensitivity to widespread, generalized signals.

Average Reference Montage: This montage uses the average voltage of all scalp electrodes as the common reference for each individual channel. It assumes that the sum of all brain potentials is zero, providing a more balanced and reference-free view of the cortical electrical activity. It is widely

used in research and quantitative EEG analysis, though its accuracy is highly dependent on having a sufficient number and even distribution of electrodes covering the scalp.

Laplacian Montage: Also known as NDD, it uses a mathematical estimate of the local current source density at each electrode. It references each electrode to a weighted average of its immediate neighbors. This method effectively highlights localized activity directly under an electrode while suppressing diffuse, widespread activity, providing excellent spatial resolution.

1.7. Fundamentals of Brain-Computer Interfaces

BCIs have shown up from collaborations between disciplines in neuroscience, computer science, engineering, and rehabilitation sciences. BCIs allow the brain to directly communicate to external devices by converting brain neural activity into control signals, which skips over standard methods like keyboards and touchscreens [30]. Their applications span multiple fields: in clinical rehabilitation, BCIs give individuals with serious motor disabilities, like paralysis, new ways to communicate and control things; in neurorehabilitation, they help people recover motor skills through feedback-based training; and in entertainment, they make gaming and virtual reality more immersive by letting people interact with their thoughts. In addition to technological advancements, BCIs also provoke significant ethical and social scientific questions, especially concerning accessibility, autonomy, and user inclusion.

1.7.1. Origins and early foundations of BCIs

The idea of a BCI started to take shape in the 1970s. A research team at the University of California, Los Angeles, funded by the National Science Foundation and DARPA, showed that EEG signals could be used to control simple external systems. These groundbreaking studies demonstrated that brain activity can serve as an independent input channel, separate from muscular activity. The decoding of brain signals was greatly enhanced in the 1990s and early 2000s by developments in machine learning and signal processing [31]. While non-invasive EEG-based BCIs have allowed humans to control cursors, spell letters, and operate assistive equipment, invasive recordings, such as those using intracortical microelectrodes, have demonstrated high-resolution control of robotic arms in monkeys. More recently, BCIs have been used in virtual reality, gaming, and human augmentation in addition to clinical rehabilitation. Commercial interest has also grown, with companies investigating both invasive and non-invasive methods for communication, control, and cognitive enhancement.

Today, BCIs are no longer viewed solely as experimental tools but as emerging technologies with the capacity to revolutionize medical care, accessibility, and human–machine interaction.

1.7.2. Classes of BCIS

A primary method for classifying BCI is classified according to the invasiveness of the signal acquisition, or how close the electrodes are to the brain. The classification between invasive, partially invasive, and non-invasive systems is essential since it determines how signal quality and usefulness are traded off. BCIs can also be classified according to their functional paradigm, which is the process by which a user's brain activity is converted into a command, in addition to this hardware-oriented classification. This leads to 4 main classes defined by the user's role: active, reactive, passive, and Hybrid BCIs. The choice of a specific paradigm is determined by the target application, user-specific factors, and the technological requirements of the system.

1.7.2.1. Active BCIs (Endogenous)

Active BCIs are designed to allow users to initiate and control actions or commands using their brain activity alone. These systems typically involve the user consciously generating specific brain signals, such as MI or mental commands, to interact with devices or applications [32]. Active BCIs are commonly used in applications where real-time control and feedback are required, such as assistive technology for individuals with motor disabilities or neuroprosthetics for limb control.

1.7.2.2. Reactive BCIs (Exogenous)

Reactive BCIs are designed to react to particular environmental events or stimuli, causing commands or actions to be triggered based on the person's brain activity responses to external cues[33]. These systems detect and interpret brain signals evoked by external cues, like visual, auditory, or tactile cues, and translate them into meaningful commands or actions. Reactive BCIs are often used in applications such as brain-controlled interfaces for gaming, attention monitoring systems, or neurofeedback training.

1.7.2.3. Passive BCIs

Without the user's active participation or conscious control, passive BCIs are made to continually track and analyze their brain activity [34]. These systems leverage pattern recognition techniques to decode patterns in ongoing brain activity and infer the user's cognitive or emotional state. Passive BCIs are commonly used in applications such as cognitive workload assessment, emotion recognition, or mental state monitoring in high-stakes environments like aviation or healthcare.

1.7.2.4. Hybrid BCIs

Hybrid BCIs combine two or more distinct BCI approaches such as active, reactive, or passive paradigms or integrate a BCI with complementary physiological signals (e.g., eye-tracking or EMG) [35]. This fusion enhances overall system performance, improving accuracy, robustness, and functionality beyond what any single method can achieve. Hybrid BCIs are particularly valuable in applications that require high reliability and multimodal interaction, such as advanced assistive communication and precision neuroprosthetics.

1.7.3. Brain patterns used in BCI systems

BCI systems depend on distinct brain signal patterns that can be identified and converted into meaningful commands for external devices. These patterns represent specific neural responses linked to sensory processing, motor activity, or cognitive events. Depending on the paradigm, they can be externally evoked by stimuli or voluntarily generated by the user. The most commonly utilized patterns in BCI research and applications include P300 potentials, Steady-State Visual Evoked Potentials (SSVEPs), Error-Related Potentials (ErrPs), Event-Related Desynchronization/Synchronization (ERD/ERS), Sensorimotor Rhythms (SMR), Slow Cortical Potentials (SCPs), and Motor Imagery (MI) [1]. Each of these signals offers unique advantages and is suited to specific BCI applications, which will be detailed in the following subsections.

1.7.3.1. P300

The P300 is a positive event-related potential (ERP) that occurs about 300 ms following the presentation of a rare or important cues, usually studied with the oddball paradigm [33]. Its latency and amplitude reflect attention and cognitive processing. In BCIs, P300 responses allow users to select items on a screen, such as spelling letters, choosing items, or navigating interfaces, making this paradigm effective for communication in patients with severe motor impairments.

1.7.3.2. Steady-State Visually Evoked Potentials (SSVEP)

SSVEPs are brainwave patterns triggered by visual cues flickering at constant frequencies [36]. They are detected mainly over the occipital cortex and reflect synchronization between neural oscillations and the flicker frequency. In BCIs, SSVEPs are used for fast and reliable control, such as selecting icons by gazing at flickering targets. SSVEPs serve as a reliable and efficient method for BCIs, offering a high information transfer rate that enables rapid control; however, this paradigm requires sustained visual focus on a specific flickering cue.

1.7.3.3. Error-Related Potentials (ErrPs)

ErrPs are neural responses generated when users perceive errors, either in their own actions or in system feedback [37]. These signals, often appearing as negative deflections in EEG recordings, are useful for adaptive BCIs that can automatically detect and correct mistakes during operation.

1.7.3.4. Sensorimotor Rhythms (SMRs)

SMRs are oscillatory patterns in the mu and beta frequency intervals recorded over the sensorimotor cortex and they are closely linked to motor functions [38]. A key phenomenon associated with SMRs is ERD/ERS where ERD denotes a decline in brainwave activity in specific frequency bands (e.g., alpha or mu rhythms) associated with cognitive or motor tasks, while ERS denotes an increase in activity following the task. These modulations are fundamental for MI-based BCIs to infer user intent.

1.7.3.5. Slow Cortical Potentials (SCPs)

SCPs are prolonged, low-frequency changes in cortical electrical activity lasting between 100ms to several seconds and they can be trained and controlled by users, offering a means to generate binary or graded commands in BCI systems [39]. However, SCP-based BCIs generally require extensive training.

1.7.3.6. Motor Imagery (MI)

a. Definition and neurophysiological basis

MI involves the cognitive rehearsal of a motor act in the absence of the execution of any physical movement. It is a mental process in which a person internally simulates an action, involving neural mechanisms associated with actual motor performance. The conceptual foundations of MI date to the late 19th century, when Angelo Mosso and other psychologists studied mental practice and the influence of imagined actions on physiological responses. Its neuroscientific foundation for BCIs, however, was established much later, particularly in the early 1990s with the discovery of the mirror neuron system [40], and neuroimaging studies showing that imagined and executed movements activate largely overlapping neural networks [41]. Specifically, MI engages the main motor, premotor, supplementary motor area, and parietal cortices, which together form the motor-related network.

These activations generate distinct and measurable patterns in EEG signals, primarily through the modulation of SMRs via the ERD/ERS phenomena. For example, imagining a right-hand movement typically induces ERD in the mu and beta rhythms over the contralateral (left) sensorimotor cortex.

Such EEG signatures provide reliable neural markers for decoding motor intent in MI-based BCI systems.

b. Importance and advantages

MI is considered a cornerstone of non-invasive BCI research due to several key advantages. First, it offers a more natural and intuitive control paradigm for neuroprosthetics and rehabilitation compared to externally paced paradigms that rely on sensory stimulation such as P300 or Steady-State Visual Evoked Potentials (SSVEP). By directly engaging the brain's native motor planning circuitry, MI enables users to interact with BCIs in a way that closely mirrors actual movement execution. This makes it especially valuable in clinical contexts such as post-stroke rehabilitation, where repeated engagement of motor-related areas through MI has been shown to promote use-dependent neural plasticity and functional recovery [42].

Second, MI represents an active paradigm, in which the user voluntarily generates the control signals rather than responding passively to external stimuli. This property enhances user agency and is particularly advantageous for continuous and self-paced control tasks, such as operating robotic arms or wheelchairs [43], [44]. Finally, MI does not depend on visual fixation, allowing users to maintain visual attention on other tasks or their environment while still operating the BCI. This independence from gaze makes MI-based BCIs versatile and adaptable to a wide range of assistive and augmentative applications.

c. Challenges and limitations of MI-BCI

Despite its promise, MI-BCI faces significant challenges. The main hurdle is the phenomenon of BCI illiteracy (or inefficiency), where an estimated 10–30% of individuals fail to acquire effective control of the system [45]. The underlying causes are multifactorial, including difficulties in producing consistent and discriminable SMR patterns, limited neurofeedback learning ability, and the inherent cognitive demand of the MI task itself.

Most prior studies have reported BCI illiteracy within the MI paradigm specifically [45]. When examined across multiple paradigms, however, investigations often involved very limited sample sizes (fewer than five users), constraining the generalizability of the findings [46]. Informal reports additionally indicate that MI-based BCIs may demonstrate a higher incidence of BCI illiteracy relative to ERP or SSVEP based paradigms. Yet, conclusive experimental evidence remains scarce due to the absence of sufficiently large and standardized datasets.

Also, MI-BCIs have other significant challenges to deal with, such as the fact that EEG signals have a low signal-to-noise ratio (SNR) by nature, brain dynamics change over time, and they need a lot of

calibration and training that is specific to each user. These problems not only make it harder for a lot of people to use the system, but they also show how important it is to have adaptive algorithms, transfer learning methodologies, and better training protocols to make the system more stable and less likely to fail.

d. Focus of this thesis

Given its strong potential in motor rehabilitation and assistive technologies, as well as the persistent challenge of BCI illiteracy, this thesis concentrates specifically on MI-based BCIs. The primary aim is to explore and develop advanced strategies in signal processing, feature extraction, and classification, to enhance classification accuracy, robustness, and overall usability. By addressing these technical and user-related challenges, the work seeks to contribute toward mitigating BCI illiteracy and advancing the reliability of MI-based BCI systems for practical applications.

1.7.4. Components of a MI-BCI system

Translating brain signals into commands that reflect user intent allows for the assistance, enhancement, or restoration of cognitive and sensorimotor functions, thereby enabling a direct brain to external devices communication pathway. Designing and implementing BCIs poses significant engineering challenges, ranging from signal acquisition to information processing and user adaptation. Developing practical BCI applications also involves addressing advanced technological difficulties that vary according to the specific application and available resources. The BCI system is generally composed of five main components, as highlighted in Figure 1.11.

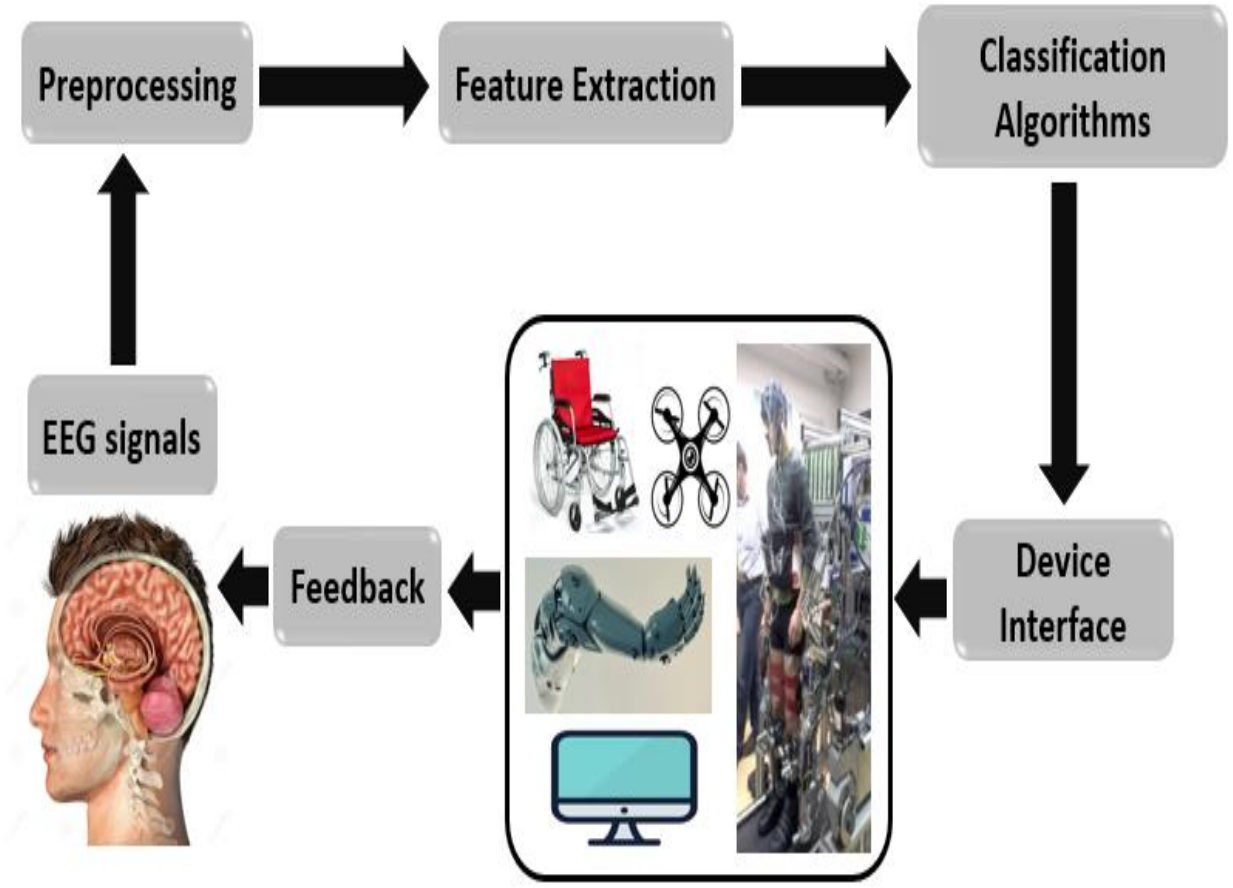

Figure 1.11. General Architecture of a BCI System.

In MI, a subject mentally simulates a motor action without executing any physical movement [47]. The associated EEG signals are initially preprocessed and then transformed into discriminative features through feature extraction. A classifier is subsequently employed to identify the imagined action, enabling the control of external devices like computers, wheelchairs, or robotic arms via electronic interfaces.

These components are regulated by an operating protocol that governs the initiation and timing of operation, the details of signal processing, the structure of device commands, and the monitoring of system performance. A well-designed operating protocol ensures the flexibility of the BCI and enables it to meet the specific needs of individual users.

After EEG signals are collected, an MI-based BCI system generally proceeds through the following stages.

1.7.4.1. Preprocessing

The primary aim of preprocessing is to enhance the quality of EEG signals, thereby facilitating easier and more reliable subsequent analysis. This involves applying a series of operations to the raw signal to improve the SNR and spatial resolution while preserving the underlying neurological information. A poor SNR indicates that the relevant brain activity is obscured by artifacts and noise, leaving it hard to detect. Artifacts can be caused by eye movement, eye blinks, facial muscle activity, electrode artifacts, power line interference, and electrical spikes [5]. Therefore, effective preprocessing is crucial for isolating and highlighting the informative components of the EEG signal for further stages like feature extraction and classification.

The raw EEG signal must be amplified and converted into digital form before it can be effectively cleaned using techniques such as temporal and spatial filtering [25]. Signal filtering plays a crucial role in eliminating unwanted components, including muscle activity and eye movement artifacts, thereby improving the SNR. With a higher SNR, the underlying neural information becomes clearer and more suitable for decoding. Before applying specific filtering techniques, EEG preprocessing commonly relies on four fundamental types of frequency filters: high-pass filters, which remove low-frequency drifts; low-pass filters, which remove high-frequency noise; band-pass filters, which separate a specific frequency range of interest; and band-stop (notch) filters, which suppress narrowband interference such as power line noise. The most widely applied preprocessing approaches to enhance brain signals are temporal and spatial filtering techniques [48].

a. Temporal filtering

This step is applied to isolate frequency bands that carry relevant neural information by suppressing bands dominated by noise or irrelevant physiological processes. For MI-BCIs, this typically involves enhancing the mu and beta rhythms, which are linked to both motor execution and imagery, while attenuating other frequencies. This process ensures that only the most informative oscillatory components are preserved for subsequent analysis.

b. Spatial filtering

Originally applied in image processing to reduce random intensity fluctuations, spatial filtering also plays a crucial role in BCI systems. It improves signal quality by emphasizing activity from brain regions of interest while attenuating signals originating from unrelated or non-relevant areas. This selective enhancement allows the decoder to focus on meaningful neural activity and ignore background noise.

1.7.4.2. Feature extraction

Following the preprocessing and artifact removal stages, the relevant information must be distilled from the cleaned neural signals. This process, known as feature extraction, is a crucial and arguably the most important stage in the BCI pipeline, as it directly determines the quality and discriminability of the information available for classification. By reducing high-dimensional raw data into a compact set of meaningful features, feature extraction enables efficient and accurate pattern recognition. The choice of features is generally guided by the specific BCI paradigm and the underlying neurophysiological signals being utilized, making it a central determinant of the system's overall performance [49].

1.7.4.3. Classification stage

Classification represents the stage in the MI-BCI processing chain where extracted features are translated into discrete commands to control an application [49]. At this stage, the classifier learns to discriminate between neural patterns corresponding to the user's intent or task-related classes. The choice of algorithm is crucial, as it determines the accuracy, speed, and robustness of the system. Among the many algorithms employed, Support Vector Machines (SVMs) are the most widely used in BCI research due to their effectiveness in handling high-dimensional data and their robustness with small sample sizes. Other commonly applied techniques include Linear Discriminant Analysis (LDA), k-Nearest Neighbors (k-NN), Random Forests, and ensemble learning methods. More recently, DL architectures such as Convolutional Neural Networks (CNNs) and Recurrent Neural Networks (RNNs) have gained increasing attention for their ability to learn complex, non-linear representations of EEG data automatically. A detailed analysis of these classification strategies will be presented in Chapter 2.

1.7.4.4. Applications of MI-BCIs

MI-BCIs have evolved from experimental research tools into practical systems with a broad range of applications. Their particular advantage lies in providing a natural and intuitive control paradigm based on the internal rehearsal of movement, making them particularly powerful for applications requiring intentional, self-paced control. across clinical and everyday contexts. Broadly, their uses are categorized into two domains: medical and assistive applications, which focus on rehabilitation and restoring motor functions, and non-medical and augmentative applications, which aim to augment human capabilities and elevate life quality [50].

a. Medical and assistive applications

The most advanced and impactful applications of MI-BCIs are seen in the medical and assistive fields. Their main goal is to restore motor control and independence for individuals. MI-BCIs are uniquely suited for this because they directly engage the brain's native motor circuitry. This is applied in motor restoration and neuroprosthetics, where individuals with spinal cord injuries or stroke can use MI to control robotic arms, prosthetic limbs, or exoskeletons by simply imagining a limb movement, the user generates a neural command that the BCI translates into action, thereby helping to regain lost motor function [51], [52]. A primary application is stroke neurorehabilitation, where BCI-mediated MI training provides reinforcing feedback that promotes use-dependent neural plasticity, thereby helping to rebuild damaged pathways and drive functional recovery [53]. Furthermore, while often slower than reactive paradigms like the P300 speller, MI-BCIs also offer a viable pathway for communication by associating distinct MI tasks like left-hand versus right-hand movement imagination, with binary commands or cursor control users who lack reliable muscle function can make selections to spell words or interact with their environment [54].

These medical and assistive applications highlight the transformative potential of BCIs in enhancing the life quality and restoring independence to individuals who otherwise face profound limitations in daily functioning.

b. Non-Medical and augmentative applications

Beyond clinical rehabilitation, MI-BCIs are increasingly explored as tools for augmenting human capabilities, offering novel forms of human–computer interaction (HCI), enhancing productivity, and enriching daily experiences. A key application is in enhanced HCI, where MI-BCIs provide hands-free control of software interfaces, such as navigating virtual environments or moving a computer cursor, offering an alternative to traditional input devices [55]. This capability is directly leveraged in gaming and virtual reality (VR), where MI-BCIs foster deeply immersive experiences by allowing users to control avatars or execute in-game actions like pushing or jumping through imagined movements, creating a more direct and engaging form of interaction [56], [57]. Furthermore, the neuroplastic principles underpinning MI-BCI therapy are applied in motor skill training for healthy individuals. By using real-time feedback during MI, MI-BCI systems can accelerate the acquisition of complex control skills in applications such as drone navigation and robotic control [58], [59].

1.7.4.5. Feedback

Feedback is the last stage of the MI-BCI pipeline and completes the bidirectional feedback loop linking system and user. In this stage, the output generated by the classifier is conveyed back to the

user to indicate the success or outcome of their mental command. Through this feedback, the user can continuously adjust and optimize their MI performance in real time. Feedback can take different modalities depending on the application context, such as visual feedback through cursor movement or changes in symbols or objects, auditory feedback through tones or spoken cues, or somatosensory feedback through vibrations or haptic responses [60].

By providing timely and meaningful feedback, the system facilitates user learning, enhances performance, and supports continuous adaptation in MI tasks

1.8. Thesis objectives and scope

This chapter has established the foundational principles of BCI, from the neurophysiological basis of EEG signals to the specific paradigms that enable neural control, with a particular emphasis on MI. Building upon this background and motivated by the need to address key challenges such as BCI illiteracy and the non-stationary nature of EEG, this thesis is motivated by the following primary objectives:

To explore, analyze, and develop effective machine learning algorithms and signal processing techniques for the classification of MI-EEG signals.

To enhance the classification accuracy, robustness, and reliability of MI-BCI systems by investigating and refining strategies for feature extraction and model adaptation.

To contribute to the mitigation of BCI illiteracy by developing methods that improve system performance and usability for a wider range of users.

The scope of this work is focused exclusively on non-invasive, MI-based BCIs. The subsequent chapters of this thesis are constructed as follows: Chapter 2 provides a comprehensive review of machine learning methodologies for MI-BCI, Chapter 3 details the datasets used for empirical validation, and Chapter 4 presents the two core contributions of this thesis.

1.9. Conclusion

This chapter has presented a foundational introduction to the human brain and its importance to BCIs. We started with an explanation of the brain's main anatomical structures and key functions, emphasizing the importance of understanding neural organization for generating electrical and hemodynamic signals. The role of neurons, especially pyramidal cells, in producing measurable brain activity was highlighted as the foundation for electrophysiological recording methods. We then overviewed the main techniques used to measure neuronal activity, from invasive to non-invasive methods, with special focus on EEG because of its practicality, portability, and time resolution. Lastly, we introduced the concept of BCIs and outlined the main brain patterns that form the basis for

translating neural activity into control signals. Within the scope of this thesis, the topics covered here offer the theoretical foundation essential to comprehending the neurophysiological basis of EEG signals in BCI, especially in relation to MI.

Chapter 02

MACHINE LEARNING FRAMEWORKS FOR MI DECODING IN BCI

2.1. Introduction

The advancement of effective MI-BCI systems significantly relies on the capability to decipher neural patterns linked to MI tasks from EEG signals[61]. This deciphering process is formulated as a machine learning challenge, where computational algorithms learn to recognize and classify brain activity into distinct categories corresponding to imagined movements. The accuracy of this deciphering is directly depending on the resilience, generalization, and interpretability of the utilized learning algorithms.

In general, the operation of a learning algorithm can be divided into two major steps [62]. The first phase, called the learning or training phase, it's involves developing a prediction model based on a labeled dataset that can generalize to new situations. The second phase, referred to as the deployment or testing phase, applies the trained model to unseen data to perform the desired task typically classification or decision-making. It is clear that the final decision's reliability is greatly affected by the model's accuracy and the quality of the learning process. For this reason, the input space of most learning systems is divided into separate training/testing subsets to objectively assess effectiveness and avoid overfitting.

Among the different paradigms of machine learning, supervised learning remains the most widely studied and applied in the field of MI-based BCIs. This is mainly because of the availability of labeled EEG datasets and the requirement for accurate classification of user intentions. Supervised approaches have demonstrated consistent success in translating brain activity into discrete control commands, building the groundwork for modern MI-BCI research.

In addition to learning-based modeling, optimization plays an equally crucial role in improving model efficiency and accuracy. Optimization techniques are essential in many stages of the MI-BCI pipeline, including parameter tuning, feature selection, and model refinement. Given that most real-world optimization problems such as selecting the most relevant EEG features are NP-hard and computationally intensive, metaheuristic algorithms like GA have become indispensable tools. Their

efficiency in exploring large, high-dimensional search spaces makes them particularly well-suited for EEG-based feature selection and model optimization.

This chapter presents a detailed overview of conventional machine learning techniques for MI-based BCIs. It begins by introducing the supervised learning paradigm and the principles underlying EEG-based classification. The next sections discuss feature extraction methods that transform raw EEG data into discriminative representations. After that, we talk about traditional classifiers like Linear Discriminant Analysis (LDA), Support Vector Machines (SVM), k-Nearest Neighbors (KNN), and Logistic Regression (LR). The chapter also explores feature selection as an optimization problem, with a focus on applying GAs in the selection of informative features. Finally, performance evaluation metrics and validation strategies are discussed to establish the methodological foundation for the experimental framework presented in later chapters.

2.2. Supervised paradigm for EEG-MI classification

The decoding of MI patterns from EEG is fundamentally a supervised learning problem [63]. This paradigm involves training the model on a set of EEG trials (the input features) where each trial is explicitly labeled with the corresponding mental task (e.g., left-hand or right-hand imagery). The objective of the model is to learn a mapping function from the high-dimensional neural data to these discrete labels, enabling it to predict the user's intent on new, unseen trials. While other paradigms like unsupervised or reinforcement learning exist in broader BCI research, the clear availability of trial labels and the primary goal of accurate classification make supervised learning the established and most effective framework for MI-BCI. More broadly, the selection of a learning paradigm relies on the data's nature and the intended objective; when labeled data are available and the aim is prediction rather than pattern discovery, supervised learning remains the most appropriate approach.

2.3. Machine Learning vs. Deep Learning for MI-BCI

We already explained why supervised learning is used. Next, we need to explain why we use classical machine learning rather than DL. DL presents a powerful alternative for MI-EEG classification, directly addressing the signal's complexity and inter-subject variability. BCI researchers have extensively explored a wide variety of DL models, encompassing CNNs, Recurrent Neural Networks (RNNs) such as LSTMs and GRUs, and hybrid architectures that integrate multiple DL components within a unified framework [47]. DL architectures, especially CNNs, can operate on raw or minimally processed data, learning hierarchical features automatically through an end-to-end learning process that bypasses traditional feature engineering and selection [64], [65]. This approach mitigates potential information loss from manual feature design and can be robust to noise and outliers [66]. Their

capacity to model complex, non-linear relationships makes them ideally suited for handling high-dimensional data like EEG, and their efficacy in MI classification has been well-documented [67], [68].

Despite these advantages, this thesis focuses on conventional machine learning techniques for several reasons. First, conventional ML pipelines with explicit feature extraction such as CSP offer high interpretability. They provide transparent insights into the neurophysiological mechanisms underlying MI, such as ERD/ERS in specific frequency bands. This level of interpretability is essential for scientific understanding and clinical validation, whereas DL architectures often operate as "black boxes," which complicates the interpretability of the decisions making process [61]. Second, conventional classifiers such as LDA and SVM are computationally efficient to train and implement. Their low computational cost makes them particularly suitable for real-time BCI systems and rapid prototyping. Moreover, they perform reliably even when training data are limited, an important advantage in MI-BCI experiments, where datasets are often small, while DL architectures normally need large datasets to prevent overfitting and achieve stable generalization [69]. Third, traditional ML methods provide well-established baselines in the BCI literature. These baselines are critical for evaluating progress in the field, as new algorithms are often benchmarked against classical approaches. Their extensive study and consistent performance make them indispensable reference points for meaningful comparison [70]. Finally, this thesis aims to investigate the full potential of the conventional MI-BCI pipeline from spatial filtering and signal processing to feature extraction and classifier optimization. This pipeline remains highly relevant for practical applications, where model transparency, computational efficiency, and ease of deployment are essential [49].

Therefore, while acknowledging the substantial advancements enabled by DL, the following sections focus on conventional machine learning methods, which offer a compelling balance of performance, efficiency, and interpretability for MI-BCI systems.

2.4. Feature extraction

Feature extraction transforms raw, high-dimensional, and noisy EEG signals into a concise and meaningful representation suitable for machine learning algorithms [63]. Unlike the human brain, which can intuitively interpret continuous patterns, computational models require structured numerical inputs called feature vectors to identify discriminative information. Therefore, feature extraction serves as the bridge between raw EEG data and effective classification, enabling the decoding of cognitive states and the development of functional MI-BCI systems. Besides improving classification accuracy, feature extraction also enhances the interpretability of EEG data. By isolating features related to specific neural rhythms or cortical regions, researchers can achieve a more profound

understanding of the brain's neural mechanisms underlying MI. This not only increases model transparency but also aids in designing more effective neurofeedback protocols and assistive BCI applications. The main goal of feature extraction is to emphasize signal characteristics that differentiate one mental task from another, such as left-hand versus right-hand imagery. Well-extracted features improve class separation, reduce dimensionality, and boost both computational efficiency and classification accuracy. Conversely, improperly designed features can lead to overfitting, misclassification, and decreased system performance. This challenge is compounded by the EEG nature itself, which is a non-stationary, stochastic signal containing sophisticated information. Consequently, a single feature extraction approach is often insufficient to fully characterize its properties. To address this, it is necessary to benefit from the complementary discriminative power of multiple feature domains [71]. The most widely adopted feature extraction strategies in MI-BCIs can be classified into four principal domains: time domain, frequency domain, time-frequency domain, and spatial domain. These categories reflect the diverse nature of EEG signals, which contain meaningful information distributed across multiple representations. Figure 2.1 illustrates the most commonly used feature families reported in the literature. Collectively, these techniques aim to transform raw EEG signals into discriminative, low-dimensional representations that facilitate accurate classification of MI patterns.

Time-domain features primarily capture statistical properties or waveform characteristics of the EEG signal directly in the temporal space. Common measures include signal amplitude, Hjorth parameters (mobility, activity, and complexity), autoregressive (AR) coefficients, root mean square (RMS), and amplitude variance [69]. These features are computationally efficient and easily interpretable, making them well-suited for real-time MI-BCI systems. However, their sensitivity to noise and limited ability to capture oscillatory patterns often reduce performance when used alone.

Frequency-domain features extract information by converting EEG signals into the spectral domain, thereby emphasizing oscillatory activity directly related to MI-induced ERD/ERS. Classical spectral techniques like the Fast Fourier Transform (FFT) [70], Power Spectral Density (PSD) estimation (e.g., Welch’s method) [71], and the Discrete Cosine Transform (DCT) [72] have been widely used. These features allow precise quantification of band-specific activity, which is strongly modulated during MI. Frequency features remain foundational in MI-BCI research owing to their strong physiological interpretability.

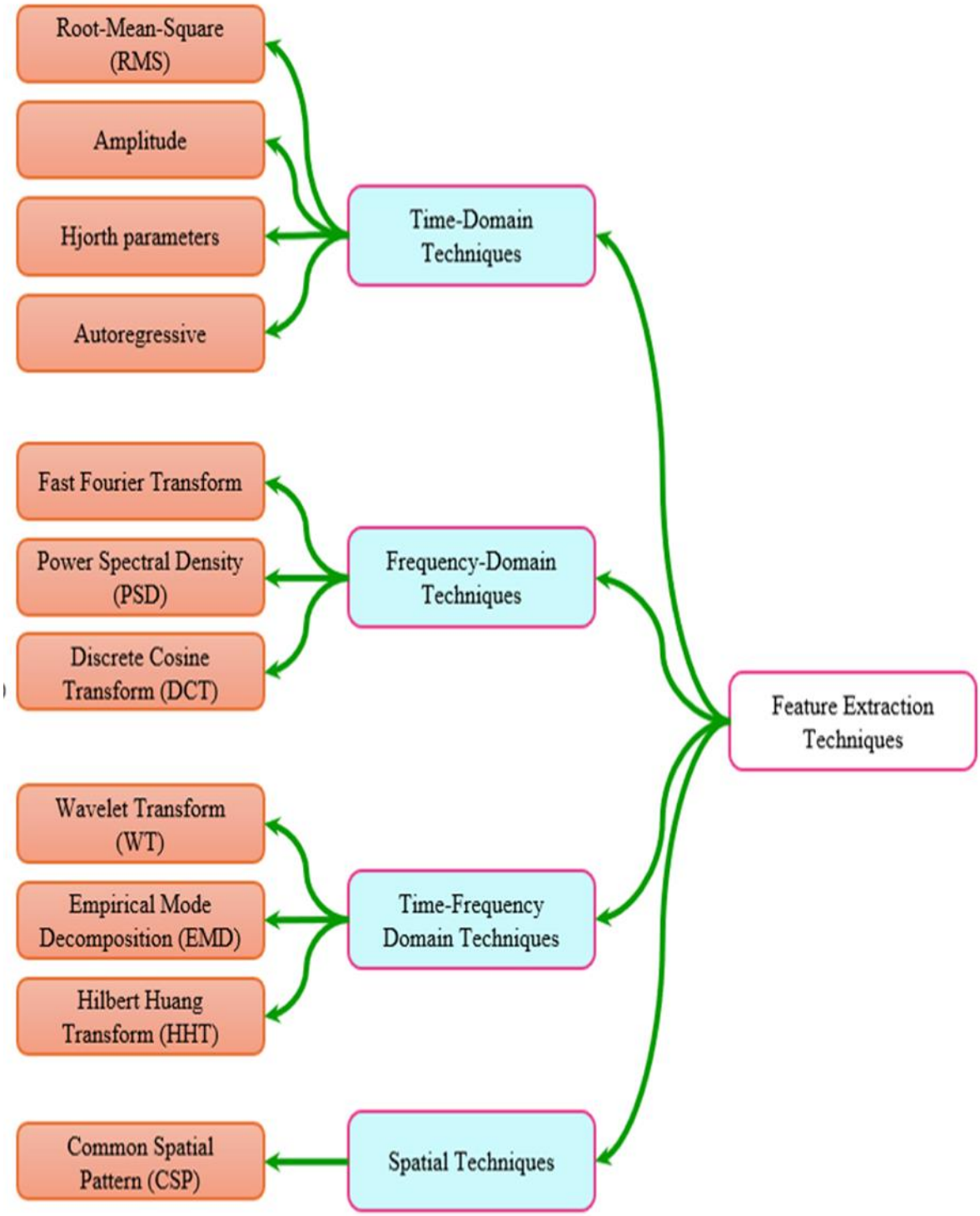

Figure 2.1. Feature Extraction.

Time–frequency-domain features provide a richer representation by simultaneously capturing temporal dynamics and spectral content. These methods describe how frequency components evolve over time, an essential capability for EEG, where MI processes are inherently non-stationary. Popular approaches include the Continuous Wavelet Transform (CWT) [72], Discrete Wavelet Transform

(DWT) [73], Wavelet Packet Decomposition (WPD) [74], Empirical Mode Decomposition (EMD) [75], and Hilbert-Huang Transform (HHT) [76]. Such methods are effective in modeling transient ERD/ERS patterns and provide multiresolution descriptions of EEG activity. Their adaptability and robustness make them highly suitable for MI classification, although they often involve higher computational expense and parameter tuning.

Spatial-domain features aim to enhance discriminability by emphasizing differences in the spatial distribution of sensor activity over the scalp. The most influential spatial method in MI-BCI is Common Spatial Patterns (CSP), which maximizes variance differences between two MI classes by learning spatial filters [77]. Variants such as Filter Bank CSP (FBCSP), Subspace CSP, and regularized CSP approaches have further improved robustness across subjects and sessions. Spatial features are essential for capturing the cortical sources underlying MI and often serve as the backbone of conventional ML pipelines.

2.5. Classification in MI-Based BCIs

Classification constitutes a core task in machine learning, wherein the goal is to construct a model that classifies data instances to predefined categories or class labels [62]. This process relies on analyzing patterns and relationships within a labeled training dataset, where every sample is associated with its true class assignment. The algorithm learns to identify discriminative features and builds a decision boundary or decision function that effectively separates the different classes. Following training, the model can be deployed to new, unseen data to predict their class memberships a process commonly referred to as inference or prediction. Despite the proliferation of numerous powerful learning methods, they all adhere to the same underlying framework, which in supervised learning consists of four stages: training data, a learning algorithm, the resulting classification function (or model), and a testing phase, as conceptually showcased in Figure 2.2.

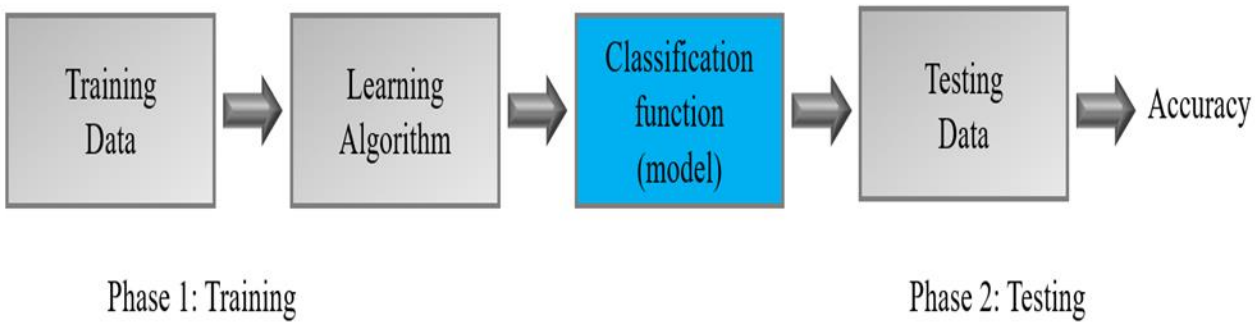

Figure 2.2. General Framework of Supervised Machine Learning.

In the context of MI-BCIs, classification represents the final and decisive stage of the signal processing pipeline. At this stage, features extracted from EEG signals are mapped to discrete control commands corresponding to imagined movements. The choice of classifier directly influences system accuracy, robustness, and real-time performance, making it a critical design decision. A diverse range of classification algorithms has been employed in MI-BCIs, including LDA, SVM, LR, and KNN [78], [79], [80]. Each algorithm is based on different theoretical principles, with specific strengths and limitations depending on data features and application needs. The following subsections highlight the most relevant classifiers in MI-BCIs, emphasizing their working principles, mathematical bases, and application considerations.

2.5.1. Linear Discriminant Analysis (LDA)

LDA is a fundamental supervised learning algorithm, widely recognized in MI-BCI research for its computational efficiency, robustness, and reliable performance. Its main objective is to identify a linear combination of features that achieves maximum class separability by projecting the data onto a hyperplane that maximizes the between-class to within-class variance ratio [49].

Mathematically, LDA determines a projection vector *w* which optimizes the Fisher criterion:

$$\boldsymbol{J(w) = \frac{w^T S_B w}{w^T S_W w}} \tag{2.1}$$

where S_B is the between-class scatter matrix, measuring the separation between class means and S_w is the within-class scatter matrix, measuring the spread of samples within every class. This criterion ensures that projected class means are pushed farther apart while minimizing intra-class variance.

The optimal projection vector is obtained by solving the generalized eigenvalue problem:

$$\boldsymbol{S_B w = \lambda S_W w} \tag{2.2}$$

Where the eigenvectors corresponding to the largest eigenvalues form the projection matrix. Once the data is projected, classification is typically performed using a linear decision rule:

$$\boldsymbol{y = w^T x + b} \tag{2.3}$$

Where x is the feature vector and b is a threshold chosen to best separate the classes.

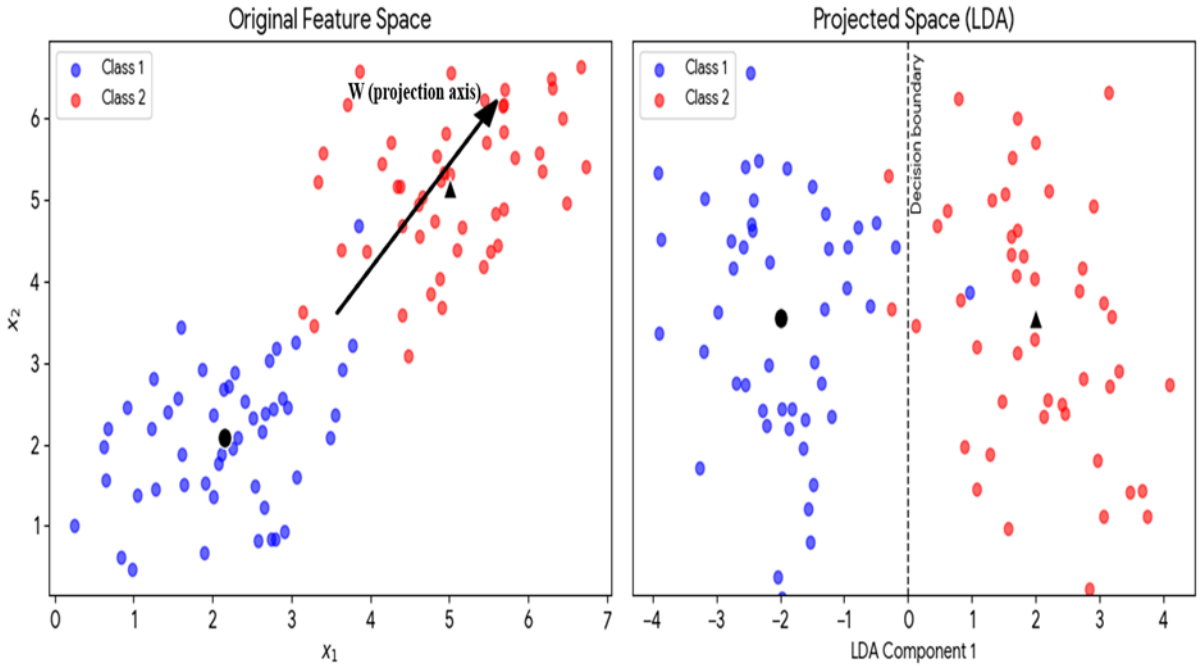

Figure 2.3. Illustration of the LDA principle.

The left panel of Figure 2.3 shows two Gaussian-distributed classes in the original feature space, with the black arrow indicating the LDA projection axis. The right panel displays the distribution of data points after they are projected onto this axis. The LDA projection line w demonstrates how it maximizes inter-class separation while minimizing intra-class variance, leading to an optimal linear decision boundary.

LDA is one of the most commonly utilized baseline classifiers in MI-BCIs because of its computational efficiency, ease of implementation, and interpretability. Constructing linear decision boundaries provides clear insights into class separation and performs reliably on small datasets, making it particularly well-suited for real-time applications. However, it relies on the strong assumption that classes are Gaussian-distributed with equal covariance matrices conditions frequently violated in EEG data. It is also sensitive to outliers, which can distort class means, and its linear nature restricts its ability to capture the non-linear relationships often present in MI patterns. Despite these limitations, LDA remains a resilient and indispensable baseline against which more sophisticated MI-BCI classifiers are evaluated.

2.5.2. Support Vector Machines (SVM)

SVMs represent a powerful supervised learning paradigm capable of modeling complex, non-linear relationships between EEG features and MI classes. The fundamental principle of an SVM is to construct an optimal separating hyperplane that splits data from distinct classes with the maximum

separating margin, thereby improving generalization and reducing the risk of misclassification [79]. Support vectors, which are the samples closest to the hyperplane, critically shape the final decision boundary.

Mathematically, for a binary classification problem, the SVM seeks a hyperplane defined as:

$$\boldsymbol{w^T x + b = 0} \tag{2.4}$$

Where w is the weight vector orthogonal to the hyperplane and b is the bias term. The optimization problem aims to maximize the margin $\frac{2}{\|w\|}$, which leads to the formulation:

$$\boldsymbol{\min_{w,b} \frac{1}{2}\|w\|^2 \quad \text{subject to} \quad y_i(w^T x_i + b) \geq 1, \forall i} \tag{2.5}$$

Where x_i are training samples and $y_i \in \{-1, +1\}$ are their class labels.

Where data are not linearly separable, SVM employs kernel functions to map data into a higher-dimensional feature space, allowing for the construction of an optimal linear hyperplane. Frequently employed kernels include the linear kernel, the Radial Basis Function (RBF) kernel and the polynomial kernel, the latter being particularly effective in capturing the non-linear dynamics of EEG signals in MI-BCIs [81]. Figure 2.4 conceptually illustrates the distinction between a linear SVM, which separates classes with a straight hyperplane, and a non-linear SVM using the RBF kernel, which enables circular or more complex decision boundaries in transformed feature spaces.

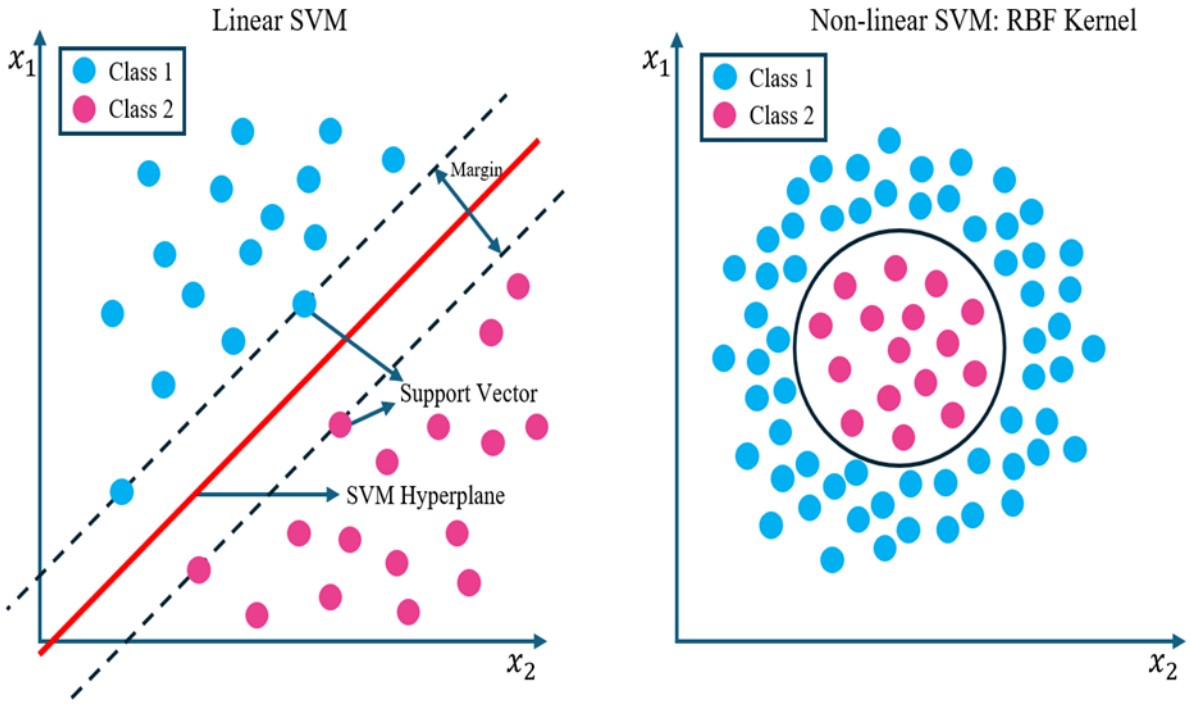

Figure 2.4. Illustration of Linear and Non-Linear SVM Decision Boundaries.

The left panel shows a linear SVM, where the optimal separating hyperplane is shown as the solid line, with dashed lines representing the margins, and the circled points correspond to the support vectors. The right panel illustrates a non-linear SVM using the RBF kernel, which successfully separates data that are non-linearly separable in the untransformed feature space.

SVMs are powerful classifiers that function effectively in high-dimensional EEG feature spaces by maximizing the margin between classes, which enhances generalization and robustness against overfitting. Their versatility is largely due to the utilization of kernel functions, specifically the RBF kernel, which allows effective modeling of the non-linear dynamics typical of MI-EEG data. SVMs are also effective with relatively small training sets, making them attractive for MI-BCI applications where data can be limited. However, these strengths come at a cost: training could be computationally intensive, specially with non-linear kernels, and performance is highly sensitive to hyperparameter tuning, such as the kernel parameters like γ and regularization parameter C. Furthermore, SVMs lack native probabilistic outputs and become less interpretable when complex kernels are employed, which can limit transparency in practical decision-making.

2.5.3. Logistic Regression (LR)

LR is a classical and commonly utilized supervised learning algorithm primarily applied to two-class classification tasks. In contrast to Linear Regression, which is designed to predict continuous numerical values, LR calculates the likelihood of an input belonging to a specific class, making it particularly suitable for distinguishing between two categories (e.g., left-hand vs. right-hand MI). It achieves this using a linear combination of features to model the relationship with class labels, followed by the application of a sigmoid (logistic) function that maps the output into the [0, 1] interval [80].

Mathematically, the logistic model can be calculated as:

$$\boldsymbol{z = w^T x + b} \tag{2.6}$$

where w represents the weight vector, b is the bias term and x is the feature vector.

The linear combination of inputs z is transformed by the sigmoid function to produce a probability:

$$\boldsymbol{\hat{y} = P(Y = 1|x) = \sigma(z) = \frac{1}{1 + e^{-z}}} \tag{2.7}$$

In this equation, $\hat{y}$ denotes the estimated probability that input x corresponds to the positive class. The sigmoid function maps any real-valued input z into the [0,1] interval, allowing the model to interpret the result as a probability.

This probability can be interpreted as the confidence level of the model's prediction. A threshold of 0.5 is commonly utilized to determine the last class label:

$$\hat{y} = \begin{cases} \textbf{Class 1}, & \textbf{if } \hat{y} \geq \textbf{0.5} \\ \textbf{Class 0}, & \textbf{otherwise} \end{cases} \quad (2.8)$$

Throughout the training stage, the model parameters w and b are estimated by maximizing the likelihood function or equivalently by minimizing the cross-entropy loss, given by:

$$L(w, b) = -\frac{1}{N}\sum_{i=1}^{N}[y_i \log(\hat{y}_i) + (1 - y_i)\log(1 - y_i)] \quad (2.9)$$

where N is the number of training samples and y_i is the true label of the ith sample. Optimization algorithms such as gradient descent are typically employed to minimize this loss and update model parameters iteratively.

LR remains a compelling choice in MI-based BCIs due to its computational efficiency, probabilistic interpretation, and straightforward implementation. The coefficients of the model directly reflect the effect of each feature on the classification outcome, offering interpretability that is valuable for understanding EEG feature relevance. Moreover, LR can be adapted to multi-class classification using techniques like One-vs-Rest (OvR) or Softmax Regression.

Despite its robustness and simplicity, LR is based on the assumption of a linear relationship between features and the log-odds of the outcome, which may limit its effectiveness when dealing with the nonlinearity and non-stationarity of EEG data. It is also sensitive to feature scaling and may overfit in high-dimensional spaces without appropriate regularization (e.g., L1 or L2). Consequently, while LR provides a strong baseline, it is often outperformed by non-linear models like neural networks or SVM in complex MI-BCI classification tasks.

2.5.4. k-Nearest Neighbors (KNN)

KNN is a simple but highly effective supervised learning approach utilised for regression and classification tasks [82]. In the context of MI-BCIs, it is primarily employed for classification, which is designed to assign an EEG feature vector to a MI class based on the similarity of that feature vector to previously labeled data. KNN is an instance-based and non-parametric method, indicating that it does not assume any specific distribution for the data and does not construct an explicit model during the training stage. Rather, it memorizes the training samples and computes only at prediction time, which is why it is often referred to as a lazy learner.

The fundamental principle of KNN is that instances of the same class are typically close to one another in the feature space. For the classification of a new sample, the algorithm computes its distance from all training points and identifies the k nearest neighbors. The class label is then determined based on a majority vote rule among these neighbors. The similarity between samples is commonly measured using the Euclidean distance [83], defined as:

$$d(x_i, x_j) = \sqrt{\sum_{k=1}^{d} (x_{ik} - x_{jk})^2} \tag{2.10}$$

Where d is the dimensionality of the feature space, and x_i and x_j are feature vectors.

Other distance metrics, such as the Manhattan and Minkowski distances, can also be applied depending on the characteristics of the dataset. However, the Euclidean distance remains the predominant metric in MI-BCI applications.

As illustrated in Figure 2.5, the KNN algorithm classifies an unseen data point via majority voting among its closest neighbors in the feature space, effectively defining flexible, non-linear decision boundaries without an explicit parametric model. KNN's simplicity, interpretability, and flexibility make it an attractive option for EEG-based MI classification, particularly when dealing with small datasets or non-linear feature distributions. Because it does not rely on strong assumptions about data structure, KNN adapts well to complex and irregular EEG feature spaces. Additionally, by basing its decision on multiple neighbors rather than a single point, KNN is relatively robust to outliers and noise. However, the algorithm has several drawbacks. It is computationally expensive during prediction since it requires calculating distances to all training samples, and its memory usage grows linearly with dataset size.

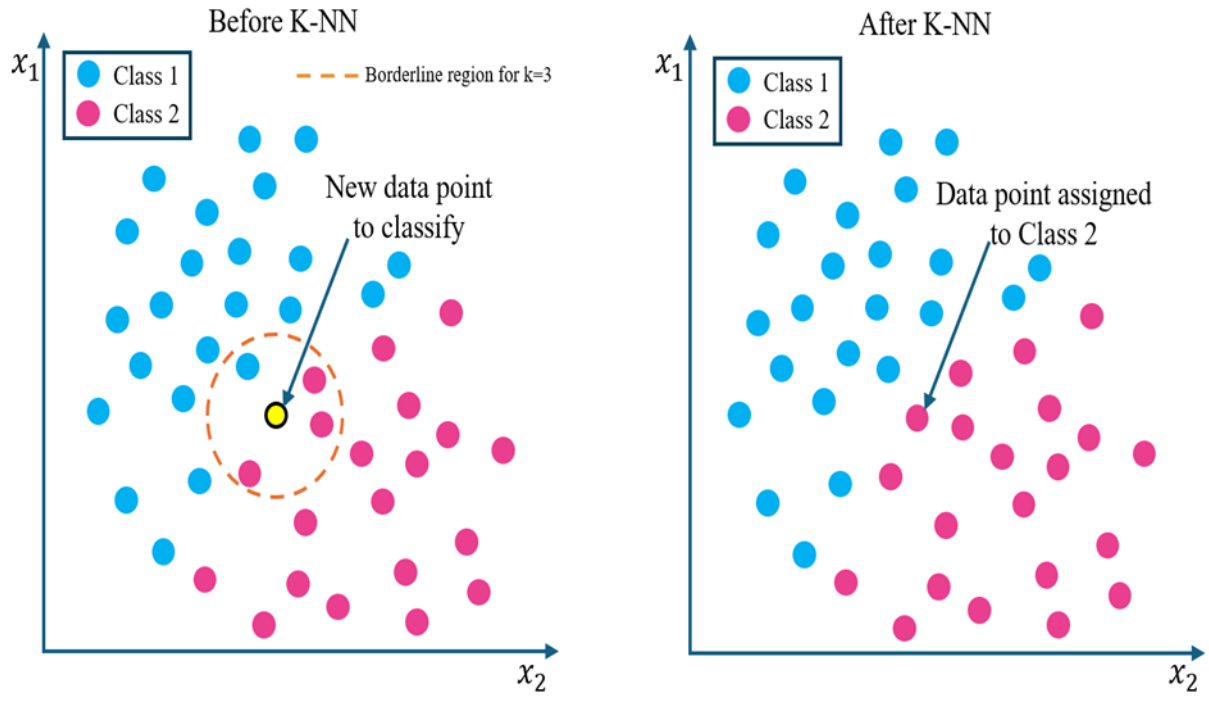

Figure 2.5. The k-Nearest Neighbors classification principle.

Moreover, its performance heavily relies on the selection of k and the distance metric, with inappropriate selections leading to underfitting or overfitting. KNN is also sensitive to feature scaling and performs poorly when there is a large class imbalance. Despite these limitations, KNN remains a valuable baseline method in MI-BCIs due to its minimal parameter tuning, conceptual simplicity, and ability to model non-linear decision boundaries.

2.6. Feature selection for dimensionality reduction

The effectiveness of a learning algorithm is not influenced by just its structure or how it processes data; several external factors especially the nature and quality of the dataset can significantly impact performance. Issues such as high dimensionality, redundant variables, and irrelevant features are known to reduce CA [84]. To address this, reducing the dimensionality of the data is often necessary to eliminate unnecessary or noisy features. Approaches to dimensionality reduction are generally split into two primary classes:

Feature selection, which involves identifying and keeping only the most informative variables from the dataset.

Feature extraction, which transforms the original feature space into a new, lower-dimensional representation. Principal Component Analysis (PCA) is the most commonly applied feature extraction approach for dimensionality reduction [85].

In this thesis, we focus specifically on dimensionality reduction through feature selection. Accordingly, the next sections present an overview of the feature selection problem and its underlying strategies.

2.6.1. Feature selection as an optimization problem

Feature selection enhances the performance of classification models by removing irrelevant, noisy, or redundant features that can lower accuracy, increase computational cost, and reduce generalization [86]. Unlike feature extraction, which creates new features by transforming original variables into a different space, feature selection maintains the original feature representations by discarding only the irrelevant or redundant ones. In EEG-based MI applications, where datasets are typically high-dimensional with many non-discriminative features, choosing an optimal subset is crucial for improving classifier performance.

Feature selection is typically treated as an optimization process in which candidate feature subsets are generated, evaluated, and refined to identify the most informative combination of variables. This process involves four core components operating iteratively [84]:

Search Strategy: A method is used to explore different combinations of features to find the best feature subsets from the initial set of features. This can include exhaustive search, heuristic algorithms, or

metaheuristic optimization techniques such as Genetic Algorithms (GA), Firefly Algorithm (FA), Ant Colony Optimization (ACO), or Particle Swarm Optimization (PSO).

Evaluation Criterion: Each feature subset is assessed based on its discriminative power, which measures the quality of the feature subsets generated in the previous step. This evaluation is typically performed using a performance indicator such as CA or error rate.

Stopping Criterion: The search process terminates when a predefined condition is satisfied. Common stopping criteria involve achieving a maximum number of iterations, reaching convergence in performance improvement, or exceeding a defined computational limit.

Validation: The final step in the feature selection process is to validate the chosen subset. This is typically done by evaluating the performance of a model trained using these features through a cross-validation or train/test split technique to verify that the chosen features genuinely enhance the model's performance.

Among the metaheuristic approaches used to address this optimization problem, GAs have achieved significant interest because of their strong global search capability and efficiency in exploring large feature spaces to identify optimal feature subsets [87].

2.6.2. Feature selection using GA

GAs are population-based metaheuristic optimization techniques inspired by the principles of natural selection and genetics. Originally developed by John Holland in the 1970s [88], and later formalized for engineering optimization by David Goldberg [89], GAs are particularly effective for feature selection in large, complex search spaces where exhaustive or deterministic methods are computationally infeasible.

GAs operate on a population of candidate solutions, simulating Darwin's "survival of the fittest" principle. Fitter individuals have a higher probability of reproducing and passing their traits to the next generation. In the context of feature selection, GAs aim to identify the most informative subset of features that maximizes classification performance while minimizing redundancy and dimensionality [87]. Each individual is represented as a binary chromosome, where each gene corresponds to a specific feature: a value of '1' indicates the feature is selected, while '0' indicates its exclusion. The quality, or fitness, of a chromosome is evaluated by a fitness function that typically incorporates a performance metric, such as classification accuracy from a model like SVM. It can be expressed as:

$$\boldsymbol{F = \alpha \times Accuracy + (1 - \alpha) \times \left(1 - \frac{|S|}{|N|}\right)} \tag{2.11}$$

where F is the fitness value, $Accuracy$ is the classifier's performance metric, $|S|$ is the number of the chosen features, $|N|$ is the total number of features, and α is a weighting factor that balances CA and subset size.

The standard GA-based feature selection process iteratively improves the population through the following biologically inspired operators [90]:

Initialization: An initial population of chromosomes (feature subsets) is generated, often randomly.

Fitness Evaluation: Each chromosome is decoded into a feature subset. A classifier is trained using this subset, and its performance (e.g., accuracy, kappa) on a validation set is assigned as the individual's fitness score.

Selection: Individuals are chosen for reproduction based on their fitness. Strategies like tournament selection or roulette wheel selection are commonly used to give fitter chromosomes a higher chance of being selected.

Crossover: Pairs of selected parent chromosomes undergo recombination (e.g., single-point crossover) to create offspring. This operator exploits existing genetic material by combining promising feature subsets from different parents, guiding the search toward promising regions of the space.

Mutation: Offspring chromosomes are subject to random bit flips with a small probability. This operator introduces new genetic material, enhances the exploration ability of the algorithm, and helps prevent premature convergence to local optima.

An intermediate population is created from the new offspring, and the fittest individuals from this pool replace the weakest in the current population to form the next generation. This iterative process of selection, crossover, and mutation continues until a stopping criterion is met, such as a maximum number of generations or convergence of the population.

By effectively balancing exploration (via mutation) and exploitation (via crossover and selection), GAs can escape local optima and discover compact, high-performing feature subsets that simpler greedy search methods might miss. This makes them highly suitable for the high-dimensional feature spaces common in MI-BCI, such as those generated by Filter Bank CSP. Beyond improving CA by eliminating redundant and non-discriminative features, GA-based selection significantly reduces the computational burden during model training and inference, enhancing the feasibility of real-time BCI applications.

2.7. Performance evaluation and benchmarking

A rigorous and standardized approach to evaluation is paramount in MI-BCI research, as it enables the fair comparison of different algorithms, provides a clear measure of progress, and ensures that reported performance reflects real-world usability [45]. This is particularly critical given the significant variability of EEG signals across participants, sessions, and trials, stemming from their

inherent non-stationarity and susceptibility to noise. Consequently, an effective evaluation strategy must include suitable metrics, strict validation protocols, and robust statistical analysis to derive meaningful conclusions and enable fair comparisons with existing studies.

MI-BCI studies are generally conducted in offline or online contexts. Offline analysis uses pre-recorded data for retrospective model development and validation, while online systems operate in real-time, providing continuous feedback to the subject. The following subsections detail the standard metrics, validation schemes, and benchmarking practices essential for credible offline MI-BCI research, which forms the foundation for any subsequent online implementation.

2.7.1. Standard metrics for MI-BCI

The evaluation of a machine learning classifier in MI-BCI typically begins with the confusion matrix, as it offers the most informative and interpretable breakdown of classification outcomes. It summarizes how the model's predictions compare to the true class labels by counting the number of correctly and incorrectly classified samples in the test data.

In a binary classification setting, as illustrated in Figure 2.6, the confusion matrix is structured as a 2×2 table consisting of:

- True Positives (TP): instances correctly predicted as belonging to the positive class
- True Negatives (TN): instances correctly predicted as belonging to the negative class
- False Positives (FP): negative instances incorrectly classified as positive
- False Negatives (FN): positive instances incorrectly classified as negative

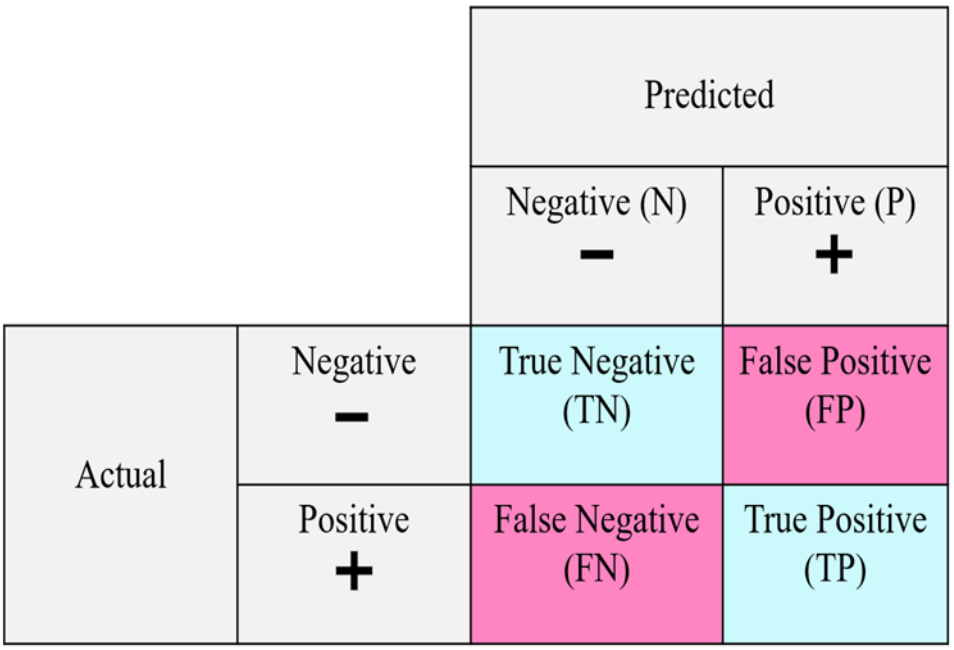

Figure 2.6. Confusion Matrix for a Binary Classification.

In this matrix, the rows represent the predicted classes from the model and the columns represent the true, actual classes. This structure provides detailed insight into the specific types of errors the classifier makes, moving beyond simple accuracy to reveal the nature of its confusions between classes.

This matrix serves as the foundation for all standard classification metrics used in MI-BCI, including accuracy, recall, precision, F1-score, and Cohen's Kappa.

Accuracy represents the proportion of successfully predicted cases compared to the total number of predicted cases, serving as a general indicator of performance. It is defined as:

$$\boldsymbol{Accuracy} = \frac{\boldsymbol{Number\ of\ correct\ predictions}}{\boldsymbol{Total\ number\ of\ predictions}} = \frac{\boldsymbol{TP + TN}}{\boldsymbol{TP + TN + FP + FN}} \quad (2.12)$$

Sensitivity (Recall), also known as the True Positive Rate, measures how well the model correctly identifies instances of the target class.

$$\boldsymbol{Sensitivity} = \frac{\boldsymbol{TP}}{\boldsymbol{TP + FN}} \quad (2.13)$$

Precision reflects the proportion of successfully classified positive predictions out of all cases predicted as positive:

$$\boldsymbol{Precision} = \frac{\boldsymbol{TP}}{\boldsymbol{TP + FP}} \quad (2.14)$$

F1-score gives a fair evaluation by merging Precision and Sensitivity into a single metric using their harmonic mean. It is useful when the dataset is uneven or when both false positives and false negatives carry significant consequences:

$$\boldsymbol{F1 - score} = \boldsymbol{2} \times \frac{\boldsymbol{Precision} \times \boldsymbol{Sensitivity}}{\boldsymbol{Precision + Sensitivity}} \quad (2.15)$$

Cohen's Kappa provides a robust evaluation by measuring the level of agreement between predicted and true labels while correcting for the agreement expected by chance. It is particularly beneficial when evaluating performance on imbalanced datasets, as it offers a more realistic measure of classifier effectiveness than accuracy alone by accounting for the underlying class distribution. It is calculated as:

$$\boldsymbol{K} = \frac{\boldsymbol{p_o - p_e}}{\boldsymbol{1 - p_e}} \quad (2.16)$$

where p_o is the observed agreement (equivalent to overall accuracy) and p_e is the probability of chance agreement, calculated from the marginal probabilities of the confusion matrix.

2.7.2. Validation strategies

To obtain a reliable estimate of a model's ability to generalize to new data, the dataset must be divided into separate subsets for model training and evaluation. Appropriate validation strategies are crucial for mitigating overfitting, ensuring the reproducibility of results, and facilitating fair comparisons across different studies. The most widely adopted validation strategies in MI-BCI comprise:

2.7.2.1. Train/Test split (Predefined)

In many MI datasets, the division between training and testing data is already provided by the dataset itself. In this case, the researcher does not manually split the data; instead, they train the model on the designated training portion and evaluate it on the predefined test set. This approach is simple and efficient, but provides only a single estimate of performance.

2.7.2.2. Hold-Out validation

When no predefined split exists, the data can be split manually into two parts, like 70% for training and 30% for testing. This method is easy to apply but may lead to biased estimates if the split is unrepresentative of the entire dataset.

2.7.2.3. k-Fold Cross-validation (10-Fold)

It is a widely adopted evaluation approach in machine learning [91], prized for its conceptual simplicity and its robust, reliable estimation of classification model performance [92]. To get a more reliable estimate of machine learning models, the dataset is divided into k equal partitions. In each iteration, (k – 1) folds are utilized for training and the remaining fold is utilized for testing. This method is repeated k times to make sure that each fold is used once as the test set. The final score is calculated as the average of all k evaluations, as shown in Figure 2.7. In MI-BCI studies, the most commonly adopted configurations are 10-fold and 5-fold cross-validation, with 10-fold being more frequently used because of its balance between evaluation reliability and computational efficiency [93]. This approach offers a more reliable and consistent performance estimate than the hold-out method because it uses all available data for both training and testing.

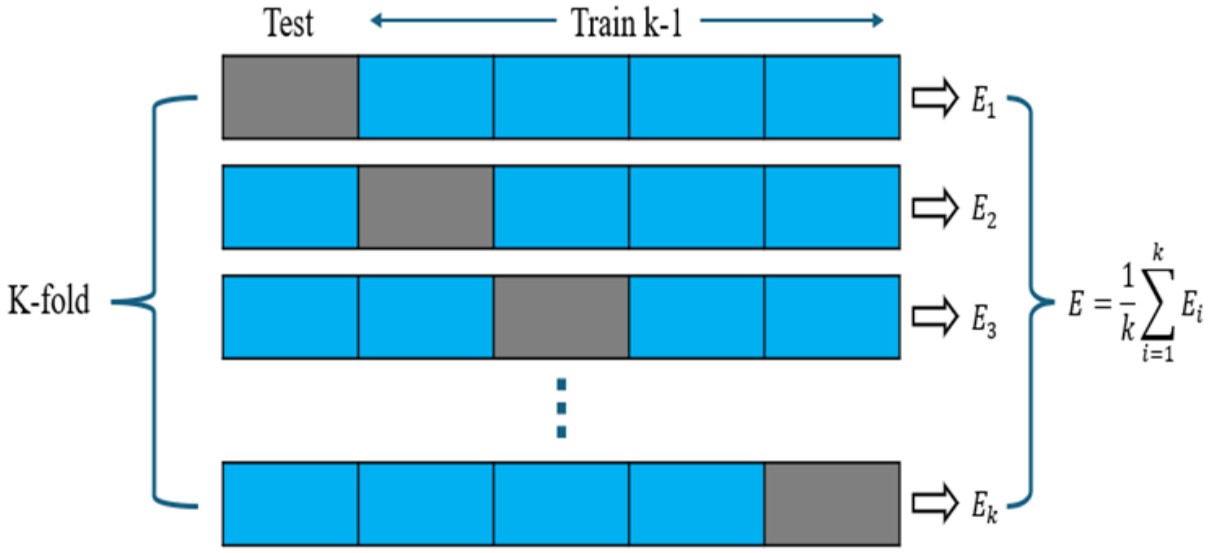

Figure 2.7. Schematic Representation of both Holdout and K-Fold Cross-Validation.

2.8. Conclusion

In this chapter, the fundamental components of the machine learning framework for MI-BCIs were presented. The discussion began with the supervised learning paradigm, which forms the foundation for EEG-based classification, emphasizing the importance of labeled data and model generalization. Subsequently, various stages of the MI-BCI signal processing pipeline were detailed, including feature extraction, classification, and performance evaluation. Feature extraction methods were categorized according to their analytical domains temporal, spectral, time–frequency, and spatial highlighting their respective contributions to improving class separability and reducing data complexity.

Several conventional classification algorithms were then explored, such as LDA, SVM, LR, and KNN. Each method was discussed in terms of its mathematical principles, advantages, and limitations in decoding MI patterns from EEG signals.

The chapter also examined feature selection as an essential step in dimensionality reduction, aiming to identify the most informative subset of features that enhance model accuracy and computational efficiency. In particular, GA were presented as a robust metaheuristic optimization approach for feature selection, capable of efficiently exploring large search spaces to identify near-optimal feature subsets.

Finally, the performance evaluation and benchmarking section provided an overview of common assessment metrics and validation strategies, including cross-validation techniques, ensuring that model results are both reliable and comparable across studies.

Overall, this chapter established the theoretical and methodological foundation for developing efficient MI-BCI systems by exploring key stages like feature extraction, feature selection, and classification. The next chapter builds upon this foundation by presenting a detailed description of the datasets used in this study, outlining their structure, acquisition protocols, and relevance to MI research.

Chapter 03

EEG DATASETS FOR MI-BASED BCI

3.1. Introduction

The development of robust BCI systems relies heavily on the availability of high-quality, well-annotated EEG datasets. MI-based BCIs, in particular, require standardized datasets for training, validation, and benchmarking machine learning models. Given the natural heterogeneity of EEG signals both within and across individuals, research typically employs multiple datasets to ensure that results are not biased toward a specific recording setup, subject group, or task design.

This chapter introduces and describes the datasets utilized in this study. It begins by outlining the general characteristics of MI EEG datasets, including standard recording setups, MI tasks, experimental protocols, and preprocessing procedures. These aspects establish a foundational understanding of how MI data are collected and prepared for analysis. The chapter then presents five benchmark datasets that are widely used within the BCI research community:

- BCI Competition III Dataset IIIb – a two-class dataset emphasizing non-stationary MI [94].
- BCI Competition II Dataset III – a single-subject dataset with continuous feedback [95].
- BCI Competition IV Dataset 2b – a dataset combining open-loop and feedback sessions [96].
- OpenBMI Dataset – a large-scale dataset enabling both cross-subject and subject-specific analyses [97].
- BCI Competition IV Dataset 2a – widely recognized as one of the most challenging four-class EEG classification benchmarks [98].

By first establishing the general characteristics of MI datasets and then examining each dataset individually, this chapter provides the necessary foundation for understanding the data that underpins the analyses conducted in subsequent chapters.

3.2. General characteristics of MI EEG datasets

This section focuses on describing the standard techniques and typical practices utilized in recording EEG data for MI-based BCI research. Data collection generally follows well-known protocols designed to ensure consistency across subjects and sessions. These include standardized electrode placement systems for reliable spatial coverage, cue-based experimental paradigms for precise timing, and carefully planned trial designs to balance task engagement with resting periods [45]. These practices are essential for ensuring reproducibility and allowing meaningful comparisons across different datasets and research groups. Additionally, understanding these common features is vital for interpreting the datasets discussed later in this chapter and for designing robust, reproducible experiments. It is essential to acknowledge that variations in parameters such as electrode setup, sampling rates, or preprocessing methods can highly impact the usability and quality of MI EEG signals, which tend to be low in amplitude, noisy, and exhibit considerable inter-individual variability. The following subsections will detail the key aspects of MI EEG datasets, including recording configurations, MI tasks, experimental protocols, labeling strategies, and preprocessing techniques. These elements collectively form the core framework for effective feature extraction, signal analysis, and model development in MI-based BCI systems.

3.2.1. EEG recording setup

To begin, it is essential to consider how EEG signals are recorded in MI experiments, as the recording configuration directly determines the reliability and quality of the data. The selection of electrode system, placement strategy, and sampling rate is critical for capturing motor-related brain activity with sufficient spatial and temporal resolution. A carefully designed setup ensures that the neural activity linked with MI can be accurately detected and later analyzed for use in BCI applications.

3.2.1.1. Electrode systems and placement

The international 10–20 system is the most frequently adopted standard electrode montage in MI studies, as it provides a consistent framework across laboratories and subjects [31]. For higher-resolution recordings, extended configurations such as the 10–10 system are frequently employed, offering denser spatial coverage and improved accuracy in localizing cortical sources of activity.

3.2.1.2. Relevant channels

Since MI tasks primarily engage the sensorimotor cortex, the most informative signals are typically recorded from electrodes positioned along the central sulcus [41]. In particular, C3, Cz, and C4 are recognized as the most critical key channels, as they directly correspond to contralateral and midline

motor regions. To enhance robustness, surrounding channels such as FC1, FC2, CP1, and CP2 are also commonly included, providing additional spatial context for decoding MI patterns.

3.2.1.3. Sampling rate

EEG data in MI experiments are generally sampled at rates between 128 Hz and 1000 Hz, depending on the research objectives and hardware constraints. A 250 Hz sampling rate is particularly common, as it balances the need to capture the frequency bands of interest, especially the mu and beta rhythms, while keeping data size manageable [98]. Higher sampling rates may be used in studies requiring finer temporal precision, but most MI-based BCI applications achieve reliable performance within this range.

3.2.2. Common MI tasks

Equally important in MI EEG datasets is the type of MI tasks employed during data acquisition. Task design, whether based on simple binary contrasts or more complex multi-class paradigms, has a direct impact on the richness, variability, and difficulty of the dataset, as well as on the choice of machine learning algorithms used for classification. In most cases, participants are directed to perform kinesthetic MI (e.g., imagining the sensation of the movement), as this approach produces stronger and more reliable cortical activations in the sensorimotor regions than purely visual imagination [99].

3.2.2.1. Binary classification tasks

The simplest and most widely used MI paradigms involve binary comparisons, such as:

- Left Hand vs. Right Hand: a fundamental paradigm that engages contralateral motor areas and provides strong lateralized EEG patterns.
- Hand (Left or Right) vs. Feet: a slightly more complex task that contrasts movements of different limbs, resulting in more distinct cortical activations.

3.2.2.2. Multi-Class classification tasks

More challenging paradigms expand beyond two classes, for example:

- Right Hand vs. Left Hand vs. Feet: a three-class paradigm commonly used in competitive BCI challenges.
- Right Hand vs. Left Hand vs. Feet vs. Tongue/Rest: a four-class paradigm that adds further complexity by engaging multiple motor representations or including a resting baseline.

The choice between binary and multi-class designs depends on the research objectives. While binary paradigms are easier to learn, yield higher classification accuracy, and provide clearer signals, multi-class paradigms better simulate real-world BCI applications by offering a wider range of possible commands, albeit at the cost of reduced accuracy and increased complexity.

3.2.3. Experimental protocol and trial structure

In addition to the tasks themselves, MI datasets typically employ a structured, cue-based experimental protocol. Such protocols are designed to ensure synchronization between brain activity and task events, thereby allowing researchers to extract time-locked epochs for further analysis [100]. A well-defined trial structure not only enhances reproducibility but also minimizes variability caused by external distractions or subject fatigue. Figure 3.1 illustrates a standard MI trial structure which generally consists of the following sequence:

Fixation Period (e.g., 0–2 s): A fixation cross or neutral symbol appears on the screen to orient the participant's attention and establish a baseline.

Cue Presentation (e.g., 2–3 s): A visual cue, such as an arrow pointing right or left, a letter, or a symbolic image of a limb, indicates the specific MI task to be performed.

MI Period (e.g., 3–7 s): The subject engages in kinesthetic MI of the cued movement without executing any physical motion. This is the most critical phase, as it contains the EEG signals of interest.

Rest Period (e.g., 7–9 s): A brief relaxation phase allows the participant to reset before the next trial begins, reducing cognitive load and preventing carry-over effects.

This repetitive, time-locked structure ensures consistency across trials and subjects. It also enables accurate segmentation of EEG data into meaningful epochs aligned to cue onset, which is essential for both preprocessing and subsequent classification tasks.

Furthermore, the duration of participant training and feedback mechanisms significantly impact MI performance, with repeated exposure enhancing the stability and vividness of kinesthetic imagery [101]. Regular training sessions help participants internalize the MI task, leading to more consistent activation patterns within the sensorimotor cortex. Visual, auditory, or proprioceptive feedback reinforces this learning process by providing real-time information about performance, enabling participants to adapt their strategies over time. Consequently, datasets integrating both open-loop and feedback-based sessions offer valuable insights into user learning dynamics, adaptation, and long-term improvements in MI-based control performance.

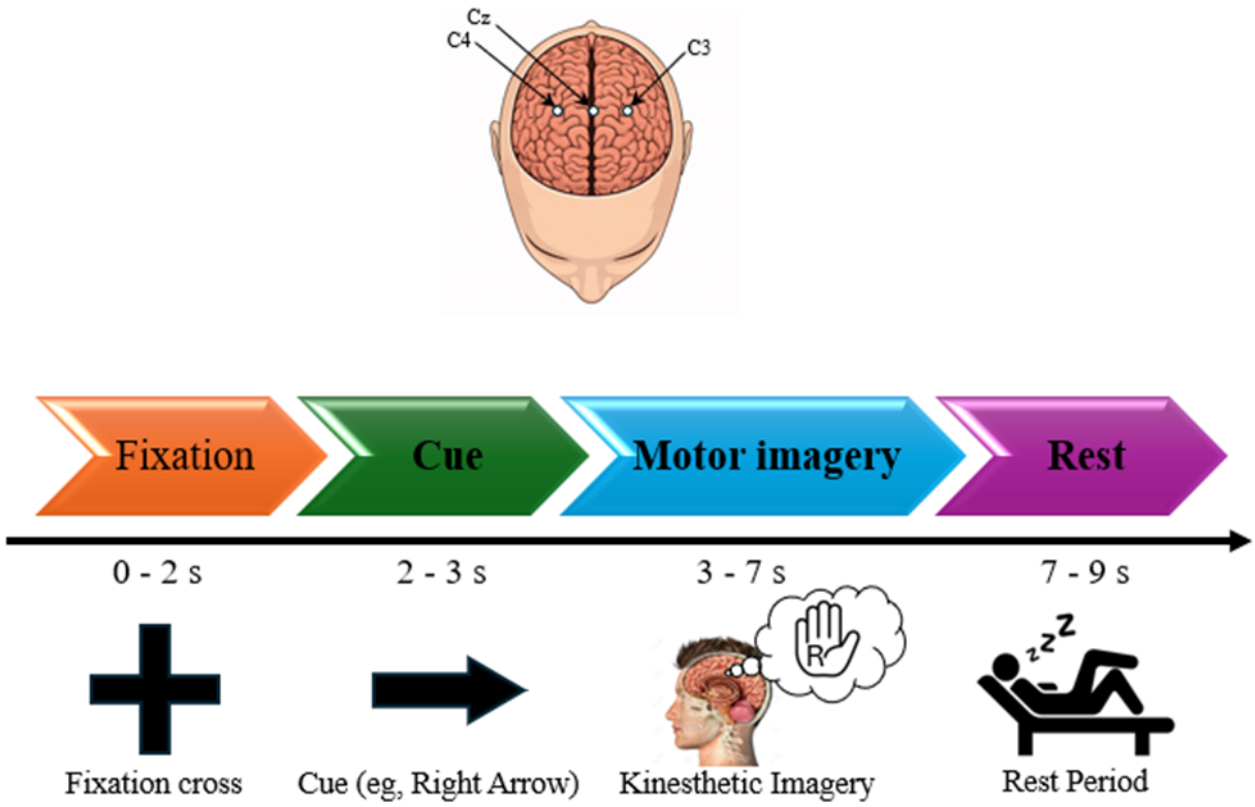

Figure 3.1. Standard Timeline structure of a single MI trial (Fixation, Cue, MI, Rest).

3.2.4. Data annotation and labeling

Accurate annotation and labeling of data are essential steps in preparing MI EEG datasets. Since machine learning approaches depend on well-defined ground truth, each trial must be precisely labeled according to the specific MI task [62]. This ensures the relationship between neural activity and task conditions stays consistent, thereby improving the reliability of both training and evaluation phases in supervised learning.

In most MI experiments, labels are automatically assigned based on the visual or auditory cue presented during the trial. For example, a left pointing arrow would correspond to a "left-hand imagery" label, while a downward pointing arrow might indicate a "foot imagery" task. These labels are typically stored alongside EEG signals in structured data files, enabling seamless alignment of task events with the corresponding neural responses. The quality and consistency of this labeling process are paramount, as mislabeled or ambiguous trials can significantly degrade classification performance.

3.2.5. Common preprocessing steps

EEG data collected during MI experiments are inherently noisy, as they are susceptible to contamination by artifacts from non-neural sources, like muscular contractions (EMG), eye movements, or external electrical interference [5]. Therefore, preprocessing is essential for enhancing data quality and ensuring that relevant neural oscillations are preserved for subsequent feature extraction and classification [25]. While specific pipelines may vary between datasets and research groups, most follow a set of well-established preprocessing steps to standardize the data and enhance reproducibility. These core steps typically include:

3.2.5.1. Band-Pass filtering

To reduce unwanted noise, a notch filter at 50 or 60 Hz is typically utilized to remove power line interference. In addition, a band-pass filter is commonly set between 0.5–30 Hz to suppress high-frequency noise and slow drifts, making sure that the neural rhythms most relevant to MI remain intact [31]. Within this range, the mu (8–13 Hz) and beta (13–30 Hz) frequency bands are of particular interest, as they originate from the sensorimotor cortex and play a critical role in distinguishing different MI tasks.

3.2.5.2. Artifact removal

Non-neural artifacts like saccades, eye blinks, and muscle activity can overshadow the relatively weak cortical signals. Independent Component Analysis (ICA) is widely regarded as the most commonly utilized method to identify and remove such components, though other approaches, such as regression-based methods or automated artifact detection algorithms, are also employed in some datasets.

3.2.5.3. Epoching

Continuous EEG recordings are segmented into shorter time intervals (epochs) aligned with the onset of task cues. These epochs typically include a short baseline, the cue presentation, and the MI period. This segmentation allows researchers to focus on time-locked neural activity associated with each trial while discarding irrelevant portions of the continuous signal [45].

Together, these preprocessing steps provide cleaner and more structured data, forming the foundation for accurate feature extraction and reliable classification in MI-BCI systems.

3.3. Dataset 1: BCI Competition III Dataset IIIb

3.3.1. Source and description

The dataset utilized in this study is BCI Competition III Dataset IIIb, a public benchmark dataset from the 3rd International BCI Competition. Validating and improving signal processing and classification techniques for MI-BCI is the primary goal of the BCI Competition series. This particular dataset was created to address a significant problem in the field: non-stationary MI, which provides a strong platform for developing adaptive classification algorithms that can handle time-varying brain dynamics.

The dataset comprises EEG recordings from three healthy subjects identified as O3, S4, and X11. Each subject performed between 3 to 4 sessions on separate days, each session included 4 to 9 experimental runs. The total number of trials varies per subject: approximately 320 trials for subject O3 and 1080 trials each for subjects S4 and X11. The core objective is a binary classification task to distinguish between right-hand and left-hand MI.

3.3.2. Experimental protocol

The trial structure and timing of the MI task are illustrated in Figure 3.2. The experiment followed a two-class MI paradigm, where subjects were instructed to imagine movements of either the right hand or the left hand. The total trial duration was 8 seconds for subject O3 and 7 seconds for subjects S4 and X11.

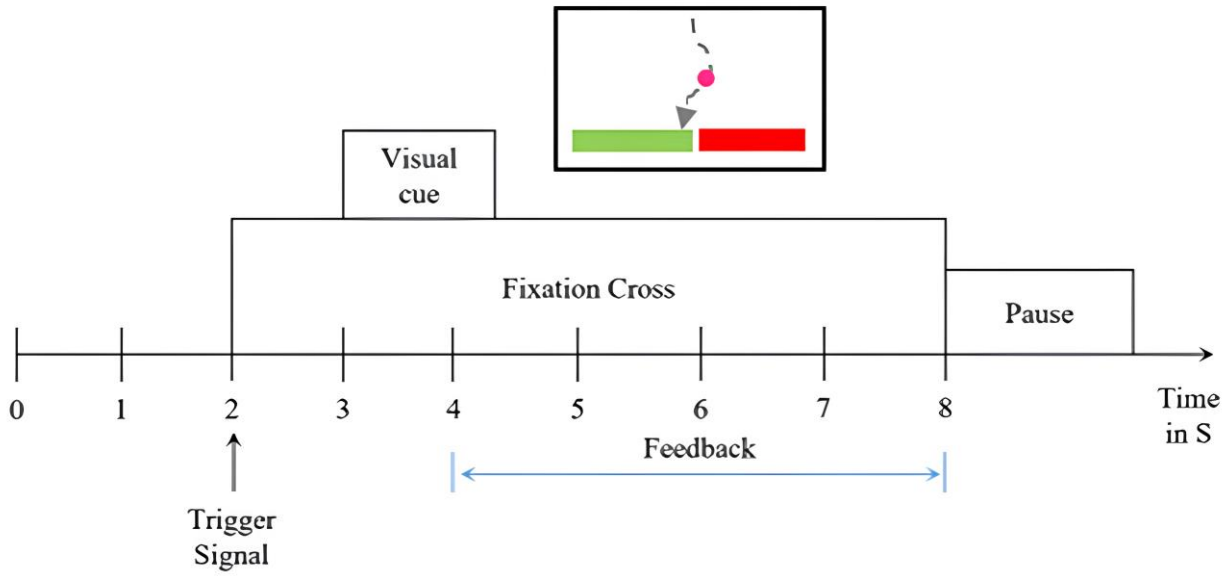

Figure 3.2. Timing scheme of the MI paradigm.

Each trial began with a trigger signal at t = 0 s, marking the beginning of the trial sequence, followed by a ready signal in the form of a fixation cross that showed up on the screen at t = 2 s, helping the subject to concentrate and maintain attention until the end of the trial. An auditory beep sounded at t=3s simultaneously with the appearance of a visual cue (lasting 1.25 seconds) that instructed the subject to perform the designated MI task. The cue indicated whether the subject should imagine moving the right or the left hand. Following the cue, the MI period began. For subject O3, the imagery and feedback phase lasted 4 seconds (4–8 s), whereas for subjects S4 and X11, the duration was 3 seconds (4–7 s). This feedback was delivered through one of two engaging paradigms designed to maintain subject motivation: a virtual reality environment for subject O3 and a "basket" paradigm for subjects S4 and X11. Finally, each trial concluded with a short rest interval, allowing subjects to relax before the next trial began.

3.3.3. Recording setup and preprocessing

EEG signals were recorded using a bipolar amplifier from g.tec, with two electrodes placed over the sensorimotor cortex at locations C3 and C4 according to the international 10–20 system (see Figure 3.3). This setup was intentionally chosen because these two sites capture the strongest oscillatory patterns linked with left versus right-hand MI, reflecting contralateral activation of the motor cortex. The EEG was sampled at 125 Hz, providing adequate temporal resolution for analyzing MI–related rhythms. A band-pass filter between 0.5 Hz and 30 Hz was employed to eliminate slow drifts and high-frequency noise, ensuring that only the physiologically relevant components were preserved. Additionally, a 50 Hz notch filter was utilized to remove the power line interference.

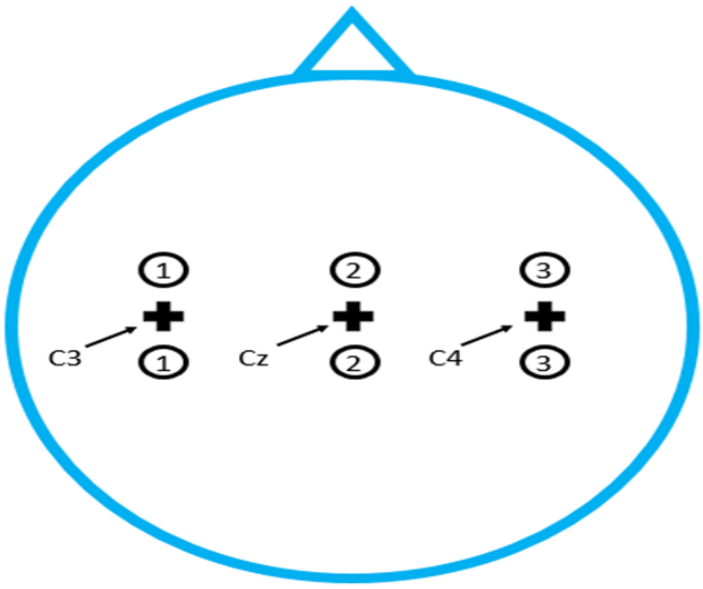

Figure 3.3. The placement of electrode positions based on dataset 1.

All data were saved in the GDF (General Data Format for Biomedical Signals), a standard format that ensures consistent metadata annotation and interoperability with analysis software. The dataset includes full trial annotation: the beginning of each trial is stored in the HDR.TRIG variable, and the class labels are stored in HDR.Classlabel, with values '1' and '2' representing right and left-hand imagery, respectively. It is important to recognize that the data may contain NaN values, which indicate either breaks between consecutive experimental runs or saturation of the analog-to-digital converter.

3.4. Dataset 2: BCI Competition II Dataset III

3.4.1. Source and description

This work also employs the BCI Competition II Dataset III, a canonical dataset provided by the Institute for Biomedical Engineering at Graz University of Technology. This dataset was contributed to the 2nd International BCI Competition to foster the development of continuous feedback decoding methods. It contains recordings from a single, healthy, 25-year-old female subject during a closed-loop BCI feedback session. The subject was seated in a comfortable, armrests equipped chair to minimize movement and muscle artifacts, thereby ensuring higher quality EEG recordings throughout the session.

The experiment comprises 7 runs conducted on a single day, with breaks in between. Each run consists of 40 trials, totaling 280 trials, each lasting 9 seconds. The objective is a binary classification task to distinguish between right and left hand MI.

3.4.2. Experimental protocol

The trial structure is depicted in Figure 3.4. Each trial lasted 9 seconds and began with a 2-second quiet period, during which the subject was at rest. At t = 2 s, an auditory stimulus signaled the start of the trial, a trigger signal was generated, and a fixation cross ("+") showed up on the screen for 1s to help the subject focus.

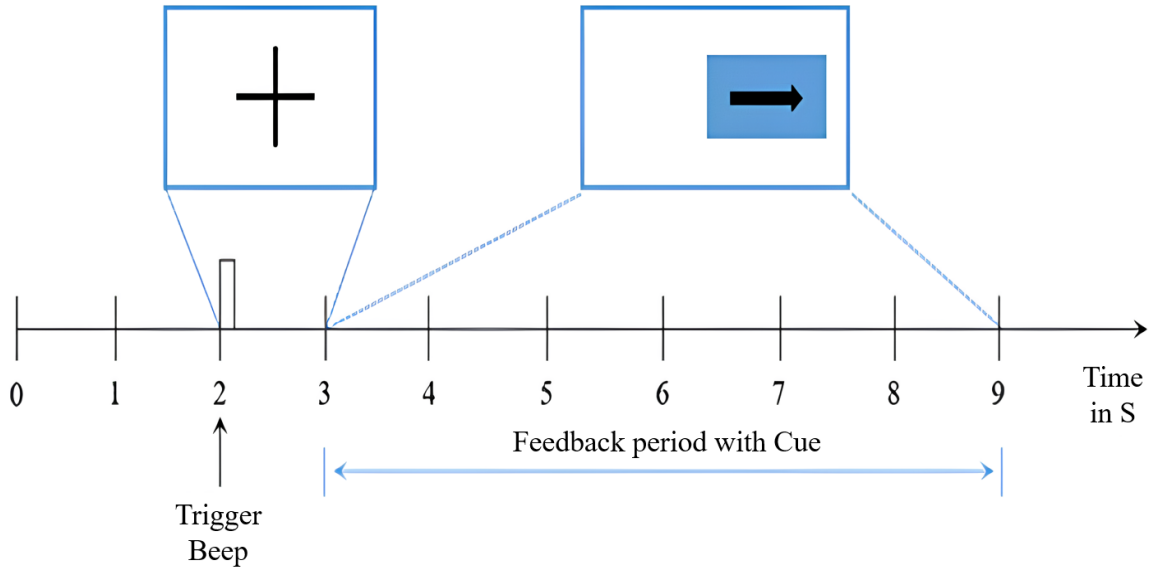

Figure 3.4. Timing scheme of the MI paradigm.

At t = 3 s, a visual cue was presented in the form of a right or left pointing arrow. The direction of the arrow was randomly arranged across trials to avoid prediction or habituation effects. Simultaneously, the subject was instructed to execute the corresponding MI task to control a feedback bar. The feedback period lasted from 3 to 9 seconds and was generated in real time using adaptive autoregressive (AAR) parameters extracted from the ongoing EEG signals. This design provided continuous visual feedback, enabling subjects to adapt their strategies during the session and making the task closer to real-world BCI applications.

3.4.3. Recording setup and preprocessing

The data were recorded by a g.tec amplifier with Ag/AgCl electrodes. The setup included three bipolar EEG channels, with electrodes placed over the sensorimotor cortex at positions C3, Cz, and C4. Each bipolar channel was arranged so that the anterior electrode served as the positive input ("+") and the posterior electrode as the negative input ("–"), which enhances sensitivity to localized cortical activity, see Figure 3.3. The EEG signals were digitized at a 128 Hz sampling rate and filtered with a band-pass filter of 0.5–30 Hz.

The dataset is provided in a MATLAB file format, which facilitates convenient analysis and easy integration into standard BCI processing pipelines. The data structure is organized into separate files for training and testing, ensuring a clear separation between model development and evaluation.

The training set consists of two files. The variable x_train contains EEG recordings from the three channels (C3, Cz, and C4) across 140 training trials, with each trial lasting 9 seconds. The

corresponding ground truth labels are stored in y_train, where the value 1 denotes right-hand MI and 2 denotes left-hand MI.

The testing set also consists of two files. The variable x_test contains EEG recordings from the same three channels for 140 testing trials. The corresponding labels are stored in y_test.

3.5. Dataset 3: BCI Competition IV Dataset 2b

3.5.1. Source and description

The third dataset analyzed in this work is the BCI Competition IV Dataset 2b, released by the BCI Laboratory at Graz University of Technology as part of the 2008 BCI Competition. It was specifically designed to evaluate subject-specific and adaptive MI decoders under realistic closed-loop feedback conditions. The dataset comprises EEG recordings from nine healthy (labeled B01-B09), right-handed subjects, all of whom possessed normal or corrected-to-normal vision, and were compensated for their participation. During the recordings, subjects were seated comfortably in armrest equiped chair and presented with visual cues on a screen positioned approximately one meter away from the participant's eye level.

Each participant completed five recording sessions. The initial two sessions, conducted on separate days over a two-week period, comprised screening runs without feedback, each including six runs of ten trials for two classes of MI. The remaining three sessions introduced real-time visual feedback using a smiley-face paradigm, with each session containing four runs of twenty trials per MI class. In total, each subject contributed 120 trials per class for training and 160 trials for evaluation, covering left- and right-hand imagery tasks.

3.5.2. Experimental protocol

The experiment followed a cue-based MI paradigm with both screening and feedback sessions. Each trial was carefully structured to synchronize visual and auditory cues with the onset of MI, thereby ensuring consistent timing across subjects and sessions. The overall trial structure for both screening and feedback sessions is shown in Figure 3.5.

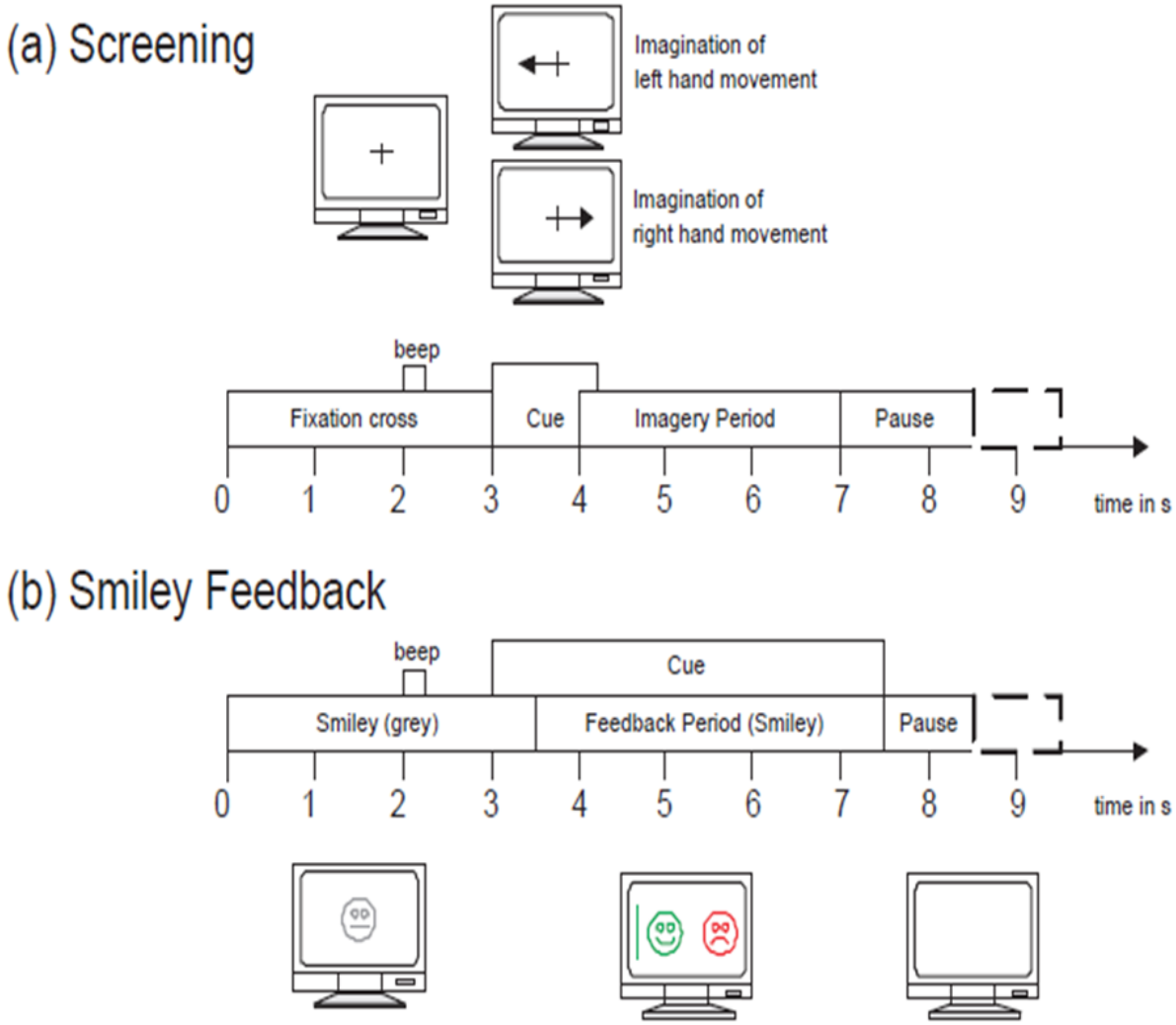

Figure 3.5. Timing scheme of the MI paradigm **[96]**. (a) Screening sessions without feedback. (b) Feedback sessions with the smiley paradigm.

During the screening sessions, every trial began with a fixation cross that showed up for two seconds in the middle of the screen to guide attention and establish a baseline. At t = 2 s, an auditory warning tone signaled the imminent task, and at t = 3 s, a visual cue was displayed for 1.25 seconds in the form of a left- or right-pointing arrow, presented in randomized order. The subject was then instructed to execute the corresponding MI task (left or right hand) for four seconds, then rested for a period of 1.5 seconds before the next trial began.

In the feedback sessions, the same trial structure was maintained (see Figure 3.5.b), but the MI phase included real-time visual feedback. Instead of simply imagining the movement after a fixation cross, the cue was replaced by a grey smiley face, which indicated the onset of the task and the direction of the required MI (right or left hand). Throughout the feedback phase, the smiley face turned green upon successful directional control, but turned red when the classification was incorrect. Subjects were

explicitly asked to maintain the smiley on the target side for as long as possible, which encouraged them to sustain the MI throughout the feedback phase.

3.5.3. Recording setup and preprocessing

The data were recorded by a g.tec amplifier with three bipolar EEG channels placed over the sensorimotor cortex at electrode positions C3, Cz, and C4, with electrode Fz serving as ground. The data provided is already down-sampled to 250 Hz with a dynamic range of ±100 μV during screening sessions and ±50 μV during feedback sessions, reflecting different sensitivity settings for offline data collection versus real-time feedback. Online preprocessing included a band-pass filter from 0.5–100 Hz, and a 50 Hz notch filter to suppress power line interference. Alongside the EEG channels, three monopolar EOG electrodes were placed to record eye movements. These auxiliary channels were intended for artifact detection and removal, but were not used in classification.

The dataset is distributed in the GDF format, with different files for each subject and session. Each file contains six channels in total: three EEG and three EOG. The training data consist of the initial three sessions (two screening sessions and one feedback session) and include class labels for each trial. Event markers specify trial onset, cue presentation, and class type (right-hand = 1, left-hand = 2). The evaluation data consist of the last two feedback sessions, which were structured to evaluate system performance during sessions with real-time feedback.

3.6. Dataset 4: OpenBMI dataset

3.6.1. Source and description

The fourth dataset employed in this study is the OpenBMI dataset, a large-scale public benchmark selected to broaden the scope of the investigation. It includes multiple EEG paradigms, but for the purposes of this thesis, only the MI component was analyzed.

The dataset comprises EEG recordings from 54 healthy participants (labeled S01-S54, ages 24–35; 25 female), 38 of whom were BCI inexperienced subjects, while the remaining 16 were previously experienced with BCI paradigms. None reported any neurological, psychiatric, or other relevant medical conditions. Every subject finished two sessions on separate days; each session consisted of a training phase and a testing phase, each comprising 100 trials balanced between right and left-hand MI tasks. This design provides a substantial amount of data suitable for both subject-specific and cross-subject analyses.

During recordings, subjects were seated comfortably in armrest equiped chair; 60 ± 5 cm from a 21-inch LCD monitor (refresh rate: 60 Hz; resolution: 1600 × 1200; approximate visual angles: 37.7° horizontal, 28.1° vertical). They were asked to remain relaxed and to limit ocular and muscle

movements to reduce artifacts. The design of this dataset, with its large participant and multiple sessions, provides a robust foundation for developing and evaluating generalized classification models for left and right-hand MI tasks.

3.6.2. Experimental protocol

Before the experiments, all subjects were provided with written instructions outlining a detailed explanation of the tasks, the experimental schedule, and necessary cautions. To systematically assess participant readiness and experience, two questionnaires were administered: one before the session (Questionnaire I [97]) and one after each experimental run (Questionnaire II [97]). Following confirmation of their understanding of the instructions, participants filled out Questionnaire I, which assessed their physical and mental health on the day of the experiment and gathered information about themselves (e.g., age, gender). It also recorded the participant's physical and mental health before the session began and provided a checklist to find external factors that could affect BCI performance.

Before commencing the main MI trials, baseline EEG recordings were collected for five types of noise-related activity typically associated with artifacts: (1) eye blinking, (2) repetitive horizontal eye movements, (3) repetitive vertical eye movements, (4) teeth clenching, and (5) flexing of both arms. These reference signals were used to facilitate artifact detection and thereby enhance the reliability of subsequent analyses.

Each trial started with a 3-second fixation cross presented at the middle of the screen to prepare participants for the task. This was followed by a visual cue in the form of a right- or left-pointing arrow, instructing the subject to perform kinesthetic imagery of grasping with the indicated hand. The imagery phase lasted 4 seconds, during which subjects were asked to mentally simulate the movement without any overt muscle activity. Following imagery, a blank screen was displayed for 6 ± 1.5 seconds, serving as a rest period before the next trial began.

The experiment comprised two phases: training and testing, with each phase comprising 100 trials equally balanced between left- and right-hand imagery. In the online test phase, real-time visual feedback was provided: the fixation cross initially showed up in the middle of the screen and then shifted left or right based on the classifier’s interpretation of the EEG activity (see Figure 3.6). This closed-loop feedback encouraged participants to adjust and sustain their MI strategies to optimize performance. After every run, subjects completed Questionnaire II to capture their current condition and to provide feedback on the preceding experimental session.

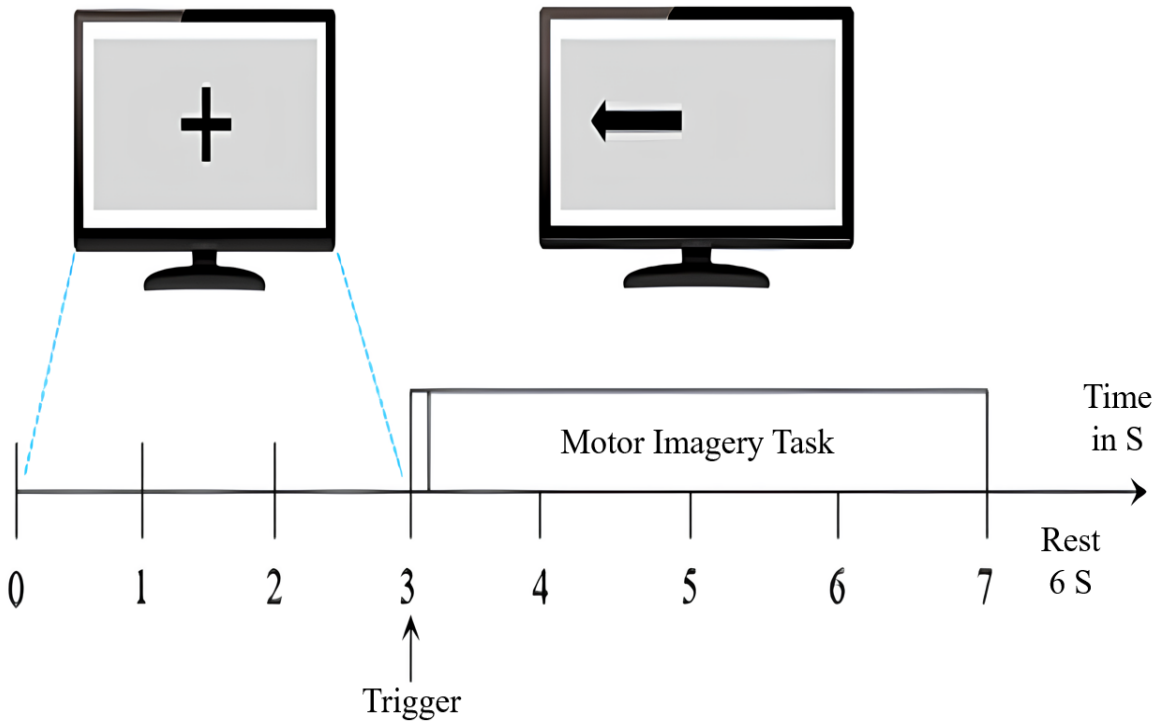

Figure 3.6. Timing scheme of the MI paradigm.

3.6.3. Recording setup and preprocessing

Data were recorded from 62 Ag/AgCl scalp electrodes arranged according to the international 10–20 system, providing full-head coverage of cortical regions relevant for MI tasks. The signals were amplified by a BrainAmp amplifier, sampled at 1,000 Hz, and filtered with a 50 Hz notch filter to remove power line interference. All electrodes were referenced to the nasion and grounded at AFz, with impedances carefully maintained below 10 kΩ during the experiment to ensure optimal signal quality.

To monitor for unintended muscle activity that could contaminate the EEG signals, electromyography (EMG) was simultaneously recorded from the flexor digitorum profundus muscles of both arms, using the olecranon as the reference site. The complete electrode layout and labeling scheme are illustrated in Figure 3.7; the left panel shows the numerical channel indexing for the 62 EEG and 4 EMG electrodes, while the right panel illustrates their corresponding anatomical locations according to the 10–20 system.

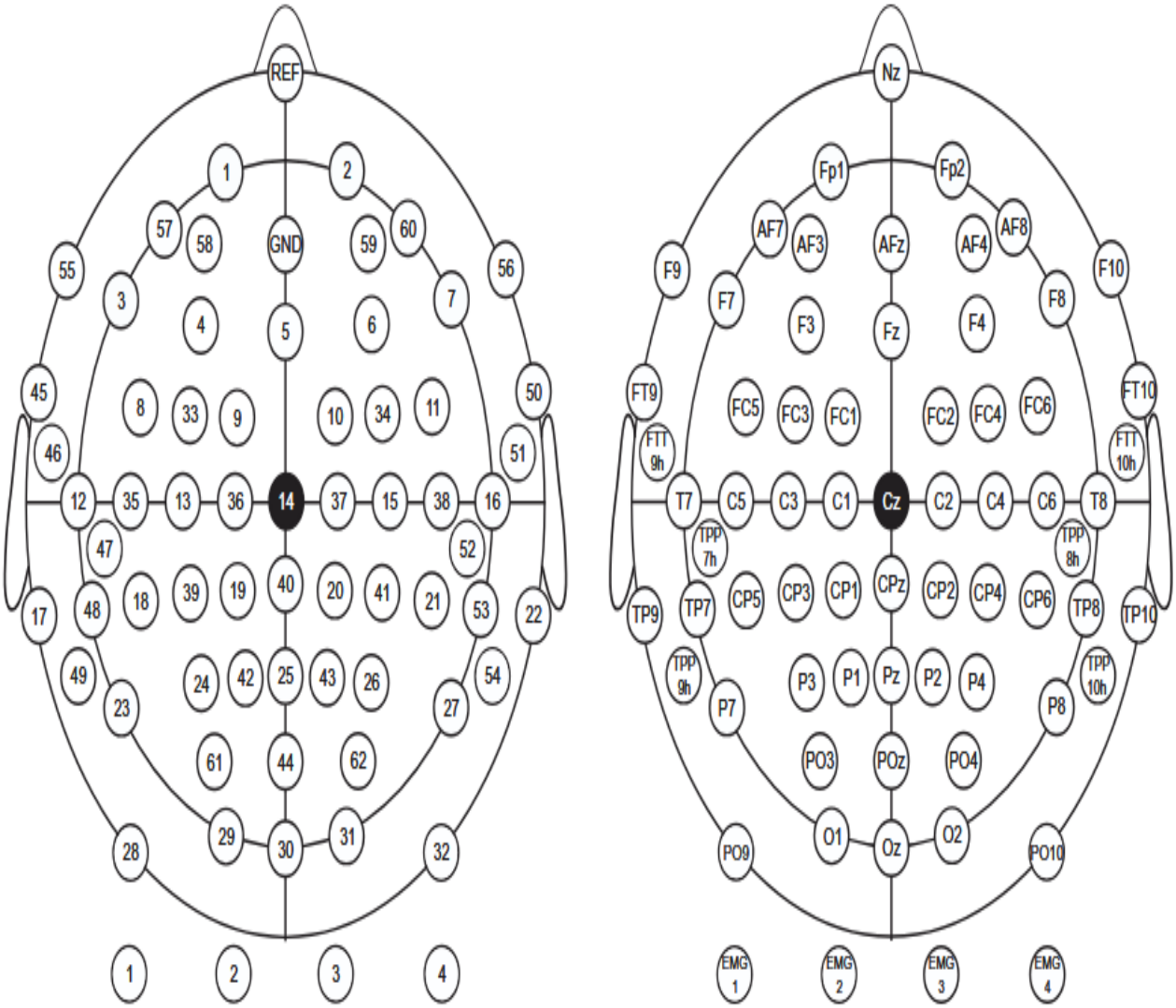

Figure 3.7. EEG/EMG Electrode Layout According to the 10–20 System **[97]**.

The dataset is provided in a MATLAB-compatible format. Each file contains the continuous EEG/EMG recordings, event markers indicating trial onset and cue presentation, and the accompanying questionnaire data, all structured to facilitate straightforward integration into standard BCI pipelines.

3.7. Dataset 5: BCI Competition IV Dataset 2a

3.7.1. Source and description

The fifth dataset included in this study is the BCI Competition IV, Dataset 2a, made publicly available by Graz University of Technology within the framework of the BCI Competition IV, 2008 edition. This benchmark dataset is widely regarded as one of the most frequently utilized in MI research,

particularly for four-class classification tasks. The recordings were conducted under controlled laboratory conditions, with subjects sitting comfortably in an armchair positioned facing a display screen on which visual cues were presented.

EEG data were collected from nine subjects (labeled S01-S09), each completing two sessions recorded on separate days. Each session comprised six runs, and every run included 48 trials (12 trials per class). This design resulted in 288 trials/session and 576 trials/subject. The MI paradigm included four different classes: right-hand, left-hand, tongue, and both feet imagery.

At the beginning of each session, a 5-minute EOG calibration block was performed to facilitate subsequent ocular artifact correction. The block included 2 minutes of eyes open watching a fixation cross on the display, 1 minute of eyes closed, and 1 minute of guided eye movements. This was followed by the main experiment, comprising sequential MI runs. The overall timing structure of a session is shown in Figure 3.8. For subject A04T, only the eye movement was available due to technical issues.

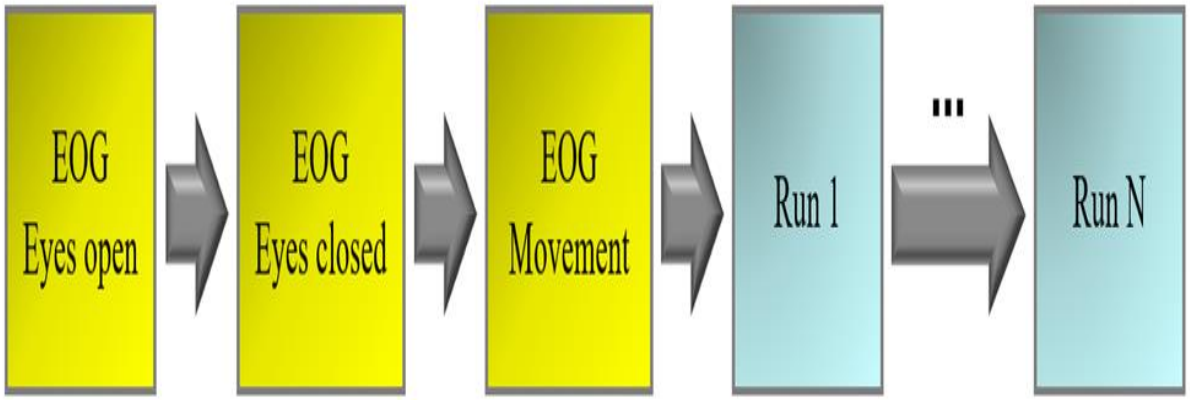

Figure 3.8. Timing preparation for a single session.

3.7.2. Experimental protocol

The experiment employed a cue-based MI paradigm without feedback. The structure of an individual trial is depicted in Figure 3.9.

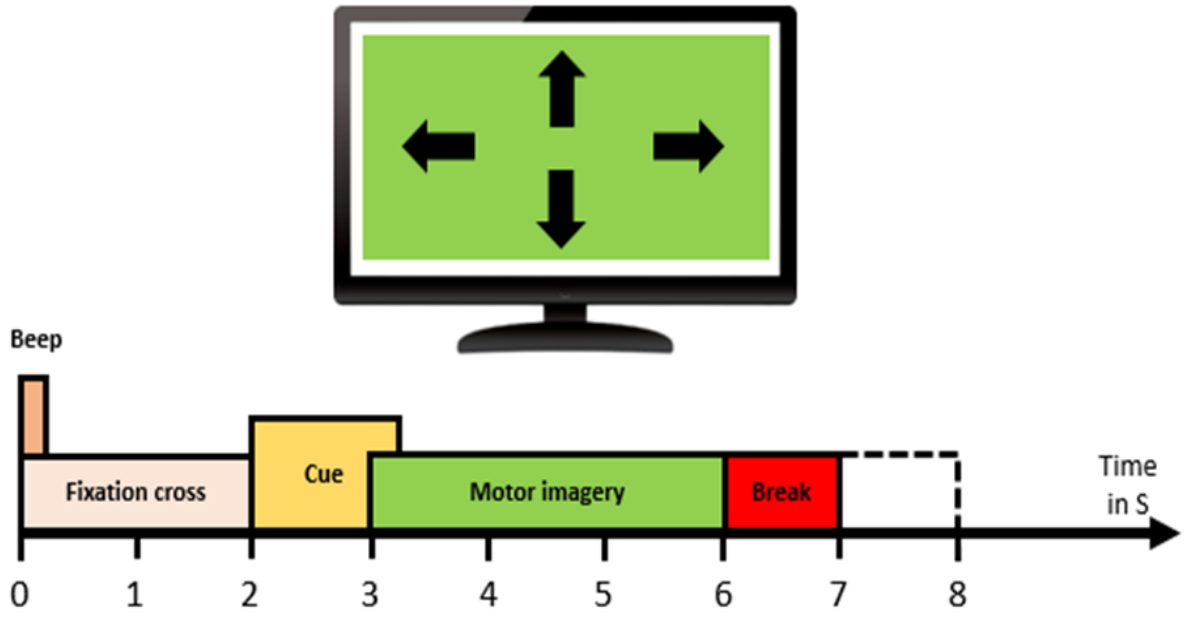

Figure 3.9. Paradigm for Four-Class Kinesthetic MI.

The experiment employed a cue-based MI paradigm without feedback. Each trial began at t = 0 s with the presentation of a fixation cross centrally on a black screen, accompanied by a short auditory warning tone. At t = 2 s, a visual cue was presented in the form of a directional arrow (pointing left, right, downward, or upward), denoting to left/right-hand, feet, or tongue imagery, respectively. The cue remained for 1.25 seconds on the displayed screen, during which subjects initiated the designated MI task.

Subjects were instructed to perform and sustain the kinesthetic MI until the fixation cross vanished at t = 6 s. Each trial concluded with a short rest interval, displaying a blank screen before the next trial commencement.

3.7.3. Recording setup and preprocessing

The data were recorded by a g.tec amplifier from 22 Ag/AgCl scalp electrodes positioned according to the 10–20 system. The amplifier sensitivity was set to 100 μV. The chosen electrodes, which provided comprehensive coverage of motor-related cortical areas, were distributed across the frontal, central, parietal, and occipital regions. The specific channels included: Fz, FC3, FC1, FCz, FC2, FC4, C5, C3, C1, Cz, C2, C4, C6, CP3, CP1, CPz, CP2, CP4, P1, Pz, P2, and POz. An electrode affixed to the left mastoid was used as the reference, and the ground electrode was positioned at Fpz. To monitor ocular artifacts, three monopolar EOG channels were also recorded. The complete electrode montage, showing all 22 EEG channels and the three EOG sensors, is demonstrated in Figure 3.10.

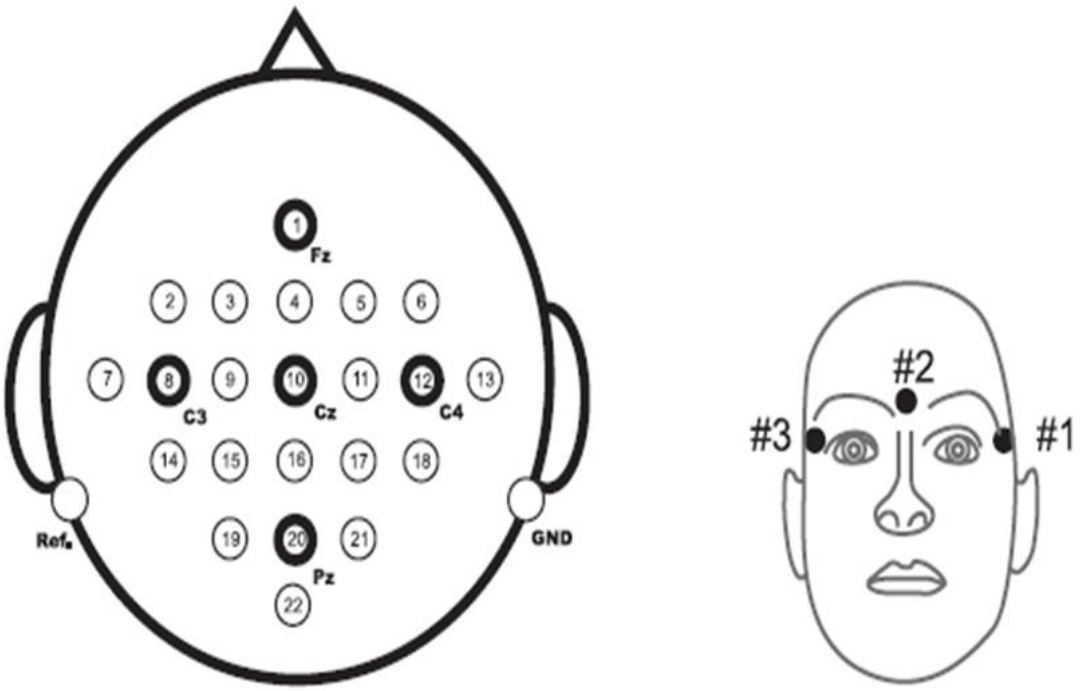

Figure 3.10. Locations of EEG and EOG electrodes **[98]**.

The data were sampled at 250 Hz and passed through a 0.5–100 Hz band-pass filter, in addition to a 50 Hz notch filter to suppress line noise. The complete dataset is provided in GDF files, with each file containing the continuous EEG/EOG recordings alongside event markers for trial onset, cue presentation, and class labels.

3.8. Summary of datasets

To conclude this chapter, Table 3.1 offers a comparative summary of the five EEG MI datasets used in this study. This comparison shows the data differences and makes it easier to see the strengths and limitations of each dataset.

The selected benchmarks provide extensive coverage of MI-BCI research scenarios. They are complementary, differing in the number of participants, recording sessions, and experimental paradigms. Datasets 1–3 have a smaller number of subjects but provide well-controlled paradigms ideal for testing adaptive decoding and feedback. In contrast, Dataset 4 (OpenBMI) is large-scale, with data from 54 subjects across multiple sessions, making it suitable for both subject-specific and cross-subject analysis. Dataset 5 (BCI Competition IV 2a) introduces a more challenging four-class paradigm that is more representative of real-world BCI applications.

Table 3.1. Overview of the EEG MI datasets used in this study.

Dataset	No. of subject	Electrodes	No. of classes	No. of trials	Sampling rate	Objective
Dataset 1	3	2 (C3, C4)	2 (Left vs. Right hand)	2480	125 Hz	Binary classification
Dataset 2	1	3 (C3, Cz, C4)	2 (Left vs. Right hand)	280	128 Hz	Binary classification
Dataset 3	9	3 (C3, Cz, C4) + 3 EOG	2 (Left vs. Right hand)	6520	250 Hz	Binary classification
Dataset 4	54	62 EEG + 2 EMG	2 (Left vs. Right hand)	10800	1000 Hz	Binary classification
Dataset 5	9	22 EEG + 3 EOG	4 (Left hand, Right hand, Feet, Tongue)	5184	250 Hz	Multi-Class classification

The technical specifications also vary significantly. The datasets were recorded with channel counts ranging from 2 to 62 and from 125 Hz to 1000 Hz sampling rates, reflecting different balances between data resolution and processing requirements. The experimental designs differ as well; some datasets (2, 3, and 4) include real-time feedback, while others (1 and 5) are open-loop. Collectively, this diverse foundation allows for a rigorous evaluation of feature extraction methods, classification strategies, and generalization performance in MI-based BCI systems.

3.9. Conclusion

This chapter provided full details of the datasets utilized in this research, beginning with an overview of the general characteristics of MI EEG datasets and concluding with a comparative summary. Each dataset was shown to possess distinct properties in terms of subject population, number of classes, electrode configurations, and recording protocols. While some datasets were recorded under controlled conditions with limited variability, others introduced more complex paradigms with larger subject pools or additional classes, thereby enhancing their realism and applicability to practical BCI scenarios.

By combining datasets of different scales and complexities, this work strategically leverages the reliability of smaller, well-established benchmarks together with the broader generalizability of large-scale collections. The comparative summary in Table 3.1 highlights the diversity of paradigms,

sampling rates, and feedback conditions across the selected datasets. This diversity is crucial for ensuring that the analyses and models developed in the subsequent chapter are thoroughly evaluated under a wide spectrum of experimental conditions.

In conclusion, this chapter provided a full description of the EEG MI datasets used throughout this research, emphasizing their paradigms, recording setups, and inherent variability. The insights gained from this analysis directly guide the methodological decisions for preprocessing, feature extraction, and classification, detailed in the next chapter. Building on this groundwork, Chapter 4 describes the full methodological framework developed to assess MI-BCI performance across different recording conditions and subject populations.

Chapter 04

Results and Contributions

Part I

AN ADAPTIVE FEATURE ENGINEERING FRAMEWORK WITH WFF FOR MULTI-DATASET MI-BCI CLASSIFICATION

4.1. introduction

Achieving reliable accuracy in EEG-based MI-BCIs remains a major challenge. Extracting meaningful features from these complex, non-stationary EEG patterns is crucial, but traditional methods often struggle due to significant individual differences and the inherent complexity of brain signals during imagined movements. Just like fingerprints are unique to each person, the brain creates distinct MI 'signatures' that differ across individuals in timing, length, and strength of activation. This personal neural variability is both an obstacle and a golden opportunity for tailoring MI-BCI systems to each user.

This study tackles that challenge with a full classification framework tested across four separate EEG datasets from 25 healthy participants over multiple sessions. Our study focuses on the fundamental binary task: left-hand vs. right-hand MI. For all analyses we exclusively utilized signals from C3 and C4 electrodes which capture contralateral sensorimotor activations critical for hand movement discrimination.

Even with this simplified electrode configuration, achieving solid performance isn't easy due to inter-session variability, individual neurophysiological differences, and the need for precise temporal alignment of MI execution.

The proposed methodology is built upon a novel 84-feature spatial-ratio set that explicitly encodes interhemispheric relationships. This set undergoes sequential refinement including optimization of the subject-specific processing duration, GA-based feature selection, and application of a weight feature function (WFF). These stages were implemented to maximize the discriminative power of the feature set, thereby improving CA and adapting the system to individual neurophysiology.

4.2. Data preprocessing pipeline

Data pre-processing constitutes a critical preparatory stage in the MI classification pipeline, serving to enhance signal quality, mitigate artifacts, and isolate task-relevant neurophysiological activity for subsequent analysis. The methodology applied in this work is detailed as follows.

4.2.1. Handling of incomplete trials

An initial inspection revealed the presence of missing data values, denoted as 'NaN' (Not a Number), within the recordings of four subjects: O3, S4, X11, and B06. The occurrence of 'NaN' values typically indicates data acquisition failures or artifacts that corrupt entire trial segments, such as signal saturation, amplifier blocking, or transient disconnection. To illustrate the nature of these invalid trials, Figure 4.1 shows the raw signals from channels C3 and C4 for a representative invalid trial (Subject O3, Trial 118, Class 1). The plot demonstrates a prolonged, high-amplitude artifact that makes a significant portion of the trial unusable, which the recording system has logged as 'NaN' values.

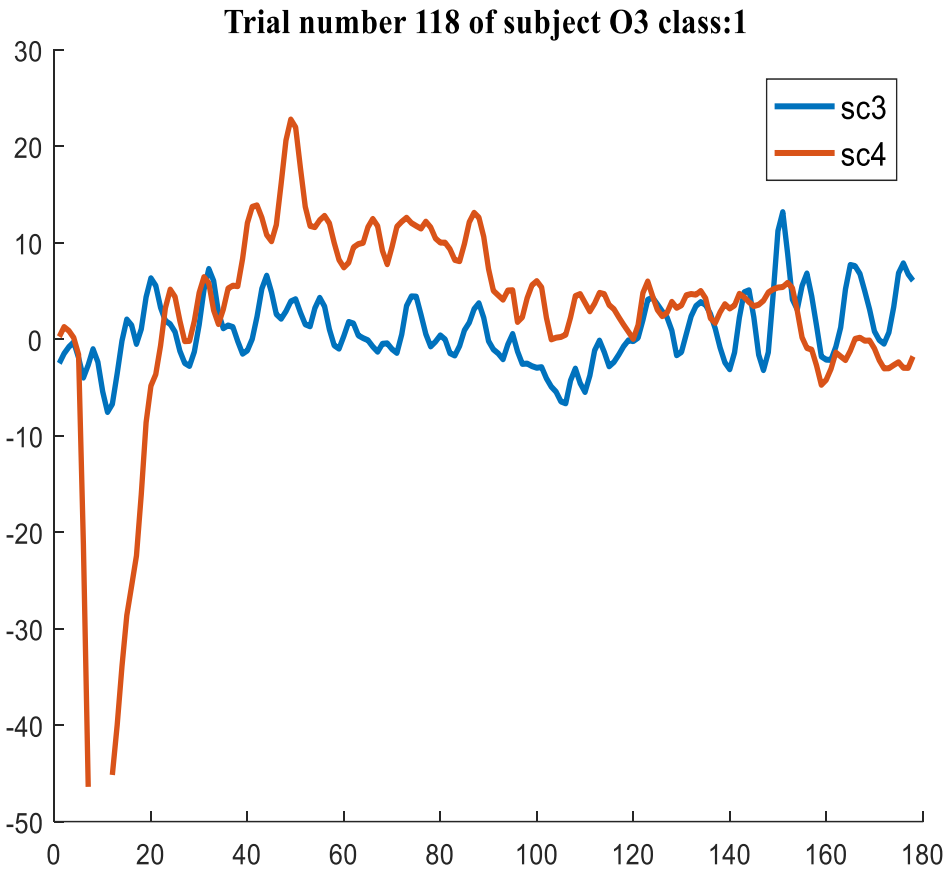

Figure 4.1. Example of a corrupted trial leading to NaN values.

To maintain data integrity and avoid analytical distortions, all individual trials containing any missing samples were systematically identified and removed from the dataset. This curation resulted in the following validated trial counts per subject: 160 trials for O3, 536 for S4, 539 for X11, and 318 for B06. Consequently, all subsequent analyses were performed on complete, contiguous data segments free from such acquisition errors.

4.2.2. Spectral filtering for feature enhancement

The spectral filtering stage was designed to isolate the frequency bands most associated with sensorimotor rhythms modulated during MI and thereby enhance the chances of discovering distinctive, class-discriminative features. To this end, two separate second-order Butterworth band-pass filters were applied to EEG signals recorded from channels C3 and C4. This filter type was selected for its maximally flat passband response. The chosen filter bands were:

Band 1 (B1): 7–24 Hz, covers the mu (8–13 Hz) and low-beta (13–24 Hz) rhythms linked to motor execution and imagery.

Band 2 (B2): 25–29 Hz, targeting the high-beta activity often involved in cortical activation.

Applying these two filters to the two channels yielded another four distinct, band-limited signals per trial, namely as SC_{31} (C3, B1), SC_{41} (C4, B1), SC_{32} (C3, B2), and SC_{42} (C4, B2).

4.3. Proposed feature set

The success of any MI BCI system comes down to turning raw, high-dimensional EEG signals into a clean set of features that clearly distinguish imagined movements. This section outlines the methodological framework for feature extraction, which forms the foundation of the proposed system. The primary objective is to construct a multi-perspective feature vector that comprehensively characterizes the brain patterns behind MI. To this end, a diverse suite of features was intentionally engineered, extracted from the time, frequency, and time-frequency domains. This variety lets us measure different aspects like signal shape, energy distribution, complexity, and spectral-temporal dynamics, thereby capturing a more complete representation of the MI-EEG response. The subsections below break down the main feature types pulled from each preprocessed EEG channel.

4.3.1. Wavelet Transform (WT)

The WT is a powerful time-frequency analysis method that decomposes a signal into components localized in both time and frequency. Unlike the classical Fourier Transform, which only provides global frequency information, WT can capture transient or non-stationary events, making it particularly suitable for EEG signals, which exhibit rapid and dynamic changes during MI tasks.
WT is commonly divided into two categories: CWT and DWT.

4.3.1.1. Continuous Wavelet Transform (CWT):

The CWT analyzes the signal at multiple scales by convolving it with a wavelet function that is continuously stretched and shifted.

The CWT Equation:

$$C_x(a,b) = \frac{1}{a}\int_{-\infty}^{\infty} x(t)\Psi\left(\frac{t-b}{a}\right)dt \tag{4.1}$$

$$\Psi(t) = \frac{1}{\sqrt{\pi f_b}} e^{j2\pi f_c t} e^{-t^2/f_b}$$

In this equation, the parameter a controls the scale of the wavelet, while b specifies its temporal position. The mother wavelet Ψ is the original wavelet shape from which all scaled and shifted wavelets are generated to analyze the signal in the time-frequency domain. For the Morlet wavelet, f_b and f_c denote the bandwidth and center frequency parameters, respectively.

The CWT was performed using the Morlet wavelet (morl), which provides a good balance between time and frequency localization. This approach provides a fine-grained time-frequency representation, enabling the detection of short-lived oscillatory patterns in the beta bands during MI.

4.3.1.2. Discrete Wavelet Transform (DWT):

The DWT decomposes the signal into a hierarchical set of frequency sub-bands using discrete scaling and shifting. At each level, DWT produces approximation and detail coefficients, which can be used to extract features such as energy, entropy, or statistical moments.

The DWT employs two filters a low-pass filter and a high-pass filter to decompose the signal into different resolution levels. The low-pass filter produces the approximation coefficients (A_1), while the high-pass filter yields the detail coefficients (D_1). The resulting approximation component is then recursively decomposed into further lower-resolution sub-bands, enabling a hierarchical multilevel representation of the signal. Figure 4.2 shows the step-by-step DWT decomposition of the signal x[n], illustrating how it is progressively broken down across three levels.

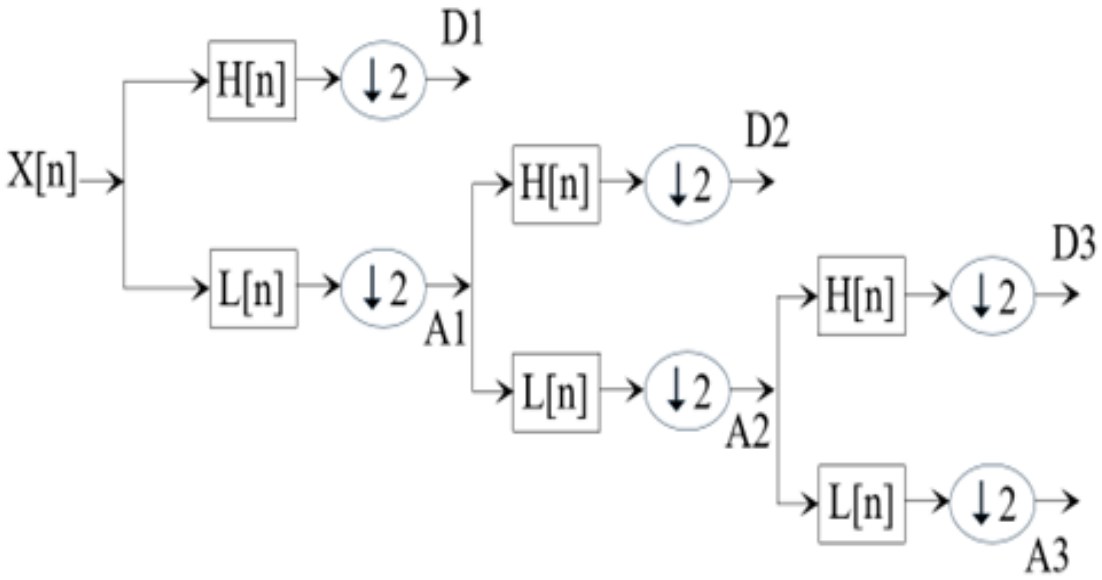

Figure 4.2. DWT decomposition of the signal up to the third level.

Mathematically, the first level of DWT decomposition is defined as follows:

$$\boldsymbol{D[k]} = \sum_{\boldsymbol{n}} \boldsymbol{x[n].H[2k-n]} \tag{4.2}$$

$$\boldsymbol{A[k]} = \sum_{\boldsymbol{n}} \boldsymbol{X[n].L[2k-n]} \tag{4.3}$$

Here, x[n] denotes the input signal, while A[k] and D[k] correspond to the approximation and detail coefficients, respectively. L[n] and H[n] represent the coefficients of the low-pass and high-pass filters, respectively, and n denotes the signal's sampling point.

In this work, a three-level decomposition was implemented using the Biorthogonal 3.3 (bior3.3) wavelet. This biorthogonal family was selected for its linear phase property, which is advantageous for preserving the temporal alignment of event-related spectral perturbations. This decomposition produces approximation and detail coefficients at each of the three levels: A1, D1, A2, D2, A3, and D3. Features were subsequently extracted from all of these coefficient sets to capture the signal's multi-resolution characteristics.

4.3.2. Power Spectral Density (PSD)

The PSD quantifies the distribution of signal power across different frequencies. For an EEG signal x(n) of length N sampled at frequency f_s, the normalized PSD is computed as:

$$\boldsymbol{P_x(f) = \frac{1}{N f_s} |fft(x)|^2} \tag{4.4}$$

where f denotes the frequency, and fft refers to the Fast Fourier Transform.

4.3.3. Variance (var)

var is a statistical measure that quantifies the spread or dispersion of a signal's amplitude values around its mean. In the context of EEG signals, variance reflects how much the signal fluctuates over time, capturing the overall level of activity or power in a given time window and it is defined as:

$$\boldsymbol{var = \frac{1}{N-1} \sum_{i}^{N} (x_i - \mu)^2} \tag{4.5}$$

In this expression, x refers to the discrete EEG signal under analysis, and N denotes the total number of samples considered within the selected time window for feature extraction.

4.3.4. Kurtosis and Skewness

Kurtosis and skewness are statistical measures that describe the shape of a signal's amplitude distribution.

Skewness quantifies the asymmetry of the signal's distribution around its mean. A positive skewness indicates that the signal has a longer tail on the right side, while a negative skewness indicates a longer tail on the left. In EEG analysis, skewness can highlight imbalances in signal fluctuations, which may differ between MI classes.

Kurtosis measures the "tailedness" or peakedness of the distribution. High kurtosis indicates a signal with sharp peaks and heavy tails, while low kurtosis reflects a flatter distribution. For EEG signals, kurtosis can capture sudden bursts or transient events that are characteristic of neural activity during imagined movements.

Mathematically, for a EEG signal x[n] of length N with mean μ and standard deviation σ:

$$\boldsymbol{Skewness} = \frac{\mathbf{1}}{\boldsymbol{N\sigma^3}} \sum_{\boldsymbol{i=1}}^{\boldsymbol{N}} (\boldsymbol{x_i} - \boldsymbol{\mu})^{\mathbf{3}} \tag{4.6}$$

$$\boldsymbol{kurtosis} = \frac{\mathbf{1}}{\boldsymbol{N\sigma^4}} \sum_{\boldsymbol{i=1}}^{\boldsymbol{N}} (\boldsymbol{x_i} - \boldsymbol{\mu})^{\mathbf{4}} \tag{4.7}$$

skewness and kurtosis provide complementary information about the distributional characteristics of the signal, helping to distinguish between different imagined movement classes.

4.3.5. Root Mean Square (RMS)

The RMS is a measure of a signal's overall amplitude or power, capturing both positive and negative fluctuations of the waveform. In MI-EEG analysis, it reflects the energy content of the signal and helps identify differences associated with distinct imagined movements, making it an effective feature for discriminating between MI classes. RMS is calculated as:

$$\boldsymbol{RMS} = \sqrt{\frac{\mathbf{1}}{\boldsymbol{N}} \sum_{\boldsymbol{i=1}}^{\boldsymbol{N}} (\boldsymbol{x_i})^{\mathbf{2}}} \tag{4.8}$$

4.3.6. Enhanced Wavelength (EWL) and Enhanced Mean Absolute Value (EMAV)

Originally developed for EMG signal classification [102], we adapt these features to EEG by applying them to wavelet coefficients of MI signals. The features emphasize the middle portion of each epoch where task-related neural activity is most prominent, addressing subject reaction time variability at epoch boundaries.

$$\boldsymbol{EWL} = \sum_{\boldsymbol{i=2}}^{\boldsymbol{N}} |(\boldsymbol{x_i} - \boldsymbol{x_{i-1}})^{\boldsymbol{P}}| \tag{4.9}$$

$$\boldsymbol{EMAV} = \frac{\mathbf{1}}{\boldsymbol{N}} \sum_{\boldsymbol{i=1}}^{\boldsymbol{N}} |(\boldsymbol{x_i})^{\boldsymbol{P}}| \tag{4.10}$$

$$\boldsymbol{P} = \begin{cases} \mathbf{0.80}, & \boldsymbol{if}\ \mathbf{0.3}\boldsymbol{N} \le \boldsymbol{i} \le \mathbf{0.7}\boldsymbol{N} \\ \mathbf{0.50}, & \boldsymbol{otherwise} \end{cases} \tag{4.11}$$

The parameter P highlights the most informative part of the signal: a larger P value (0.80) is used for the 30–70% region because it contains the clearest MI patterns, while samples near the edges receive a lower value (0.50).

4.3.7. Mean Curve Length (MCL)

MCL is a measure of the complexity and variability of a signal's waveform over time. It quantifies the cumulative absolute differences between consecutive samples, reflecting how "rough" or "smooth" the signal is. The MCL is calculated as:

$$\boldsymbol{MCL = \frac{1}{N}\sum_{i=2}^{N} |x_i - x_{i-1}|} \tag{4.12}$$

Where x represents the EEG signal, and N is the length of the signal.

In EEG analysis, higher MCL values indicate greater signal variability, which can correspond to stronger or more complex neural activity.

4.3.8. Mean Energy (ME)

ME quantifies the average power of an EEG signal segment and is computed as:

$$\boldsymbol{ME = mean(x)^2} \tag{4.13}$$

4.3.9. First Difference (FD)

The FD measures the average absolute change between consecutive samples, measuring the signal's short-term variability. It is calculated as:

$$\boldsymbol{FD = \frac{1}{N-1}\sum_{i}^{N-1} |x_{i+1} - x_i|} \tag{4.14}$$

After the pre-processing stage described in Section 4.2, which produces another four band-limited signals SC_{31}, SC_{32}, SC_{41}, and SC_{42}, the next step is the computation of features from these signals. The signal processing methodology and feature extraction pipeline are illustrated in the flowchart provided in Figure 4.3.

To explicitly encode the spatial information crucial for discriminating lateralized MI, the proposed feature set is fundamentally designed around inter-hemispheric relationships. Rather than using absolute feature values from individual channels, features are formulated as ratios that compare either identical or distinct metrics computed from corresponding C3 and C4 derived signals.

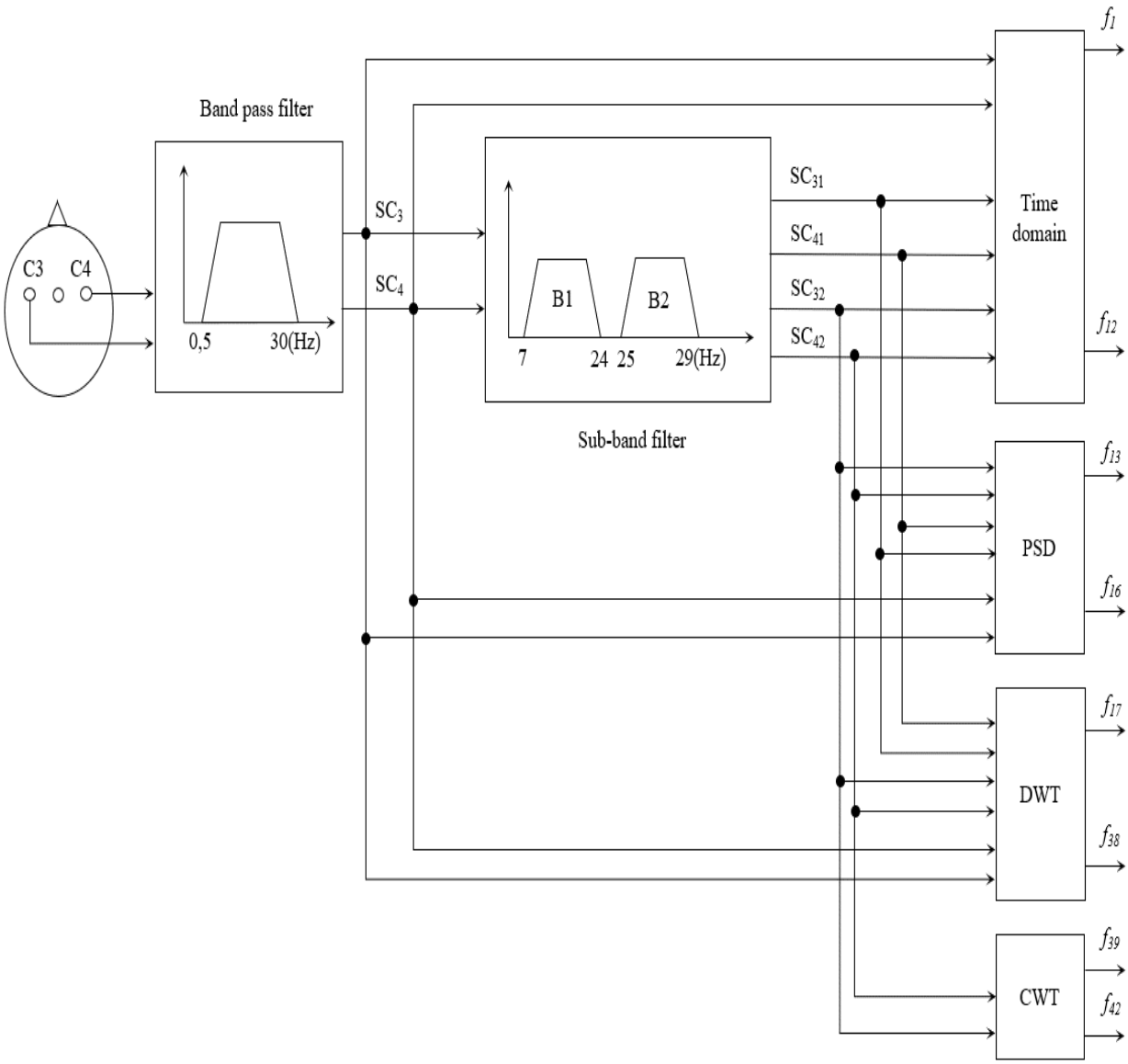

Figure 4.3. Flowchart of the signal processing with feature extraction.

From the six signals comprising the primary channels (SC_3, SC_4) and their filtered derivatives (SC_{31}, SC_{32}, SC_{41}, SC_{42}) this ratio-based approach yields a comprehensive set of 84 spatial features. The first 42 features along with their mathematical definitions are detailed in Table 4.1. The remaining 42 features constitute a complementary symmetric set, mathematically defined as the inverses of the first 42 features. This design ensures a balanced representation of the inter-channel relationship from both perspectives. For example, feature f_{43} is the inverse of f_1 (i.e., f_1^{-1}), feature f_{44} is the inverse of f_2 (f_2^{-1}), and this pattern continues for the remaining features. This comprehensive set of 84 features forms the input vector for the subsequent classification stage.

Table 4.1. Proposed Features and Their Mathematical Expressions

Features	Expressions
f_1	$\boldsymbol{MCL(SC_{31})/MCL(SC_{41})}$
f_2	$\boldsymbol{sum(SC_3)/sum(SC_4)}$
f_3	$\boldsymbol{mad(SC_{31})/mad(SC_{41})}$
f_4	$\boldsymbol{ME(SC_{31})/ME(SC_{41})}$
f_5	$\boldsymbol{FD(SC_{32})/FD(SC_{42})}$
f_6	$\boldsymbol{kurt(SC_3)/kurt(SC_4)}$
f_7	$\boldsymbol{\left(\frac{sum(SC_3{}^2)}{length(SC_3)}\right)/\left(\frac{sum(SC_4{}^2)}{length(SC_4)}\right)}$
f_8	$\boldsymbol{\left(\frac{mean(SC_3{}^2)}{length(SC_3)}\right)/\left(\frac{mean(SC_4{}^2)}{length(SC_4)}\right)}$
f_{j+8}	$\boldsymbol{\left(\frac{mean(SC_{3j}{}^2)}{length(SC_{3j})}\right)/\left(\frac{mean(SC_{4j}{}^2)}{length(SC_{4j})}\right)\ j=1\dots2}$
f_{j+10}	$\boldsymbol{\left(\frac{rms(SC_{3j}{}^2)}{length(SC_{3j})}\right)/\left(\frac{rms(SC_{4j}{}^2)}{length(SC_{4j})}\right)j=1\dots2}$
f_{13}	$\boldsymbol{var(P_3)/var(P_3+P_4)}$
f_{14}	$\boldsymbol{max(P_3)/max(P_4)}$
f_{15}	$\boldsymbol{kurt(P_{31})/var(P_{41})}$
f_{16}	$\boldsymbol{kurt(P_{31})/median(P_{41})}$
f_{17}	$\boldsymbol{STD(D3_{32})/STD(D3_{42})}$
f_{18}	$\boldsymbol{skew(D1_{32})/skew(D1_{42})}$
f_{j+17}	$\boldsymbol{kurt(Dj_{32})/kurt(Dj_{42})\ \ j=2,3}$
f_{21}	$\boldsymbol{sum(D3_{32}{}^2)/sum(D3_{42}{}^2)}$
f_{j+20}	$\boldsymbol{MCL(Dj_{32})/MCL(Dj_{42})\ \ j=2,3}$
f_{24}	$\boldsymbol{mad(D3_{32})/mad(D3_{42})}$
f_{j+24}	$\boldsymbol{EWL(Dj_{32})/EWL(Dj_{42})\ \ j=1\dots3}$
f_{28}	$\boldsymbol{EMAV(D2_{32})/EMAV(D2_{42})}$
f_{29}	$\boldsymbol{sum(A1_3{}^2)/sum(A1_4{}^2)}$
f_{30}	$\boldsymbol{mean(\lvert A1_{32}\rvert)/mean(\lvert A1_{42}\rvert)}$
f_{31}	$\boldsymbol{rms(\lvert A1_{31}\rvert)/rms(\lvert A1_{41}\rvert)}$
f_{32}	$\boldsymbol{median(\lvert A1_{32}\rvert)/MCL(\lvert A1_{42}\rvert)}$
f_{33}	$\boldsymbol{EWL(A1_3)/EWL(A1_4)}$
f_{j+33}	$\boldsymbol{EWL(A1_{3j})/EWL(A1_{4j})\ \ j=1,2}$
f_{36}	$\boldsymbol{EMAV(A1_3)/EMAV(A1_4)}$
f_{37}	$\boldsymbol{EMAV(A1_{32})/EMAV(A1_{42})}$

f_{38}	$\boldsymbol{max(A1_3)/max(A1_4)}$
f_{i+37}	$\frac{\boldsymbol{sum}(\boldsymbol{C_{SC32}}(\boldsymbol{i},:)^2)}{\boldsymbol{sum}(\boldsymbol{C_{SC42}}(\boldsymbol{i},:)^2)} \quad \boldsymbol{i = 2 \ldots 5}$

4.4. Initial classification performance and classifier selection

An initial comparative analysis was conducted to select the optimal classifier for the proposed feature set. The CA was evaluated across the four datasets using three standard classifiers: SVM with a linear kernel, KNN, and LDA. The EEG data window for feature extraction was empirically defined, with a start time of 3.85 seconds post-cue, as adopted from previous research [79], and a duration of 1 second.

Table 4.2. CA of Different Classifiers Across All Datasets

Datasets	Subjects	Classifiers		
		LSVM	***KNN***	***LDA***
Datasets 1	O3	75.8	74.4	**71.9**
	S4	76.7	74.1	**73.7**
	X11	76.9	74.2	**73.8**
Mean (%)		**76.47**	**74.2**	**73.1**
Datasets 2	S1	**82.1**	**80.7**	**82.1**
Datasets 3	B01	68.1	65.6	**65**
	B02	52.2	51.8	**52**
	B03	59.4	55	**52**
	B04	91.4	90.5	**91**
	B05	81.4	81.6	**80**
	B06	71.3	66.3	**68.8**
	B07	66.3	61.9	**64.1**
	B08	77.4	73.2	**75.3**
	B09	72.8	74.2	**75.3**
Mean (%)		**71.14**	**68.9**	**69.49**
Datasets 4	S04	75	73	**75**
	S11	75	74.3	**74.5**
	S20	75	71.3	**74.8**
	S24	75.8	74	**75**
	S25	76	75	**75**
	S27	77.3	77.8	**76.3**
	S34	76.5	74.3	**75**
	S35	85	78	**79.5**
	S40	79.5	75	**79.3**
	S42	79.8	77.8	**78**
	S46	75	74.3	**75**
	S47	75	76.8	**75.3**
Mean (%)		**77.07**	**75.13**	**76.05**

To ensure a fair and rigorous performance assessment, the evaluation protocol was tailored to the characteristics of each dataset. A rigorous 10-fold cross-validation protocol was applied to Datasets 1 and 4 to ensure an unbiased estimate of generalization performance and for Datasets 2 and 3, the CA was assessed using the holdout evaluation technique with the predefined training and testing partitions imposed by these benchmark datasets.

The results of this comparative analysis are summarized in Table 4.2. The linear SVM classifier consistently yielded the highest mean CA for all datasets, achieving 76.5% for Dataset 1, 82.1% for Dataset 2, 71.14% for Dataset 3, and 77.07% for Dataset 4. Based on this superior and consistent performance, the linear SVM was selected as the primary classifier for all subsequent, in-depth analyses reported in this work.

4.5. Subject-Specific optimization of processing duration

MI responses exhibit significant inter-subject variability in timing and duration. Consequently, using a fixed time window for feature extraction across all subjects is suboptimal. To address this, we incorporated a subject-specific optimization step to tailor the temporal segment for analysis.

For each subject, the processing duration (the length of the signal segment following a fixed start time of 3.85s) was treated as an optimization variable. The objective was to identify the duration that maximized the CA for that individual, using the previously selected linear SVM classifier. This optimization was performed using the Firefly Algorithm, a metaheuristic search technique effective for such non-linear problems.

The resulting optimal durations and their corresponding CA for all subjects are presented in Table 4.3. The results demonstrate significant inter-subject variability in the optimal window length, with durations ranging from 0.34 seconds to over 3.7 seconds.

The overall efficacy of the optimization is evident when comparing the mean classification accuracy per dataset against the baseline using a fixed 1-second window (LSVM results from Table 4.2). The subject-specific optimization yielded a clear improvement in the mean accuracy for every dataset:

Dataset 1: Increased from 76.47% to 80.28% (+3.81%)
Dataset 2: Increased from 82.1% to 90.0% (+7.9%)
Dataset 3: Increased from 71.14% to 79.82% (+8.68%)
Dataset 4: Increased from 77.07% to 80.25% (+3.18%)

Table 4.3. Subject-Specific Optimal Processing Durations and Corresponding CA

Datasets	Subjects	Processing Duration (s)	CA (%)
Datasets 1	O3	1.8720	**76.13**
	S4	3.5047	**84.29**
	X11	3.4420	**80.43**
Mean (%)			**80.28**
Datasets 2	S1	3.6056	**90**
Datasets 3	B01	0.5981	**68.43**
	B02	2.8743	**60.71**
	B03	0.8054	**64.68**
	B04	1.8122	**95**
	B05	2.2322	**90.29**
	B06	3.4624	**84.27**
	B07	0.7429	**72.18**
	B08	2.2914	**91.87**
	B09	3.2189	**90.93**
Mean (%)			**79.82**
Datasets 4	S04	0.4187	**79.25**
	S11	0.7440	**78.5**
	S20	1.5449	**80.5**
	S24	0.6414	**79.5**
	S25	0.8355	**78.75**
	S27	3.7015	**80**
	S34	1.7820	**79.75**
	S35	0.5322	**88.75**
	S40	2.1925	**79.5**
	S42	2.0043	**79.75**
	S46	0.3359	**79.25**
	S47	0.8034	**79.5**
Mean (%)			**80.25**

This consistent, dataset-wide improvement demonstrates that tailoring the feature extraction window to individual neurophysiological timing is a crucial step for maximizing the discriminative power of the extracted features. These subject-specific, optimized processing durations were subsequently used for all feature extraction, ensuring that the calculated features were derived from the most informative and discriminative neural activity period for each individual.

4.6. Dimensionality reduction and feature selection

Following the temporal optimization, a GA was employed to perform feature selection. The objective was to identify the most discriminative subset of features from the initial set of 84, thereby reducing dimensionality, mitigating the risk of overfitting, and potentially improving classification performance for the binary (left-hand vs. right-hand) MI task.

The GA operated on a population of binary-encoded chromosomes, where each gene represented the inclusion (1) or exclusion (0) of a specific feature. The fitness of each chromosome (feature subset) was evaluated as the classification accuracy achieved by a LSVM classifier. The complete set of algorithm parameters used to control the evolutionary process, including population size, selection, crossover, and termination criteria are detailed in Table 4.4. These parameters were selected to ensure a thorough exploration of the vast combinatorial search space (2^{84} possible subsets) and robust convergence.

Table 4.4. GA Configuration Parameters

Parameters	Definition or value
Population type	**Bit string / double victor**
Population size	**200**
Scaling function	**Shift linear**
Selection function	**Remainder**
Mutation function	**Constraint dependent**
Generations	**2000 / 10000**
Elite count	**0.05*Population size**
Crossover fraction	**0.8**
Crossover function	**Constraint dependent**
Migration direction	**Forward**
Migration fraction/interval	**0.2/20**
Termination Criteria	**Stall generations = 5000**

4.6.1. Results of feature selection

The results of the GA-based feature selection are summarized in Table 4.5, which compares the CA before and after selection, along with the number of selected features (SF) for each dataset.

The analysis reveals two primary outcomes:

First, the algorithm achieved a substantial dimensionality reduction, discarding redundant and non-discriminative features. On average, the size of the feature set was reduced by approximately 60%, with the number of SF ranging from 21 to 44 across subjects.

Second, this refinement directly translated into improved classification performance. The mean CA increased for every dataset: by about 10% for Dataset 1 and by approximately 5% for Datasets 2, 3, and 4. Figure 4.4 illustrates the GA's convergence patterns for top-performing subjects across each dataset. These plots show how classification error steadily drops across generations, leading to compact optimal feature subsets that deliver impressive final accuracies: 92.53% for

Subject O3 (35 features), 95.71% for Subject S1 (42 features), 98.23% for Subject B04 (35 features), and 92% for Subject S35 (21 features).

Table 4.5. CA (%) Before and After Feature Selection, with SF Count for Each Dataset

Datasets	Subjects	All features (84)	Mean (%)	Selected features (SF)	Mean (%)
Datasets 1	O3	76.13	**80.29**	92.53 (35)	**90.1**
	S4	84.30		90.32 (37)	
	X11	80.44		87.45 (35)	
Datasets 2	S1	90	**90**	95.71 (42)	**95.71**
Datasets 3	B01	68.43	**79.82**	75.5 (30)	**86.73**
	B02	60.71		71.78 (30)	
	B03	64.68		75 (44)	
	B04	95		98.23 (35)	
	B05	90.29		94.41 (39)	
	B06	84.27		89.3 (34)	
	B07	72.18		82.5 (31)	
	B08	91.87		96.25 (21)	
	B09	90.93		95.62 (21)	
Datasets 4	S04	79.25	**80.25**	82 (29)	**83.83**
	S11	78.5		81.5 (31)	
	S20	80.5		84.5 (38)	
	S24	79.5		85.75 (27)	
	S25	78.75		84.25 (22)	
	S27	80		82.5 (38)	
	S34	79.75		83.5 (21)	
	S35	88.75		92 (21)	
	S40	79.5		83.5 (32)	
	S42	79.75		83 (36)	
	S46	79.25		82.25 (21)	
	S47	**79.5**		**81.25 (36)**	

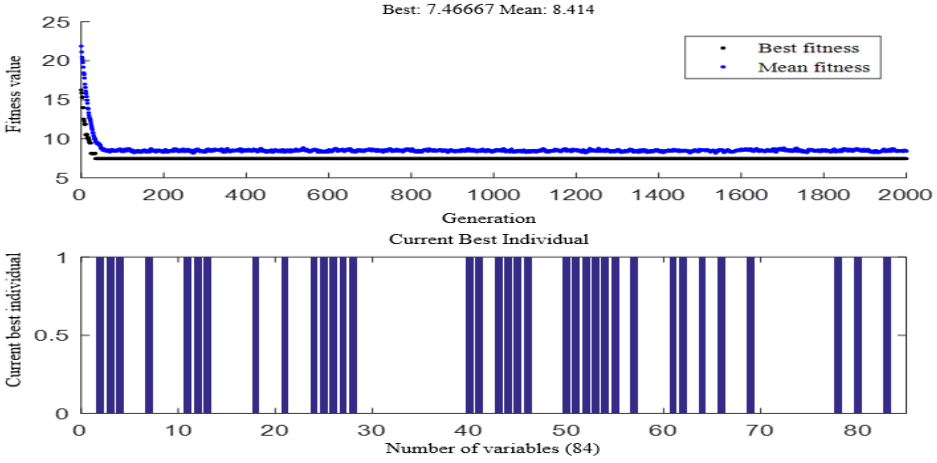

(a)

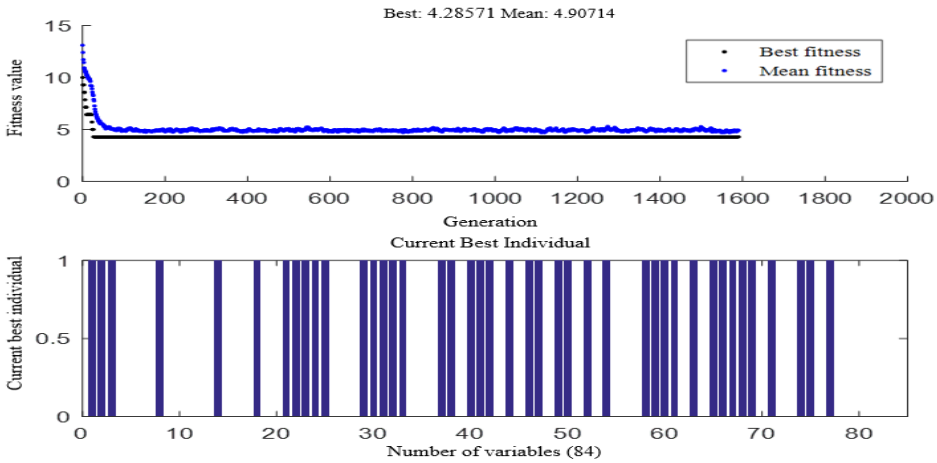

(b)

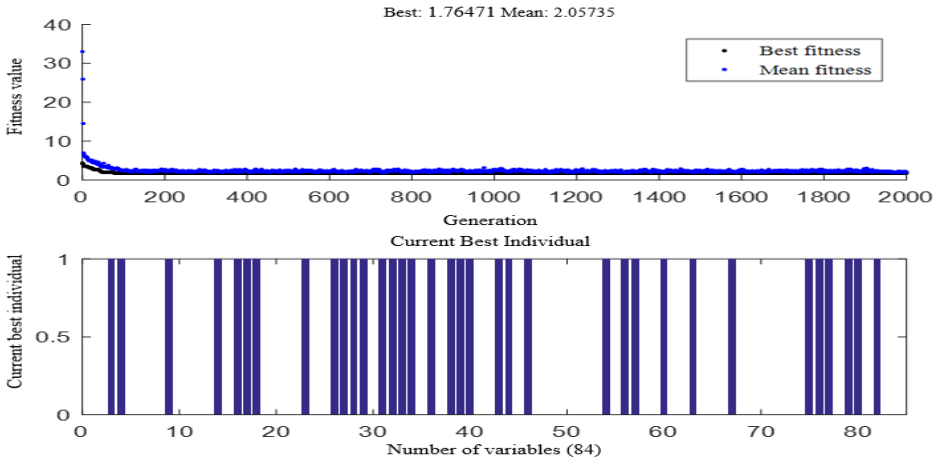

(c)

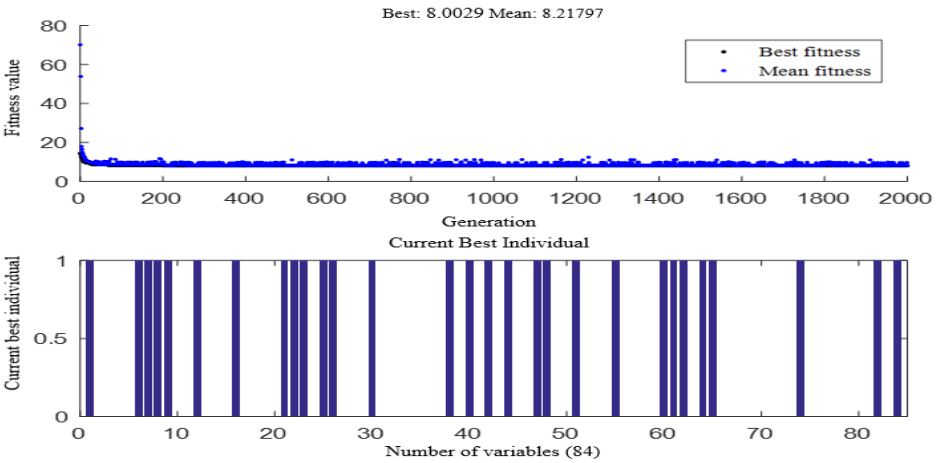

(d)

Figure 4.4. Feature Selection Using GA Optimization for High-Performing Subjects: (a) Subject O3, (b) Subject S1, (c) Subject B04, (d) Subject S35.

These results demonstrate that the GA successfully identified compact, highly discriminative feature subsets tailored to each subject, thereby enhancing the overall efficacy of the binary MI classification system.

4.7. Feature space transformation via the Weight Features Function (WFF)

Building upon the SF, a final Weighted Feature Function (WFF) transformation was applied. The WFF introduces a parameterized nonlinear mapping designed to warp the feature space, making the representations of left/right hand MI more linearly separable before classification by the LSVM.

The WFF implements a parameterized double nonlinearity on each selected feature. For a given feature X_i the transformed feature X_i' is defined as:

$$\boldsymbol{X_i' = WFF(X_i) = \tan\left(w_{1i} + w_{2i}X_i + w_{3i}X_i^2\right),} \quad \text{where } \boldsymbol{i = 1, \dots, SF} \tag{4.15}$$

Here, w_{1i}, w_{2i}, and w_{3i} are three adaptive weights associated with feature X_i. The transformation first applies a second-order polynomial, which captures local curvature, and then passes the result through the periodic tangent (tan) function. This function was selected after an empirical comparison against alternative nonlinear candidates including asin, sin, cos, acos, and atan, which consistently demonstrated superior classification performance across preliminary validation tests. The periodicity of tan enables the model to non-linearly warp different regions of the feature space independently, accommodating asymmetric class distributions that a simple polynomial alone could not address.

The three optimal weights (w_{1i}, w_{2i}, w_{3i}) for every selected feature is determined by a GA, with the fitness function set to minimize the misclassification rate. This direct optimization ensures that the transformation is explicitly tuned to improve classification performance.

Conceptually, the WFF acts as a customized, learned nonlinear projection that maps the original feature set into a new space of the same dimensionality, where the two MI classes become more linearly separable. By enhancing class separability in this transformed space, the subsequent LSVM classifier can operate more effectively, achieving higher CA with a simpler decision boundary.

4.7.1. Classification performance with Weight Features Function (WFF)

The resulting classification accuracies for all subjects after WFF transformation are presented in Table 4.6. The application of the WFF technique yielded a consistent and marked improvement in performance for every subject across all datasets.

Table 4.6. Final CA (%) After WFF Transformation

Datasets	**Subjects**	**Using WFF**	**Mean (%)**
Datasets 1	O3	100	**96.1**
	S4	95.48	
	X11	92.81	
Datasets 2	S1	100	**100**
Datasets 3	B01	84.68	**94.2**
	B02	85	
	B03	87.81	
	B04	100	
	B05	100	
	B06	99.05	
	B07	92.18	
	B08	100	
	B09	99.06	
Datasets 4	S04	86.25	**88.70**
	S11	86.75	
	S20	88	
	S24	88.75	
	S25	88.5	
	S27	87.75	
	S34	87.75	
	S35	97	
	S40	88.25	
	S42	90	
	S46	88.25	
	S47	**87.25**	

The process of optimizing the WFF weights via the GA is illustrated in Figure 4.5, which shows the convergence of classification error for a high-performing subject from each dataset. These findings demonstrate how the GA successfully minimized the misclassification rate, directly leading to the final, enhanced accuracies reported in Table 4.6.

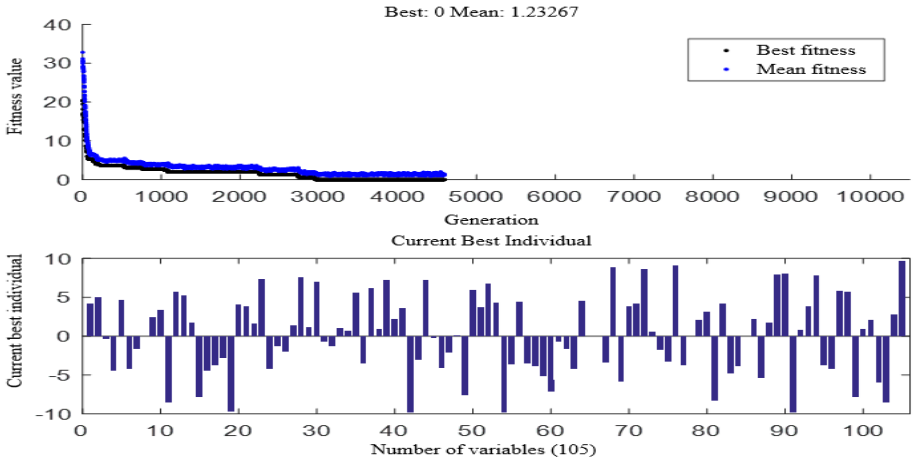
Best: 0 Mean: 1.23267
Best fitness
Mean fitness
Fitness value
Generation
Current Best Individual
Current best individual
Number of variables (105)

(a)

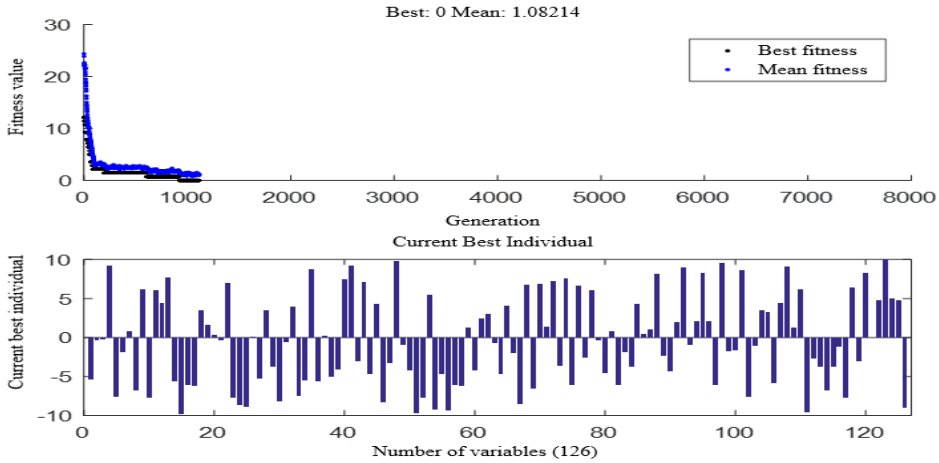
Best: 0 Mean: 1.08214
Best fitness
Mean fitness
Fitness value
Generation
Current Best Individual
Current best individual
Number of variables (126)

(b)

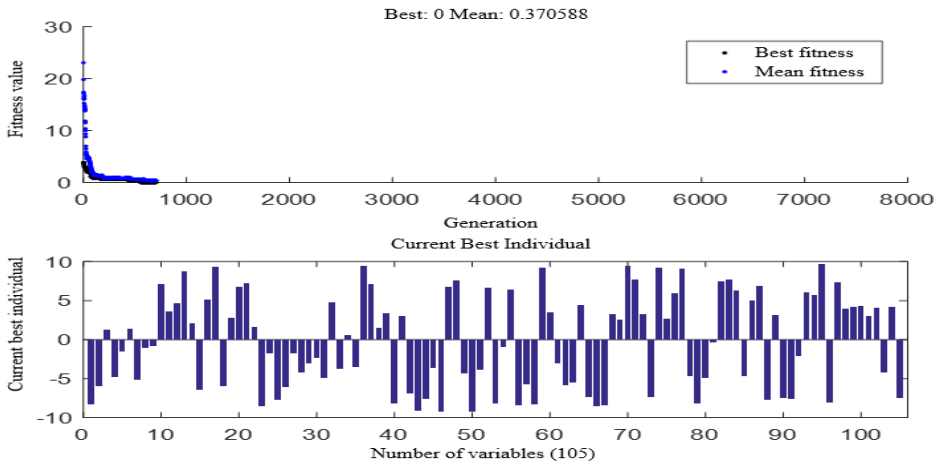
Best: 0 Mean: 0.370588
Best fitness
Mean fitness
Fitness value
Generation
Current Best Individual
Current best individual
Number of variables (105)

(c)

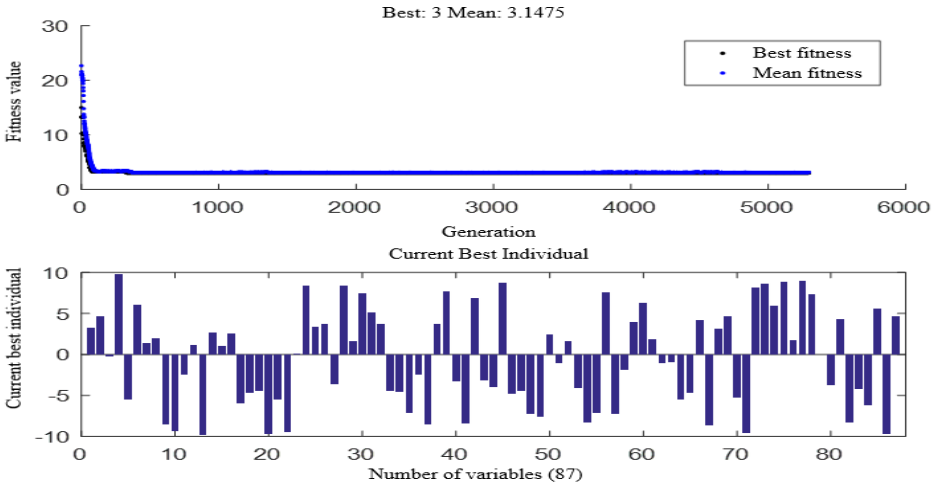

(d)

Figure 4.5. GA Optimization for WFF Across Subjects. (a) O3, (b) S1, (c) B04, (d) S35.

The contribution of the WFF technique is visually summarized in Figure 4.6, which compares the mean CA for each dataset before and after WFF application. The bar plot clearly demonstrates a significant and consistent performance gain across all datasets.

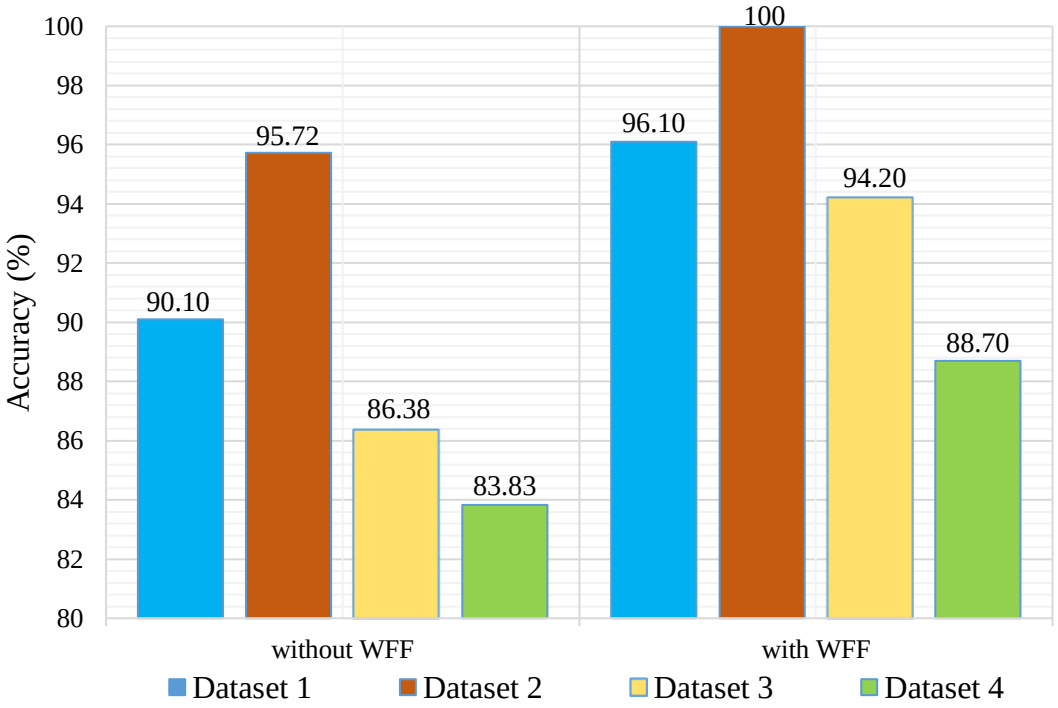

Figure 4.6. Comparison of CA Before and After WFF Application.

Quantitatively, the mean accuracy improved from 90.10% to 96.10% for Dataset 1, from 95.72% to 100% for Dataset 2, from 86.38% to 94.2% for Dataset 3, and from 83.83% to 88.70% for Dataset 4. This corresponds to an average improvement of approximately 5% per dataset. These results confirm that the WFF is a highly effective post-processing step. By nonlinearly transforming the selected feature space to enhance class separability, the WFF directly leads to a substantial improvement in the identification of left/right hand MI movements.

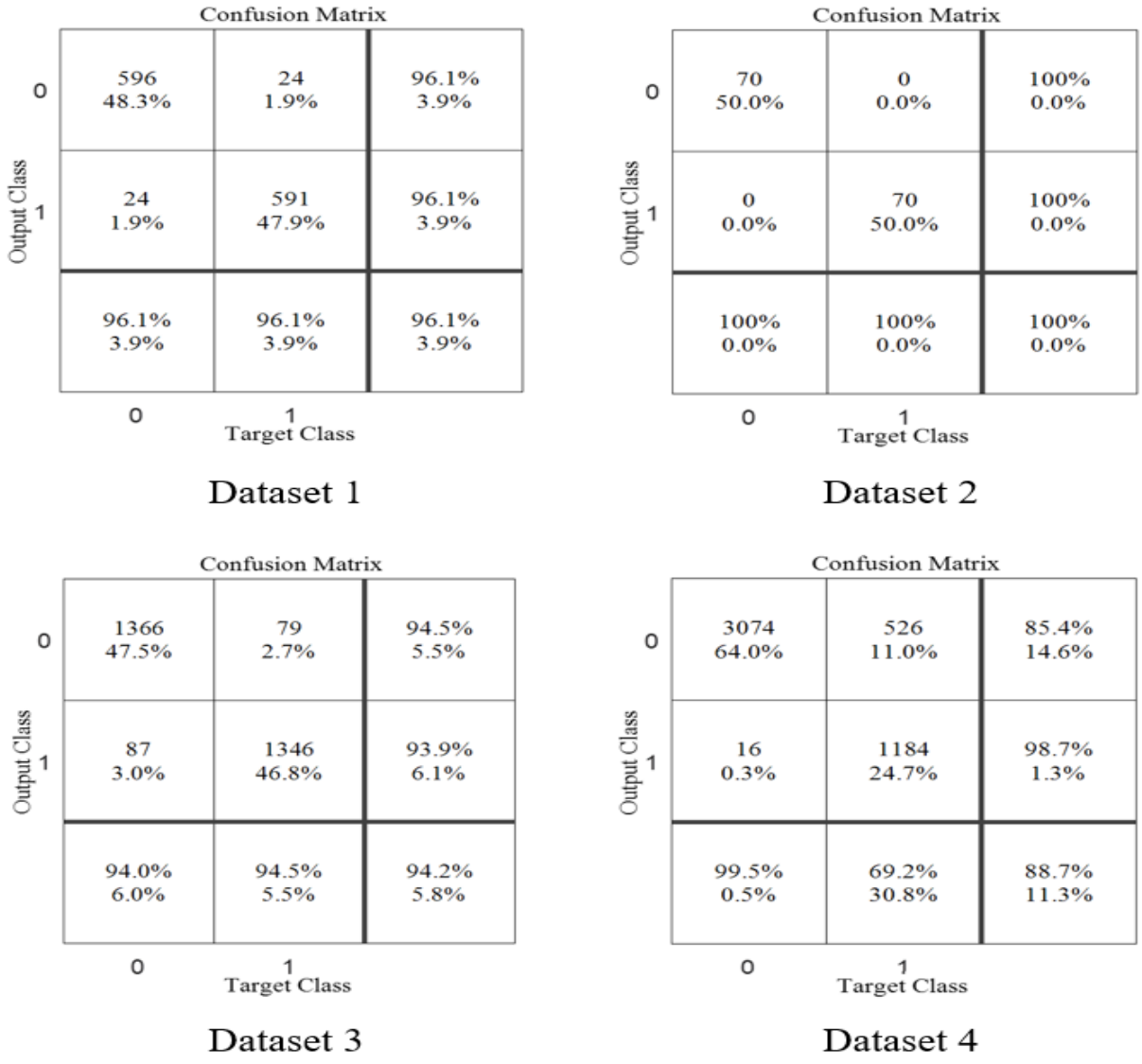

Figure 4.7. Confusion matrices of the proposed method for MI-EEG classification across four datasets.

To provide a detailed performance analysis for each class, the mean confusion matrices for the four datasets are presented in Figure 4.7. These matrices summarize the final classification outcomes using the complete optimized pipeline which is built upon the proposed 84-feature set and includes personalized time windows, GA feature selection, WFF transformation, and LSVM classification.

For Dataset 1, the classifier achieves balanced performance across both classes, with a high and symmetric recognition rate (96.1%), indicating good class separability and stable decision boundaries. Dataset 2 exhibits perfect classification, with no misclassifications observed for either class, demonstrating the effectiveness of the proposed method under controlled conditions. In Dataset 3, the classifier maintains strong performance, achieving an overall accuracy of approximately 94.2%. The confusion matrix reveals a small increase in misclassification rates for both classes, which may be attributed to increased inter-trial variability or subject-dependent differences. Dataset 4 presents the most challenging scenario, with an overall accuracy of 88.7%. While Class 0 is recognized with very high sensitivity (99.5%), Class 1 shows a reduced recognition rate (69.2%), indicating class imbalance and increased overlap between MI patterns.

Overall, these results confirm the strong generalization ability of the proposed method across diverse datasets. Although performance decreases in more challenging scenarios due to EEG variability and noise, the proposed WFF-based technique effectively enhances feature sensitivity and discriminability, reducing class confusion in MI classification.

4.8. Comparison with state-of-the-art methods

To evaluate the proposed method's performance within the current research literature, we conducted a comparative analysis against state-of-the-art techniques on identical benchmark datasets. Table 8 summarizes CA from relevant prior works alongside their methodologies and feature types for direct comparison with our results.

The analysis shows that the proposed method achieves superior performance. For Dataset 1, the previous best result of 94.11% was achieved using a complex ensemble of three optimized SVM classifiers. Our method, employing a single linear SVM on an optimized feature set, surpasses this with a CA of 96.1%. In Dataset 2, a DL CNN approach achieved an accuracy of 99.29%. Our method achieves perfect separation on this dataset with a CA of 100%. For Dataset 3, the best prior performance was 89.02%, obtained via a DL-based transfer learning CNN. Our method provides a substantial improvement, reaching a CA of 94.2%. The most striking contrast is seen in Dataset 4. The comparative study by M.-H. Lee et al., which used CSP features from 20 channels with an LDA classifier, reported a CA of 51.98%. In contrast, our method, utilizing only two electrodes (C3 and C4), achieves a significantly higher CA of 88.70%, representing an improvement of over 36%. This consistent and significant outperformance, particularly the efficiency gain demonstrated on Dataset 4, highlights the strength of the proposed feature engineering and optimization pipeline.

Table 4.7. Comparative Summary of CA from Relevant Studies Across the Four Datasets

Datasets	Works	Features	Classifiers	Mean (%)
Dataset 1	Lotte et al. (2007) [103]	Band Power	SVM	79.36
	Zhong et al. (2008) [104]	Band Power	VB	78.96
	Brodu et al. (2011) [105]	Wavelet features (Morlet)	LDA	80.95
	Brodu et al. (2012) [106]	BP, Multifractal, Complexity	LDA	81.30
	Bashashati et al. (2015) [107]	Wavelet features (Morlet)	LR	81.47
	Wang et al. (2019) [108]	TQWT	LDA	81.75
	You et al. (2020) [109]	FAWT	LDA	86.66
	Mebarkia and Reffad. (2019) [79]	16 Diversified features	Three optimized SVMs	94.11
	This work	**84 Diversified features with optimized WFF**	**SVM**	**96.1**
Dataset 2	Liu et al. (2010) [110]	Common spatial pattern (CSP)	SVM	82.86
	Jang et al. (2016) [111]	STFT	KNN	83.57
	Khasnobish et al. (2010) [112]	Average band power of alpha and beta	KNN	84.29
	Wang et al. (2019) [108]	TQWT	LDA	88.11
	Tabar and Halici. (2016) [113]	STFT	Deep learning	90
	You et al. (2020) [109]	FAWT	LDA	94.29
	Kant et al. (2020) [72]	CWT Filter-bank	Deep Transfer-learning	95.71
	Salimpour et al. (2022) [114]	CNN-based features from Stockwell TFM	SVM	99.29
	This work	**84 Diversified features with optimized WFF**	**SVM**	**100**
Dataset 3	Degdevir et al. (2021) [115]	Hjorth algorithm	SVM	82.58
	Han et al. (2022) [116]	STFT	PCNN	83
	Malan and Sharma. (2022) [117]	Dual-tree complex wavelet, NCA	SVM	84.02
	Lu et al. (2017) [118]		Deep learning based on restricted Boltzmann machines	84.2
	Liu et al. (2023) [119]		CMO-CNN	87.19
	Salimpour et al. (2022) [114]	CNN-based features from Stockwell TFM	SVM	89.02
	This work	**84 Diversified features with optimized WFF**	**SVM**	**94.2**
Dataset 4	M.-H. Lee et al. (2019) [97]	CSSP	LDA	51.98
	This work	**84 Diversified features with optimized WFF**	**SVM**	**88.70**

4.9. Conclusion

This thesis introduces a novel methodology that substantially enhances left- and right-hand MI classification from EEG signals. The core contribution is a comprehensive processing pipeline that transforms raw, high-dimensional EEG data into a compact, highly discriminative feature space through a sequence of optimized stages tailored for LSVM classification.

The proposed method integrates several key innovations:

- A Novel Hybrid Feature Set: comprising 84 spatial-ratio features. These were engineered by extracting time, frequency, and time-frequency domain metrics from six

key signals (the primary C3/C4 channels and their filtered derivatives) with ratios between corresponding C3- and C4-derived metrics explicitly encoding inter-hemispheric relationships for enhanced lateralized MI discrimination.

- Subject-specific temporal optimization: addresses inter-subject variability in MI response timing through personalized FA tuning. For each subject, the algorithm identifies the optimal processing duration (with fixed start time) that maximizes feature discriminative power, ensuring analysis targets the most informative neural activity period for that individual.
- Dimensionality reduction and feature selection: employed a GA to navigate the vast combinatorial space of 84 features, identifying compact, subject-specific subsets of the most discriminative ones. This step typically reduced the feature set by approximately 60% while simultaneously boosting CA.
- Feature transformation via the WFF: applies a tan-based transformation to the selected features. This mechanism weights and enhances the feature space, improving linear separability and emphasizing the most discriminative dimensions for the subsequent classifier.

The efficacy of this integrated approach was rigorously validated through extensive experiments across four public datasets, yielding consistent and substantial performance gains. The method outperformed a broad spectrum of state-of-the-art techniques including complex SVM ensembles and DL models achieving superior CA on every dataset. Notably, on Dataset 4, the approach delivered 88.70% CA using just two electrodes, a 36% improvement over a prior 20-channel study demonstrating the exceptional efficiency of the engineered 84-feature set, further amplified by WFF transformation and personalized optimization.

In conclusion, this work demonstrates that a carefully engineered feature pipeline centered on a novel 84 dimensional spatial-ratio feature set and enhanced by personalized temporal optimization, intelligent feature selection, and the WFF dramatically elevates MI-BCI performance and efficiency. The success of the LSVM classifier reveals that high accuracy need not rely on complex nonlinear models or dense electrode arrays; rather, extracting and optimally transforming neurophysiologically meaningful information renders the classification problem far more tractable. This approach yields a robust, interpretable framework for practical MI-BCI systems

Part II

Enhanced Decoding of Four-Class Motor Imagery through NDD and Personalized Temporal Optimization

4.10. introduction

Four-class MI classification presents substantially greater challenges than binary paradigms. Neural activation patterns for different movements exhibit significant cortical overlap in sensorimotor regions while lacking clear separability, further complicated by increased inter-class variability and classification complexity. Consequently, Effective feature extraction is critical for decoding the complex, non-stationary patterns in EEG signals used in MI-BCIs. This work presents a method for MI classification, evaluated on the widely used Dataset 5 (BCI Competition IV Dataset 2a). This benchmark dataset contains four-class MI data (left hand, right hand, feet, tongue) from nine subjects, recorded using 22 EEG electrodes, providing a standard for comparing algorithmic performance.

Previous study using this dataset has explored a variety of methodologies for instance, in [120], Ang et al. used the Filter Bank Common Spatial Pattern (FBCSP) algorithm to optimize the subject-specific frequency band for CSP, handling multi-class data. However, its reliance on a fixed set of pre-defined spectral filters may limit its adaptability to more complex, non-stationary signal components. Advancing beyond standard spatial filtering, more complex hybrid approaches have been proposed like in [121], who introduced a method combining Phase Space Reconstruction (PSR) with CSP to extract features in a high-dimensional state-space, which were then classified using a novel Relevance Vector Machine (RVM) with a custom hybrid kernel function, demonstrating gains in accuracy for multi-task MI. Others shifted significantly towards DL; for example, [122] proposed two sophisticated CNN-based approaches for EEG decoding: a multi-CNN fusion model (MCNN) and a cross-encoding CNN model (CCNN). The MCNN architecture employs several parallel CNNs with different depths

and filter characteristics to extract complementary spatial and temporal features from raw EEG, after which their feature maps are fused for improved classification. Meanwhile, the CCNN model uses an autoencoder-based cross-encoding strategy to enhance cross-subject generalization rather than to fuse CNN outputs.

However, most existing MI-BCI approaches stick to the same rigid time window right after the visual cue, which doesn't capture how differently people experience the timing, duration, and patterns of their brain responses during MI. To address this gap, we introduce a personalized framework that adapts both space and time for each subject, automatically finding the best MI EEG analysis window to maximize the useful signals for classification. On top of that, we reduce the number of electrodes from 22 down to just 10 by using the NDD configuration.

4.11. Spatial filtering and channel reduction with NDD

Spatial filtering in EEG analysis refers to the process of combining signals from multiple electrodes to enhance specific neural sources while attenuating noise and activity from irrelevant cortical areas. This sharpens focus on the regions we care about for MI and can also slim down the number of channels without losing the important information.

Here, we use the NDD configuration as a smart combination of spatial filtering and channel reduction. Each NDD channel is calculated as a weighted combination of five original electrodes: a central electrode and its four closest neighbors. For example, the first NDD signal is computed from central electrode C4 and its neighbors C1, C3, C5, and C10, following the formula:

$$\boldsymbol{NDD_1 = 4 \times C_4 - (C_1 + C_3 + C_{10} + C_5)} \quad (4.16)$$

Where C_1 represents channel 1. This process was repeated for a selected set of 10 central electrodes (channels 4, 8, 9, 10, 11, 12, 15, 16, 17, and 20 from the original montage), as illustrated in Figure 4.8.

The resulting 10 NDD signals highlight local sensorimotor activity, reduce diffuse noise and common artifacts, and keep the discriminative spatial patterns essential for distinguishing MI tasks, all while dropping from 22 channels to a more practical 10 channels.

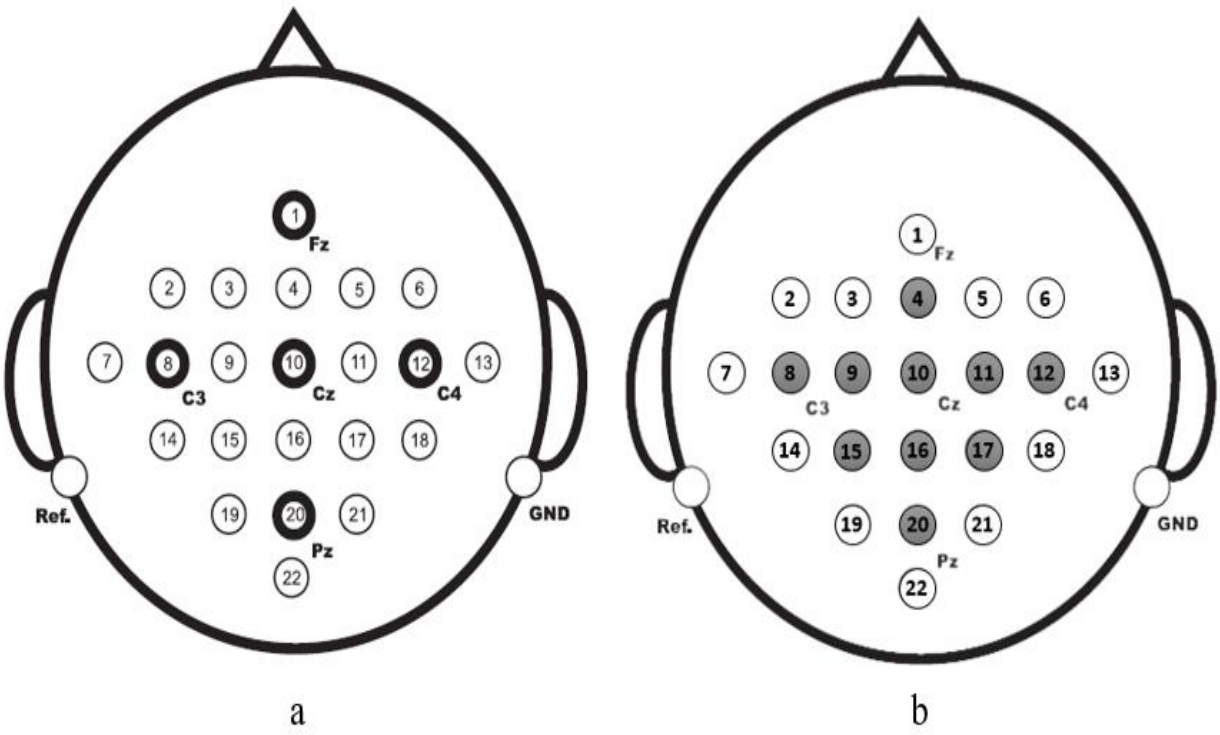

Figure 4.8. Reduction of EEG Channels Using NDD: Electrode placement following the international 10–20 system. (b) Resulting 10 NDD derived from the original 22 electrodes.

4.12. Data preprocessing pipeline

Extracting discriminative MI patterns from raw EEG is challenging because the signals are often buried in noise from physiological sources and the environment. To address this, a well-designed preprocessing pipeline is required to improve the SNR and highlight the brain activity most relevant for deciphering imagined movements. After using the NDD method to sharpen spatial features, the EEG data undergoes further preprocessing to prepare it for feature extraction and analysis.

4.12.1. Spectral filtering for mi-relevant rhythms

As introduced in Chapter 1, MI-BCIs primarily rely on changes of sensorimotor rhythms, especially in the mu (8–13 Hz) and beta (13–30 Hz) frequency bands. This study focuses specifically on the beta band because it tends to show stronger and more consistent activity during imagined movement tasks. To capture these MI-relevant oscillations, each of the 10 NDD channels is passed through a special band-pass filter, a zero-phase second-order Butterworth filter with cutoff frequencies set at 13 Hz and 30 Hz. The Butterworth filter was chosen for its smooth and flat response in the passband, ensuring no artificial boosts or cuts in signal strength within the beta band frequencies. The zero-phase implementation, achieved by filtering the signal forward and backward, eliminates any phase delays, meaning the timing and shape of the EEG waveforms remain true to the original EEG waveform.

To illustrate the impact of the filter phase characteristics, Figure 4.9 shows the difference between a regular second-order Butterworth band-pass filter and this zero-phase version on the NDD1 channels. The regular Butterworth introduces a clear linear phase delay, visible as a slight temporal shift between the original and filtered signals, while the zero-phase version keeps everything perfectly aligned. Although filtering twice effectively doubles the filter order resulting in a sharper frequency roll-off and slightly stronger attenuation near the cutoff frequencies, this trade-off is acceptable for the current processing stage.

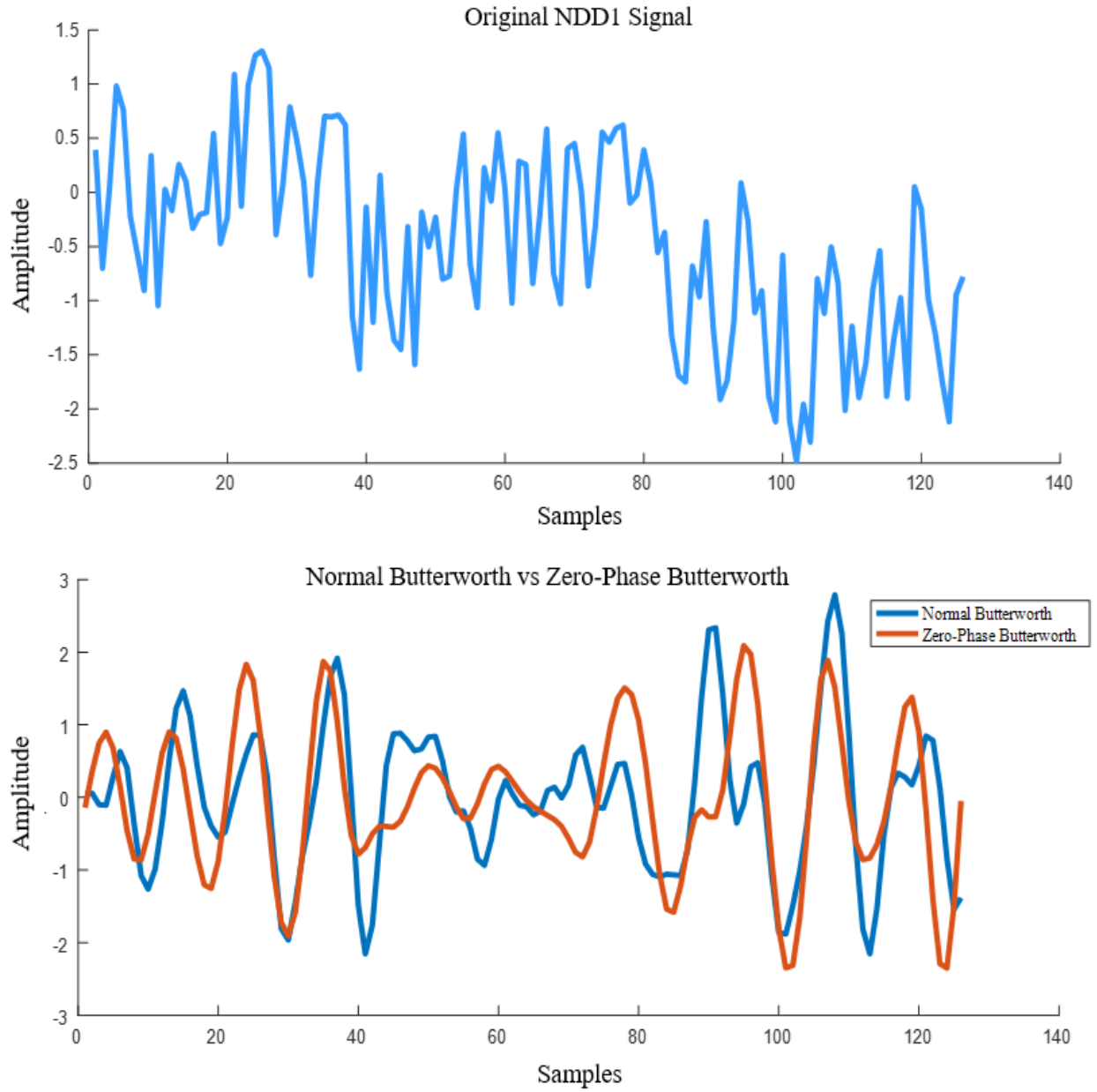

Figure 4.9. Comparison of Normal and Zero-Phase Butterworth Filters on NDD1 Signals.

Cleaning artifact and Noise: It cuts out low-frequency junk below 13 Hz—like eye blinks, slow brain waves, and sweat artifacts while toning down high-frequency noise above 30 Hz from muscle twitches (EMG) and external interference.

4.12.2. Task-Specific feature emphasis

Narrowing to the beta band highlights MI-related cortical rhythms that show strong ERD/ERS patterns during imagined limb movements. This focused filtering shrinks the data size while boosting the power of later feature extraction and personalized optimization steps.

4.13. Proposed feature set

After spectral filtering cleans the raw EEG signal and focuses on task-specific MI rhythms, the MI-BCI pipeline proceeds to feature extraction, which transforms those complex, noisy EEG waveforms into meaningful insights. Feature extraction has a crucial role, which pulls out key descriptors capturing the timing, frequency patterns, and spatial layouts of brain activity associated with imagined movements while suppressing irrelevant fluctuations and artifacts. By converting continuous EEG signals into compact numerical representations, these features become suitable inputs for downstream machine-learning classifiers. These classifiers rely on such structured feature representations to accurately distinguish between different MI tasks such as left-hand, right-hand, foot, or tongue imagery, thereby enabling accurate decoding of the user's intended movement. Conversely, poorly chosen features may obscure meaningful MI patterns, increase intra-class variability, and ultimately degrade CA. For this reason, identifying an informative, diverse, and physiologically meaningful feature set is one of the most decisive factors influencing the performance of any MI-BCI classification system.

In this work, we employ a comprehensive hybrid feature set designed to maximize inter-class separability for the four-class MI task. The proposed hybrid model utilizes an expanded set of 220 features, building upon the foundational time and time-frequency domain features defined in Section 4.3. A multi-resolution time-frequency analysis was performed, implemented through a CWT using the Morlet (morl) wavelet and a DWT with a three-level decomposition using the sym2 wavelet and from the time-domain preprocessed signals, a comprehensive suite of established metrics is extracted, including Variance (var), RMS, Skewness, Kurtosis, and Mean Curve Length (MCL). The set is further augmented with new descriptors introduced in this model: Log Detector (LD), Standard Deviation (STD), and Mean Absolute Deviation (MAD).

4.13.1. The Log detector (LD)

The LD is a time-domain feature that quantifies the amplitude characteristics of a signal by computing the geometric mean of its absolute values. It is particularly useful for highlighting subtle fluctuations in EEG signals while reducing the influence of large spikes or outliers. In the following feature definitions, x_i is the i-th sample in the analysis window, μ is the window mean, and N is the total number of samples in the window. The LD can be expressed as:

$$\boldsymbol{LD = \exp\left(\frac{1}{N}\sum_{i=1}^{N} log(|x_i|)\right)} \tag{4.17}$$

The procedure involves first taking the logarithm of each sample's absolute value, averaging these logarithms, and then applying the exponential function to return to the linear scale. LD enhances the detection of subtle amplitude variations associated with different imagined movements, providing a discriminative feature for classifiers.

4.13.2. Mean Absolute Deviation (MAD) and Standard Deviation (STD)

Both MAD and STD are time-domain features that quantify the variability of a signal. MAD measures the average absolute deviation from the mean, providing a robust estimate less sensitive to extreme values or spikes. It is calculated as:

$$\boldsymbol{MAD = \frac{1}{N}\sum_{i=1}^{N} |x_i - \mu|} \tag{4.18}$$

STD measures the average squared deviation, emphasizing larger deviations. It is computed as:

$$\boldsymbol{STD = \sqrt{\frac{1}{N-1}\sum_{i=1}^{N} (x_i - \mu)^2}} \tag{4.19}$$

Together, they capture complementary aspects of variability in EEG signals, helping to distinguish different imagined movements in MI tasks.

After describing the individual features and their mathematical formulations, the following table summarizes all 220 proposed features in one comprehensive overview. Table 4.8 presents a detailed compilation of the 220 proposed features extracted from the EEG signals, covering both time-domain and time-frequency-domain features. For each feature, the table provides the corresponding mathematical formula, offering a comprehensive overview of the descriptors used for MI classification.

Table 4.8. Summary of the Proposed Features and Their Mathematical Expressions

features	mathematical formulas
f_n	$sum(cw_i(i1+1)^2)$ i =1...10 ; $i1$=1...4 ; n =1…40
f_n	$sqrt(f1_{n-40}/f1_{(n-40)+4})$ n =41…44
f_n	$sqrt(f1_{(n-44)+8}/f1_{(n-44)+12})$ n =45…48
f_n	$sqrt(f1_{(n-48)+16}/f1_{(n-48)+20})$ n =49…52
f_n	$sqrt(f1_{(n-52)+24}/f1_{(n-52)+28})$ n =53…56
f_n	$sqrt(f1_{(n-56)+32}/f1_{(n-56)+36})$ n =57…60
f_n	$sum(NDD_i{}^2)$ n =61…70
f_n	f_{n1}/f_{n1+1} $n1 = 61,63,65,67,69$; n =71…75
f_n	$mad(NDD_i)$ n =76…85
f_n	f_{n2}/f_{n2+1} $n2 = 76,78,80,82,84$ n =86…90
f_n	$var(NDD_i)$ n =91…100
f_n	f_{n3}/f_{n3+1} $n3 = 91,93,95,97,99$ n =101…105
f_n	$MCL(NDD_i)$ n =106…115
f_n	f_{n4}/f_{n4+1} $n4 = 106,108,110,112,114$ n =116…120
f_n	$skewness(NDD_i)$ n =121…130
f_n	f_{n5}/f_{n5+1} $n5 = 121,123,125,127,129$ n =131…135
f_n	$std(NDD_i)$ n =136…145
f_n	f_{n6}/f_{n6+1} $n6 = 136,138,140,142,144$ n =146…150
f_n	f_t/f_{t+15} $t = 121 \dots 130$ n =151…160
f_n	$kurtosis(NDD_i)$ n =161…170
f_n	f_{n7}/f_{n7+1} $n7 = 161,163,165,167,169$ n =171…175
f_n	$rms(NDD_i)$ n =176…185
f_n	f_{n8}/f_{n8+1} $n6 = 176,178,180,182,184$ n =186…190
f_n	$LD(NDD_i)$ n =191…200
f_n	f_{n9}/f_{n9+1} $n6 = 191,193,195,197,199$ n =201…205
f_n	$sum(A_{t3}{}^2/A_{t3+1}{}^2)$ $t3 = 1,3,5,7,9$ n =206…210
f_n	$mean(abs(A_{t3}/A_{t3+1}))$ n =211…215
f_n	$rms(abs(A_{t3}/A_{t3+1}))$ n =216…220

4.14. Optimization of temporal segmentation and feature classification results

In MI experiments, people don't all start imagining at the same time, nor do they imagine for exactly the same duration. As illustrated in Figure 4.10, each subject has their unique MI timing; some subjects begin immediately after seeing the visual cue, while others need more processing time. Some sustain the imagination briefly, while others maintain it longer. Therefore, using a fixed time window, such as 0-4 seconds after the visual cue, for all subjects is inherently suboptimal, as it fails to accommodate individual differences.

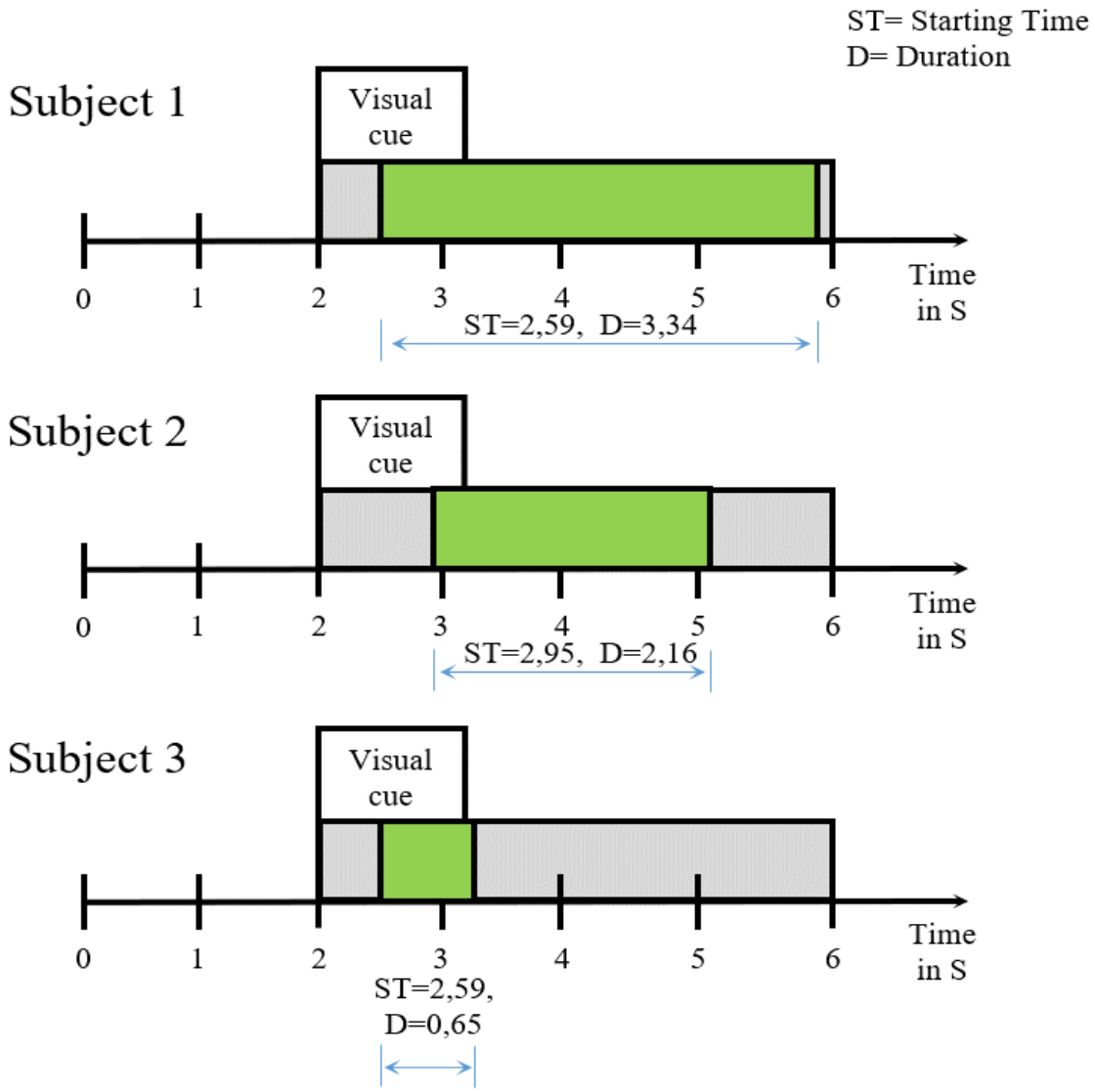

Figure 4.10. Subject-Specific MI Onset and Duration.

To address this critical challenge of inter-subject variability in task execution timing, we developed an integrated optimization framework. After extracting our comprehensive set of 220 features from each MI trial, this framework simultaneously finds the optimal subject-specific time window for analysis while assessing the discriminative ability of our feature set. By considering individual timing

differences, our approach makes sure that feature extraction happens during the most informative neural activity periods for each participant.

4.14.1. Optimization framework

Our approach employs the FA to search for subject-specific epoch parameters: the starting time and processing duration relative to the visual cue. The key innovation is that the optimization is directly guided by classification performance. For each candidate time window proposed by the Firefly Algorithm, we:

1. Segment the EEG data according to the candidate start time and duration
2. Extract all 220 features from this specific time window
3. Train and evaluate an LSVM classifier using 10-fold cross-validation
4. Use the resulting CA as the "fitness score" or "brightness" for that firefly

4.14.2. Firefly algorithm implementation

The FA operates by maintaining a population of candidate solutions (fireflies), where each firefly represents a possible (start time, duration) combination. Brighter fireflies, those yielding higher SVM CA attract other fireflies in the search space. Through iterative attraction and movement, the population converges toward the optimal time window that maximizes the separability of different MI classes based on our 220 features.

4.14.3. Classifier integration

The Linear SVM serves a dual role in our framework: first as the fitness evaluator during the Firefly optimization loop and second as the final classification model for four-class MI discrimination. We chose a linear kernel for its interpretability and computational efficiency with high-dimensional feature spaces, implementing a one-vs-one multi-class strategy. We employ a rigorous 10-fold cross-validation protocol to ensure that optimization and final evaluation remain strictly separate, providing an unbiased estimate of generalization performance.

4.14.4. Temporal optimization results

Table 4.9 presents the optimized temporal parameters and corresponding CA for all nine subjects. Our Firefly optimization identified substantial inter-subject variability in both starting times (range: 2.52-2.95s) and processing durations (range: 0.65-3.34s). Despite this diversity, every subject

showed improved CA compared to the fixed 2-4s window, with a mean improvement of 10.05%, and individual improvements ranged from +2.58% to +27.93%.

Table 4.9. CA of the Proposed Feature Set with Firefly-Optimized Parameters vs. Fixed Window

Subjects	Starting Time positions (S)	Processing Durations (S)	CA%	Fixed window (2-4s) CA%
S1	2.62	2.93	73.79	66.07
S2	2.59	3.34	62.36	52.78
S3	2.7	2.79	81.64	70.28
S4	2.59	2.70	45.5	42.92
S5	2.95	2.16	46.64	38.07
S6	2.59	0.73	56	45.57
S7	2.59	2.61	79.5	76.92
S8	2.52	2.81	78.36	68.64
S9	2.59	0.65	86.71	58.78
Mean			67.83%	57.78%

Our analysis reveals that optimal MI decoding requires personalized optimization of two key temporal parameters: starting time (onset latency) and processing duration. These parameters interact uniquely for each individual, forming distinct temporal signatures. The optimal combination varies substantially across subjects, explaining why fixed temporal parameters fail and cannot accommodate diverse individual timing strategies.

Notably, subjects with the shortest optimized durations (S6: 0.73s, S9: 0.65s) demonstrated that brief, precisely timed analysis windows can yield excellent performance (56.00% and 86.71% respectively). The optimized parameters reveal three distinct MI patterns: (1) brief, intense imaginers (S6, S9: <0.75s), (2) sustained processors (S2: 3.34s), and (3) moderate duration users (majority: 2.16-2.93s).

These findings demonstrate that MI decoding success depends on the optimal combination of starting time and duration, which varies substantially between individuals. The patterns range from brief, late-onset imagery (S9: 0.65s duration, 86.71% accuracy) to sustained processing (S2: 3.34s duration, 62.36% accuracy), with no universal optimal timing. Each subject has a unique temporal signature that our Firefly optimization discovers. This has practical implications for BCI design: rather than prescribing fixed temporal windows or training users toward standardized timing, systems must adapt to individual temporal patterns. Our framework accomplishes this by simultaneously optimizing both starting time and duration for each subject, validating the effectiveness of our subject-specific temporal optimization framework for personalized MI decoding.

4.15. Feature selection via GA

Following the identification of subject-specific optimal time windows through Firefly optimization, we extract the complete set of 220 features from these temporally aligned segments. To further enhance classification performance, we employ GA exclusively for feature selection. The GA operates on binary-encoded chromosomes where each bit represents the inclusion or exclusion of a corresponding feature, allowing the algorithm to explore different feature subset combinations. CA obtained via 10-fold cross-validation with a standard Linear SVM serves as the fitness function, guiding the evolutionary search toward the most discriminative feature subsets for each individual subject.

The GA optimization addresses a combinatorially vast search space comprising 2^{220} possible feature subsets. This astronomical number renders exhaustive search computationally infeasible, necessitating intelligent optimization heuristics. Using evolutionary principles of selection, crossover, and mutation, the GA navigates this immense search space, converging on feature subsets that maximize discriminative power for MI EEG classification. The algorithm balances exploration of novel feature combinations with exploitation of high-performing subsets, systematically evolving solutions over successive generations.

4.15.1. Feature selection results

This feature selection procedure achieves two key optimization objectives. First, it improves classification performance by concentrating on the most informative signal characteristics while discarding redundant or irrelevant features that could introduce noise or reduce classifier effectiveness. Second, it significantly lowers the feature dimensionality by approximately 77% in our results as detailed in Table 4.10, thereby alleviating high-dimensionality effects and minimizing computational costs. Despite representing only a small portion of the original feature set, the selected

subsets exhibit strong discriminative power across the four MI classes, demonstrating that classification performance is driven by the quality rather than the quantity of features.

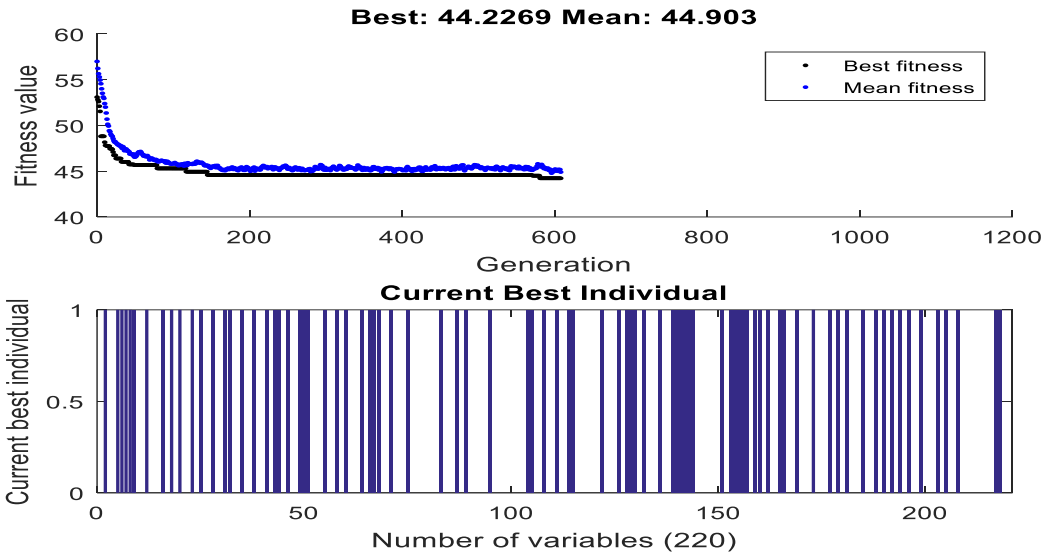

(a)

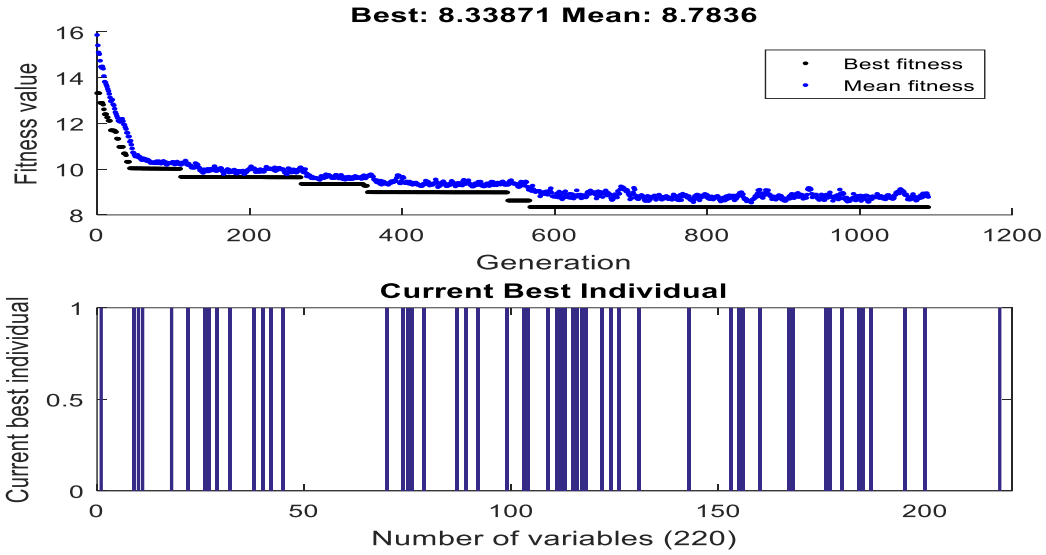

(b)

Figure 4.11. GA Feature Selection: (a) Selected features for subject 4 and (b) Selected features for subject 9.

Figure 4.11 presents two examples of the GA optimization process, showcasing feature selection for subject 4 with the lowest CA and subject 9 with the highest CA. These visualizations reveal how the algorithm converges toward optimal feature subsets while maintaining population diversity throughout the evolutionary process. As presented in Table 4.10, the GA-optimized feature selection achieves a mean CA of 78.30% across subjects, representing a 10.47% improvement over the full 220

features extracted from Firefly-optimized time windows while simultaneously reducing feature dimensionality by approximately 77%. This performance-dimensionality trade-off demonstrates the GA's effectiveness in identifying the most discriminative feature subsets from the complete feature set.

Table 4.10. Classification Performance After GA-Based Feature Selection

Subjects	SF	CA%
S1	49	87.07
S2	44	75.93
S3	37	89.71
S4	84	55.78
S5	93	65.43
S6	55	70.07
S7	51	90.36
S8	37	87.72
S9	53	91.67
Mean		78.30

4.16. Analysis of inter-subject performance variability through topographic mapping

The GA optimization combined with Linear SVM showed significant variation in performance between Subject 4 and Subject 9, with accuracies of 55.78% and 91.67%, respectively. This large gap of 35.89% led to a focused investigation into the neurophysiological reasons for these different results through topographic analysis of bioelectric signal distributions.

We conducted an in-depth examination of spatial activation patterns using the 10 channel NDD configuration. The analysis focused on RMS values of differential voltages, mapped topographically to visualize cortical activation strength and distribution during each MI condition. The color scale in Figure 4.12 represents RMS amplitude, with red regions indicating elevated activity and blue regions signifying reduced activity.

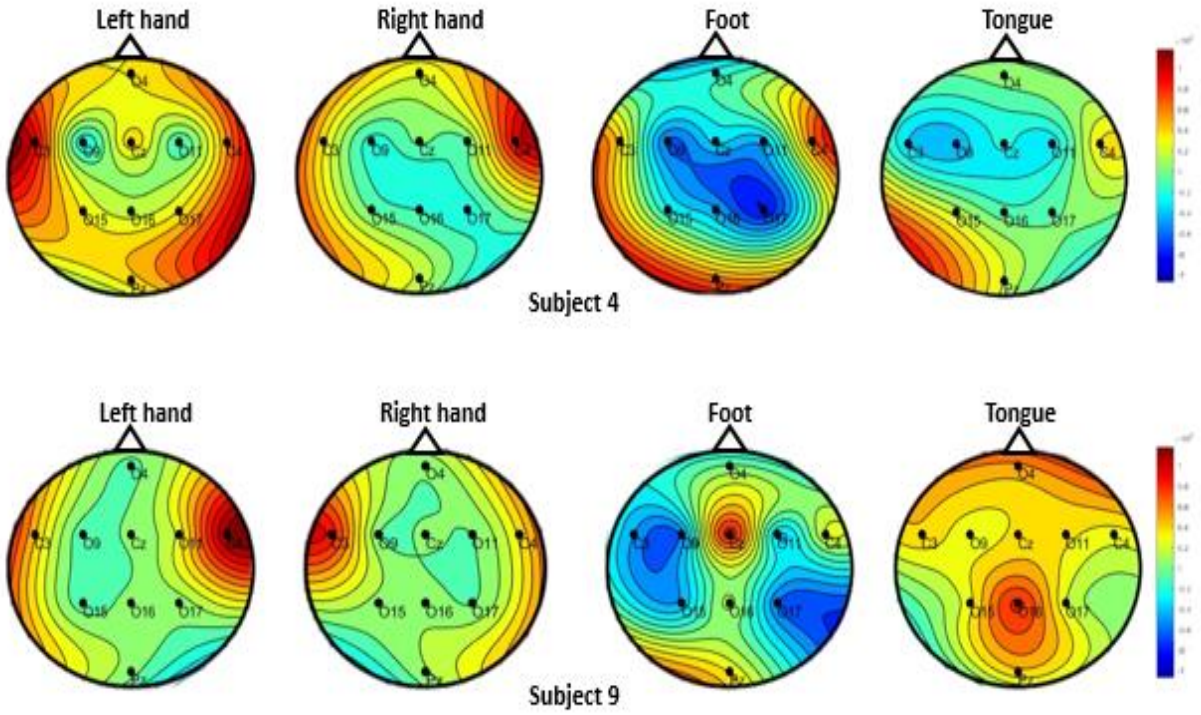

Figure 4.12. Comparative Topographic Maps of Cortical Activation During Four MI Tasks in Subjects 4 and 9.

As discussed in Chapter 1, MI tasks follow well-documented cortical activation patterns. Figure 4.12 presents comparative topographic distributions for subjects 4 and 9 across all four MI tasks, offering insight into the observed differences in CA. Subject 9 exhibits precise, task-appropriate spatial localization. Elevated RMS values appear over neuroanatomically correct regions: left-hand mouvement over the right sensorimotor cortex (C4 region), right-hand mouvement over the left sensorimotor cortex (C3 region), foot movements over the medial central region (Cz area), and tongue movements over the inferior sensorimotor cortex. These well-defined and anatomically consistent patterns yield class-separable feature representations that facilitate effective discrimination by the GA-optimized classifier. In contrast, Subject 4 demonstrates mislocalized activation patterns across all tasks. We can see that elevated activity appears in neuroanatomically incongruent regions, with foot and tongue activations particularly deviating from expected medial and inferior central distributions, even in left- and right-hand tasks, which exhibit diffuse or reversed lateralization, indicating poor spatial fidelity in the execution of MI. As a result, the extracted features for Subject 4 become highly overlapping and ambiguous, reducing classification separability.

This performance disparity arises not from algorithmic limitations but from fundamental differences in the neurophysiological quality of MI execution across all limb representations, highlighting the

importance of both proper task execution and accurate neural signal acquisition for optimal BCI outcomes.

4.17. Comparison with state-of-the-art methods

In the following subsection, we evaluate the performance of our proposed approach against established MI-BCI methods that use the same Dataset 5 (BCI competition IV Dataset 2a) to determine its comparative effectiveness

Table 4.11. CA comparison on Dataset 5

	Works	**methods**	**Acc (%)**
Dataset	K.K. Ang, et al 2012 [120].	FBCSP	67.42
	Ahn et al 2023 [123].	MS-TSformer-DS	70
	Dong et al 2020 [121].	PSCSP	74.39
	Amin et al 2019 [122].	MCNN	75.72
	Our work	**NDD with 220 features**	**78.30**

Table 4.11 provides a detailed comparison showing that our method, with an average accuracy of 78.30%, surpasses all other approaches listed, including both traditional machine-learning pipelines and recent DL models. Remarkably, this achievement is reached using a simple linear SVM classifier. This outcome illustrates that a well-designed preprocessing and feature engineering pipeline can match or even outperform the performance of much more complex and computationally intensive neural network architectures for MI classification.

4.18. Conclusion

This work presents a comprehensive EEG-based MI classification system that balances computational efficiency with high discriminative performance. The proposed pipeline introduces several methodological innovations:

1. Channel reduction using the NDD method, decreasing electrodes from 22 to 10 while preserving discriminative information.
2. Determining the optimal time windows for each person with the FA to match their unique MI response timing.

3. Extraction of the 220 proposed features from these personalized time windows.
4. GA-based feature selection to identify the most discriminative subset from the extracted features.

Combined with a linear SVM classifier, this approach achieved a CA of 78.30%, surpassing both traditional machine learning methods and several modern DL models.

The NDD channel reduction demonstrated that meaningful MI-related information can be preserved while mitigating computational complexity, despite decreasing the spatial dimensionality of the EEG montage. Moreover, the Firefly temporal parameter optimization identifies subject-specific analysis windows that capture the most discriminative neural activity periods and GA-based feature selection smartly tackled high-dimensional data by focusing on features that maximize class separability while minimizing redundancy.

A notable finding of this study is that the performance varies wildly between subjects. Subject 9 reached 91.67% CA, whereas Subject 4 achieved only 55.78% (a 35.89% gap). Through topographic RMS analysis, we demonstrated that this disparity stems from differences in the neurophysiological quality of MI execution. These results confirm that classification performance depends critically on the subject's ability to generate stable and neurophysiologically valid MI, not just on algorithmic sophistication.

Overall, these results show that carefully engineered signal processing strategies, even when combined with a simple classifier, can match or beat complex DL setups. They also spotlight how crucial proper MI execution and personal brain differences are for reliable BCIs. Future research should explore adaptive calibration strategies to mitigate inter-subject variability, as well as extend the NDD-based channel reduction approach to other BCI paradigms.

General Conclusions and Perspectives

The development of reliable and efficient MI-BCIs is still a major challenge in neural engineering, largely because EEG signals are highly non-stationary and subject-specific nature. This thesis was motivated by the need for interpretable, adaptive, and computationally efficient frameworks that can transform raw EEG activity into accurate MI commands without relying exclusively on opaque DL architectures. By combining neurophysiological foundations, machine learning methodologies, systematic use of public datasets, and original algorithmic developments, the work offers a coherent and holistic pathway for advancing MI-BCI system design.

The thesis begins with a comprehensive overview of the anatomical and functional principles of the human brain, with particular emphasis on the role of the sensorimotor cortex in MI. It further detailed the electrophysiological foundations of EEG and the operating principles of BCIs, providing the essential background for understanding the characteristics and challenges of EEG-MI signal decoding. Subsequent chapters review supervised and DL approaches for MI classification and analyze five widely used EEG datasets, emphasizing their variability in terms of subjects, tasks, recording setups, and labeling protocols. This critical examination highlights the limitations of current approaches, especially with respect to subject-specific adaptation and the interpretability of extracted features, which directly motivates the development of the novel processing pipeline introduced in this work.

Building on this foundation, the thesis advances two primary contributions that address complementary stages of the MI-BCI pipeline: the first targets robust adaptability across multiple datasets, while the second focuses on optimizing a single more challenging dataset (Dataset 5), which contains four-class MI tasks, using the NDD method for spatial filtering and channel reduction, combined with subject-specific tuning.

In Contribution 1, a comprehensive feature set derived from the time, frequency, and time–frequency domains was proposed within a systematically optimized, subject-specific pipeline. This began with identifying the optimal time processing duration, followed by feature selection to reduce dimensionality and enhance discriminability, and culminated in a novel WFF for feature-space transformation. This tailored approach achieved superior CA across four datasets (Dataset 1, Dataset 2, Dataset 3, and Dataset 4), outperforming several contemporary methods and reaffirming that a systematic, subject-tailored feature engineering pipeline remains highly competitive.

In Contribution 2, focus shifted to the Dataset 5 (BCI Competition IV 2a dataset), a substantially more challenging four-class MI benchmark encompassing left hand, right hand, feet, and tongue tasks. The pipeline began with spatial filtering and channel reduction using the NDD method, thereby enhancing signal discriminability while reducing computational complexity. Following feature extraction, a Firefly optimization algorithm was employed to find the optimal subject-specific processing windows (start time and duration), paired with GA-based feature selection to further refine the feature space, achieving a final CA of 78.30%. Furthermore, topographic mapping of inter-subject performance variability provided valuable insights into cortical activation differences, reinforcing the essential role of personalized BCI calibration.

Collectively, these contributions demonstrate that hybrid methodologies including signal processing, feature extraction/selection, and machine learning produce robust, efficient, and practical MI-BCIs without requiring complex DL architectures. Their consistent emphasis on subject-specific adaptability and interpretable features directly meets the real-world demands of BCI applications, where reliability, transparency, and personalized calibration remain paramount.

From a future perspective, several complementary research directions can extend and strengthen these EEG-based MI-BCI findings. First, developing inter- and intra-subject adaptation strategies incorporating transfer learning or adaptive mechanisms would better address EEG non-stationarity and variability. Second, advancing feature extraction and selection to yield more discriminative, physiologically interpretable representations would minimize class overlap and enhance system robustness. Third, adapting the framework for real-time, clinical, or embedded applications while reducing calibration time and computational demands would represent a significant step toward practical MI-BCI deployment.

In summary, this thesis has systematically addressed key challenges in MI-BCI design by introducing interpretable, subject-specific pipelines that balance performance, adaptability, and transparency. By validating the proposed frameworks on multiple public datasets, including the particularly challenging four-class dataset (Dataset 5), the work not only advances the state-of-the-art in CA but also reaffirms the enduring relevance of structured feature engineering in an era increasingly dominated by DL. The insights gained into inter-subject variability and the necessity of personalized calibration underscore a central tenet of practical BCI development: that the path to robust, real-world brain–computer interaction lies in harmonizing algorithmic innovation with the inherent neurophysiological diversity of individual users. This research thus contributes both methodologically and conceptually to the ongoing pursuit of accessible, reliable, and human-centered BCI technology.

Bibliographical References

[1] J. R. Wolpaw, J Del R. Millán, and N. F. Ramsey, "Brain-computer interfaces: Definitions and principles," in *Handbook of Clinical Neurology*, vol. 168, Elsevier, 2020, pp. 15–23. doi: 10.1016/B978-0-444-63934-9.00002-0.

[2] H. Berger, "Über das Elektrenkephalogramm des Menschen," *Arch. Für Psychiatr. Nervenkrankh.*, vol. 87, no. 1, pp. 527–570, Dec. 1929, doi: 10.1007/BF01797193.

[3] S. A. Cortez, C. Flores, and J. Andreu-Perez, "A Smart Home Control Prototype Using a P300-Based Brain–Computer Interface for Post-stroke Patients," *in Proc. 5th Brazilian Technology Symposium*, Cham, Switzerland, 2021, pp. 131–139. doi: 10.1007/978-3-030-57566-3_13.

[4] Z. Liu, J. Shore, M. Wang, F. Yuan, A. Buss, and X. Zhao, "A systematic review on hybrid EEG/fNIRS in brain-computer interface," *Biomed. Signal Process. Control*, vol. 68, p. 102595, Jul. 2021, doi: 10.1016/j.bspc.2021.102595.

[5] Xinyi Yong, R. K. Ward, and G. E. Birch, "Facial EMG contamination of EEG signals: Characteristics and effects of spatial filtering," in *2008 3rd International Symposium on Communications, Control and Signal Processing*, St. Julian's, Malta: IEEE, Mar. 2008, pp. 729–734. doi: 10.1109/ISCCSP.2008.4537319.

[6] S. Herculano-Houzel, *The Human Advantage: A New Understanding of How Our Brain Became Remarkable*. The MIT Press, 2016. doi: 10.7551/mitpress/9780262034258.001.0001.

[7] E. R. Kandel, J. Koester, S. Mack, and S. Siegelbaum, Eds., *Principles of neural science*, Sixth edition. New York: McGraw Hill, 2021.

[8] J. E. H. Pittella, "The uniqueness of the human brain: a review," *Dement. Neuropsychol.*, vol. 18, p. e20230078, 2023, doi: 10.1590/1980-5764-dn-2023-0078.

[9] J. S. O'Brien and E. L. Sampson, "Lipid composition of the normal human brain: gray matter, white matter, and myelin," *J. Lipid Res.*, vol. 6, no. 4, pp. 537–544, Oct. 1965.

[10] L. R. Squire, D. Berg, F. E. Bloom, S. du Lac, A. Ghosh, and N. C. Spitzer, Eds., *Fundamental neuroscience*, Fourth edition. Amsterdam Boston Heidelberg: Elsevier, Academic Press, 2012.

[11] R. Douglas Fields, "White Matter Matters," *Sci. Am.*, vol. 298, no. 3, pp. 54–61, Mar. 2008, doi: 10.1038/scientificamerican0308-54.

[12] M. Mesulam, "From sensation to cognition," *Brain*, vol. 121, no. 6, pp. 1013–1052, Jun. 1998, doi: 10.1093/brain/121.6.1013.

[13] S. E. Petersen and O. Sporns, "Brain Networks and Cognitive Architectures," *Neuron*, vol. 88, no. 1, pp. 207–219, Oct. 2015, doi: 10.1016/j.neuron.2015.09.027.

[14] S. Standring, Ed., *Gray's Anatomy: the anatomical basis of clinical practice*, 42nd edition. Amsterdam: Elsevier, 2021.

[15] T. W. Vanderah and D. J. Gould, *Nolte's the human brain: an introduction to its functional anatomy*, 8. edition. Philadelphia, PA: Elsevier, 2020.

[16] M. F. Bear, B. W. Connors, and M. A. Paradiso, *Neuroscience: exploring the brain*, 3. ed. Baltimore, Md.: Lippincott Williams & Wilkins, 2006.

[17] D. S. Bassett and O. Sporns, "Network neuroscience," *Nat. Neurosci.*, vol. 20, no. 3, pp. 353–364, Mar. 2017, doi: 10.1038/nn.4502.

[18] Z. He and Y. Jin, "Intrinsic Control of Axon Regeneration," *Neuron*, vol. 90, no. 3, pp. 437–451, May 2016, doi: 10.1016/j.neuron.2016.04.022.

[19] N. J. Allen and B. A. Barres, "Glia — more than just brain glue," *Nature*, vol. 457, no. 7230, pp. 675–677, Feb. 2009, doi: 10.1038/457675a.

[20] B. Pakkenberg and H. J. Gundersen, "Neocortical neuron number in humans: effect of sex and age," *J. Comp. Neurol.*, vol. 384, no. 2, pp. 312–320, Jul. 1997.

[21] G. Buzsáki, C. A. Anastassiou, and C. Koch, "The origin of extracellular fields and currents — EEG, ECoG, LFP and spikes," *Nat. Rev. Neurosci.*, vol. 13, no. 6, pp. 407–420, Jun. 2012, doi: 10.1038/nrn3241.

[22] A. L. Hodgkin and A. F. Huxley, "A quantitative description of membrane current and its application to conduction and excitation in nerve," *J. Physiol.*, vol. 117, no. 4, pp. 500–544, Aug. 1952, doi: 10.1113/jphysiol.1952.sp004764.
[23] V. Pizzella, L. Marzetti, S. Della Penna, F. de Pasquale, F. Zappasodi, and G. L. Romani, "Magnetoencephalography in the study of brain dynamics," *Funct. Neurol.*, vol. 29, no. 4, pp. 241–253, 2014.
[24] G. H. Glover, "Overview of Functional Magnetic Resonance Imaging," *Neurosurg. Clin. N. Am.*, vol. 22, no. 2, pp. 133–139, Apr. 2011, doi: 10.1016/j.nec.2010.11.001.
[25] D. L. Schomer, F. H. Lopes da Silva, and E. Niedermeyer, Eds., *Electroencephalography: basic principles, clinical applications, and related fields*, Seventh edition. New York, NY: Oxford University Press, 2018.
[26] J. S. Kumar and P. Bhuvaneswari, "Analysis of Electroencephalography (EEG) Signals and Its Categorization–A Study," *Procedia Eng.*, vol. 38, pp. 2525–2536, 2012, doi: 10.1016/j.proeng.2012.06.298.
[27] M. Aldayel, M. Ykhlef, and A. Al-Nafjan, "Deep Learning for EEG-Based Preference Classification in Neuromarketing," *Appl. Sci.*, vol. 10, no. 4, p. 1525, Feb. 2020, doi: 10.3390/app10041525.
[28] J. N. Acharya, A. Hani, J. Cheek, P. Thirumala, and T. N. Tsuchida, "American Clinical Neurophysiology Society Guideline 2: Guidelines for Standard Electrode Position Nomenclature," *J. Clin. Neurophysiol.*, vol. 33, no. 4, pp. 308–311, Aug. 2016, doi: 10.1097/WNP.0000000000000316.
[29] O. Mecarelli, "Electrode Placement Systems and Montages," in *Clinical Electroencephalography*, O. Mecarelli, Ed., Cham: Springer International Publishing, 2019, pp. 35–52. doi: 10.1007/978-3-030-04573-9_4.
[30] J. Cheng *et al.*, "EEG feature extraction methods in motor imagery-based brain-computer interfaces: a systematic review and network meta-analysis," *Brain-Appar. Commun. J. Bacomics*, vol. 4, no. 1, Dec. 2025, doi: 10.1080/27706710.2025.2523303.
[31] H. Ramoser, J. Muller-Gerking, and G. Pfurtscheller, "Optimal spatial filtering of single trial EEG during imagined hand movement," *IEEE Trans. Rehabil. Eng.*, vol. 8, no. 4, pp. 441–446, Dec. 2000, doi: 10.1109/86.895946.
[32] X. Lun, Z. Yu, F. Wang, T. Chen, and Y. Hou, "A novel approach of CNN for human motor imagery recognition using the virtual electrode pairs," *J. Intell. Fuzzy Syst.*, vol. 40, no. 3, pp. 5275–5288, Mar. 2021, doi: 10.3233/JIFS-202046.
[33] P. Tufvesson and F. Heskebeck, "Automatic control of reactive brain computer interfaces," *IFAC J. Syst. Control*, vol. 27, Mar. 2024, doi: 10.1016/j.ifacsc.2024.100251.
[34] T. O. Zander and C. Kothe, "Towards passive brain–computer interfaces: applying brain–computer interface technology to human–machine systems in general," *J. Neural Eng.*, vol. 8, no. 2, Apr. 2011, doi: 10.1088/1741-2560/8/2/025005.
[35] G. Pfurtscheller *et al.*, "The hybrid BCI," *Front. Neurosci.*, vol. 4, 2010, doi: 10.3389/fnpro.2010.00003.
[36] H. Yang, K. A. Paller, and M. Van Vugt, "The steady state visual evoked potential (SSVEP) tracks 'sticky' thinking, but not more general mind-wandering," *Front. Hum. Neurosci.*, vol. 16, Aug. 2022, doi: 10.3389/fnhum.2022.892863.
[37] I. Demchenko, T. Shavit, M. Benyamini, and M. Zacksenhouse, "Self-correcting brain computer interface based on classification of multiple error-related potentials," *J. Neural Eng.*, vol. 22, no. 2, Apr. 2025, doi: 10.1088/1741-2552/adbcda.
[38] S. K. Mudgal, S. K. Sharma, J. Chaturvedi, and A. Sharma, "Brain computer interface advancement in neurosciences: applications and issues," *Interdiscip. Neurosurg.*, vol. 20, Jun. 2020, doi: 10.1016/j.inat.2020.100694.
[39] H. Gevensleben *et al.*, "Neurofeedback of slow cortical potentials: neural mechanisms and feasibility of a placebo-controlled design in healthy adults," *Front. Hum. Neurosci.*, vol. 8, no. 990, Dec. 2014, doi: 10.3389/fnhum.2014.00990.

[40] G. Di Pellegrino, L. Fadiga, L. Fogassi, V. Gallese, and G. Rizzolatti, "Understanding motor events: a neurophysiological study," *Exp. Brain Res.*, vol. 91, no. 1, pp. 176–180, Oct. 1992, doi: 10.1007/BF00230027.

[41] M. Jeannerod, "Neural Simulation of Action: A Unifying Mechanism for Motor Cognition," *NeuroImage*, vol. 14, no. 1, pp. S103–S109, Jul. 2001, doi: 10.1006/nimg.2001.0832.

[42] K. K. Ang *et al.*, "A Randomized Controlled Trial of EEG-Based Motor Imagery Brain-Computer Interface Robotic Rehabilitation for Stroke," *Clin. EEG Neurosci.*, vol. 46, no. 4, pp. 310–320, Oct. 2015, doi: 10.1177/1550059414522229.

[43] J. Meng, S. Zhang, A. Bekyo, J. Olsoe, B. Baxter, and B. He, "Noninvasive Electroencephalogram Based Control of a Robotic Arm for Reach and Grasp Tasks," *Sci. Rep.*, vol. 6, no. 1, p. 38565, Dec. 2016, doi: 10.1038/srep38565.

[44] O. R. Pinheiro, L. R. G. Alves, and J. R. D. Souza, "EEG Signals Classification: Motor Imagery for Driving an Intelligent Wheelchair," *IEEE Lat. Am. Trans.*, vol. 16, no. 1, pp. 254–259, Jan. 2018, doi: 10.1109/TLA.2018.8291481.

[45] M. Ahn and S. C. Jun, "Performance variation in motor imagery brain–computer interface: A brief review," *J. Neurosci. Methods*, vol. 243, pp. 103–110, Mar. 2015, doi: 10.1016/j.jneumeth.2015.01.033.

[46] M. C. Thompson, "Critiquing the Concept of BCI Illiteracy," *Sci. Eng. Ethics*, vol. 25, no. 4, pp. 1217–1233, Aug. 2019, doi: 10.1007/s11948-018-0061-1.

[47] H. Altaheri *et al.*, "Deep learning techniques for classification of electroencephalogram (EEG) motor imagery (MI) signals: a review," *Neural Comput. Appl.*, vol. 35, no. 20, pp. 14681–14722, Jul. 2023, doi: 10.1007/s00521-021-06352-5.

[48] D. Wu, J.-T. King, C.-H. Chuang, C.-T. Lin, and T.-P. Jung, "Spatial Filtering for EEG-Based Regression Problems in Brain–Computer Interface (BCI)," *IEEE Trans. Fuzzy Syst.*, vol. 26, no. 2, pp. 771–781, Apr. 2018, doi: 10.1109/TFUZZ.2017.2688423.

[49] F. Lotte *et al.*, "A review of classification algorithms for EEG-based brain–computer interfaces: a 10 year update," *J. Neural Eng.*, vol. 15, no. 3, p. 031005, Jun. 2018, doi: 10.1088/1741-2552/aab2f2.

[50] B. Blankertz *et al.*, "The Berlin Brain–Computer Interface: Non-Medical Uses of BCI Technology," *Front. Neurosci.*, vol. 4, no. 198, 2010, doi: 10.3389/fnins.2010.00198.

[51] X. Wang, H. Lu, X. Shen, L. Ma, and Y. Wang, "Prosthetic control system based on motor imagery," *Comput. Methods Biomech. Biomed. Engin.*, vol. 25, no. 7, pp. 764–771, May 2022, doi: 10.1080/10255842.2021.1977800.

[52] Z.-Z. Ma *et al.*, "Motor imagery-based brain–computer interface rehabilitation programs enhance upper extremity performance and cortical activation in stroke patients," *J. NeuroEngineering Rehabil.*, vol. 21, no. 1, p. 91, May 2024, doi: 10.1186/s12984-024-01387-w.

[53] Á. Costa-García *et al.*, "Model for prompt and effective classification of motion recovery after stroke considering muscle strength and coordination factors," *J. NeuroEngineering Rehabil.*, vol. 16, no. 1, p. 130, Dec. 2019, doi: 10.1186/s12984-019-0611-z.

[54] S. Akuthota *et al.*, "Enhancing Real-Time Cursor Control with Motor Imagery and Deep Neural Networks for Brain–Computer Interfaces," *Information*, vol. 15, no. 11, p. 702, Nov. 2024, doi: 10.3390/info15110702.

[55] L. Yang and M. M. Van Hulle, "Real-Time Navigation in Google Street View® Using a Motor Imagery-Based BCI," *Sensors*, vol. 23, no. 3, p. 1704, Feb. 2023, doi: 10.3390/s23031704.

[56] P. Arpaia *et al.*, "Endless Runner Game in Virtual Reality Controlled by a Self-paced Brain-Computer Interface Based on EEG and Motor Imagery," *in Proc. Extended Reality*, Cham, Switzerland, 2024, pp. 208–225. doi: 10.1007/978-3-031-71704-8_16.

[57] A. Korik *et al.*, "Competing at the Cybathlon championship for people with disabilities: long-term motor imagery brain–computer interface training of a cybathlete who has tetraplegia," *J. NeuroEngineering Rehabil.*, vol. 19, no. 1, p. 95, Sep. 2022, doi: 10.1186/s12984-022-01073-9.

[58] S. M. Christensen, N. S. Holm, and S. Puthusserypady, "An Improved Five Class MI Based BCI Scheme for Drone Control Using Filter Bank CSP," in *2019 7th International Winter Conference on Brain-Computer Interface (BCI)*, Gangwon, Korea (South): IEEE, Feb. 2019, pp. 1–6. doi: 10.1109/IWW-BCI.2019.8737263.

[59] Q. Ai, M. Zhao, K. Chen, X. Zhao, L. Ma, and Q. Liu, "Flexible coding scheme for robotic arm control driven by motor imagery decoding," *J. Neural Eng.*, vol. 19, no. 5, p. 056008, Oct. 2022, doi: 10.1088/1741-2552/ac84a9.

[60] L. Pillette, B. N'Kaoua, R. Sabau, B. Glize, and F. Lotte, "Multi-Session Influence of Two Modalities of Feedback and Their Order of Presentation on MI-BCI User Training," *Multimodal Technol. Interact.*, vol. 5, no. 3, p. 12, Mar. 2021, doi: 10.3390/mti5030012.

[61] N. Tibrewal, N. Leeuwis, and M. Alimardani, "Classification of motor imagery EEG using deep learning increases performance in inefficient BCI users," *PLOS ONE*, vol. 17, no. 7, p. e0268880, Jul. 2022, doi: 10.1371/journal.pone.0268880.

[62] C. C. Aggarwal, *Data classification: algorithms and applications*, Online-Ausg. in Chapman & Hall, no. Volume 35. Boca Raton, Florida: CRC Press, Taylor & Francis Group, 2015.

[63] M. Saeidi *et al.*, "Neural Decoding of EEG Signals with Machine Learning: A Systematic Review," *Brain Sci.*, vol. 11, no. 11, p. 1525, Nov. 2021, doi: 10.3390/brainsci11111525.

[64] S. Albawi, O. Bayat, S. Al-Azawi, and O. N. Ucan, "Social Touch Gesture Recognition Using Convolutional Neural Network," *Comput. Intell. Neurosci.*, vol. 2018, p. 6973103, 2018, doi: 10.1155/2018/6973103.

[65] H. Yang, S. Sakhavi, K. K. Ang, and C. Guan, "On the use of convolutional neural networks and augmented CSP features for multi-class motor imagery of EEG signals classification," in *2015 37th Annual International Conference of the IEEE Engineering in Medicine and Biology Society (EMBC)*, Milan: IEEE, Aug. 2015, pp. 2620–2623. doi: 10.1109/EMBC.2015.7318929.

[66] W. Qiao and X. Bi, "Deep Spatial-Temporal Neural Network for Classification of EEG-Based Motor Imagery," in *Proceedings of the 2019 International Conference on Artificial Intelligence and Computer Science*, Wuhan Hubei China: ACM, Jul. 2019, pp. 265–272. doi: 10.1145/3349341.3349414.

[67] Z. Tang, C. Li, and S. Sun, "Single-trial EEG classification of motor imagery using deep convolutional neural networks," *Optik*, vol. 130, pp. 11–18, Feb. 2017, doi: 10.1016/j.ijleo.2016.10.117.

[68] R. Mane, N. Robinson, A. P. Vinod, S.-W. Lee, and C. Guan, "A Multi-view CNN with Novel Variance Layer for Motor Imagery Brain Computer Interface," in *2020 42nd Annual International Conference of the IEEE Engineering in Medicine & Biology Society (EMBC)*, Montreal, QC, Canada: IEEE, Jul. 2020, pp. 2950–2953. doi: 10.1109/EMBC44109.2020.9175874.

[69] S. Wu, K. Bhadra, A.-L. Giraud, and S. Marchesotti, "Adaptive LDA Classifier Enhances Real-Time Control of an EEG Brain–Computer Interface for Decoding Imagined Syllables," *Brain Sci.*, vol. 14, no. 3, p. 196, Feb. 2024, doi: 10.3390/brainsci14030196.

[70] Y. El Ouahidi, V. Gripon, B. Pasdeloup, G. Bouallegue, N. Farrugia, and G. Lioi, "A Strong and Simple Deep Learning Baseline for BCI Motor Imagery Decoding," *IEEE Trans. Neural Syst. Rehabil. Eng.*, vol. 32, pp. 3338–3347, 2024, doi: 10.1109/TNSRE.2024.3451010.

[71] V. Jusas and S. G. Samuvel, "Classification of Motor Imagery Using Combination of Feature Extraction and Reduction Methods for Brain-Computer Interface," *Inf. Technol. Control*, vol. 48, no. 2, pp. 225–234, Jun. 2019, doi: 10.5755/j01.itc.48.2.23091.

[72] P. Kant, S. H. Laskar, J. Hazarika, and R. Mahamune, "CWT Based Transfer Learning for Motor Imagery Classification for Brain computer Interfaces," *J. Neurosci. Methods*, vol. 345, p. 108886, Nov. 2020, doi: 10.1016/j.jneumeth.2020.108886.

[73] X. Ma, D. Wang, D. Liu, and J. Yang, "DWT and CNN based multi-class motor imagery electroencephalographic signal recognition," *J. Neural Eng.*, vol. 17, no. 1, p. 016073, Feb. 2020, doi: 10.1088/1741-2552/ab6f15.

[74] W. Ren, M. Han, J. Wang, D. Wang, and T. Li, "Efficient feature extraction framework for EEG signals classification," in *2016 Seventh International Conference on Intelligent Control and Information Processing (ICICIP)*, Siem Reap, Cambodia: IEEE, Dec. 2016, pp. 167–172. doi: 10.1109/ICICIP.2016.7885895.

[75] C. Park, D. Looney, N. Ur Rehman, A. Ahrabian, and D. P. Mandic, "Classification of Motor Imagery BCI Using Multivariate Empirical Mode Decomposition," *IEEE Trans. Neural Syst. Rehabil. Eng.*, vol. 21, no. 1, pp. 10–22, Jan. 2013, doi: 10.1109/TNSRE.2012.2229296.

[76] L. Wang, G. Xu, J. Wang, S. Yang, and W. Yan, "Motor Imagery BCI Research Based on Hilbert-Huang Transform and Genetic Algorithm," in *2011 5th International Conference on Bioinformatics and Biomedical Engineering*, Wuhan, China: IEEE, May 2011, pp. 1–4. doi: 10.1109/icbbe.2011.5780181.

[77] M. Z. Baig, N. Aslam, H. P. H. Shum, and L. Zhang, "Differential evolution algorithm as a tool for optimal feature subset selection in motor imagery EEG," *Expert Syst. Appl.*, vol. 90, pp. 184–195, Dec. 2017, doi: 10.1016/j.eswa.2017.07.033.

[78] S. Bhattacharyya, A. Khasnobish, S. Chatterjee, A. Konar, and D. N. Tibarewala, "Performance analysis of LDA, QDA and KNN algorithms in left-right limb movement classification from EEG data," in *2010 International Conference on Systems in Medicine and Biology*, Kharagpur, India: IEEE, Dec. 2010, pp. 126–131. doi: 10.1109/ICSMB.2010.5735358.

[79] K. Mebarkia and A. Reffad, "Multi optimized SVM classifiers for motor imagery left and right hand movement identification," *Australas. Phys. Eng. Sci. Med.*, vol. 42, no. 4, pp. 949–958, Dec. 2019, doi: 10.1007/s13246-019-00793-y.

[80] R. A. Khan *et al.*, "A novel framework for classification of two-class motor imagery EEG signals using logistic regression classification algorithm," *PLOS ONE*, vol. 18, no. 9, p. e0276133, Sep. 2023, doi: 10.1371/journal.pone.0276133.

[81] A. Mandilara, A. D. Papadopoulos, and D. Syvridis, "Learning kernels with quantum optical circuits," 2025, *arXiv*. doi: 10.48550/ARXIV.2509.12072.

[82] S. Har-Peled, P. Indyk, and R. Motwani, "Approximate nearest neighbors: towards removing the curse of dimensionality," *Theory Comput.*, vol. 8, no. 1, pp. 321–350, 2012, doi: 10.4086/toc.2012.v008a014.

[83] K. Chomboon, P. Chujai, P. Teerarassammee, K. Kerdprasop, and N. Kerdprasop, "An Empirical Study of Distance Metrics for k-Nearest Neighbor Algorithm," in *The Proceedings of the 2nd International Conference on Industrial Application Engineering 2015*, The Institute of Industrial Applications Engineers, 2015, pp. 280–285. doi: 10.12792/iciae2015.051.

[84] M. Dash and H. Liu, "Feature selection for classification," *Intell. Data Anal.*, vol. 1, no. 1–4, pp. 131–156, 1997, doi: 10.1016/S1088-467X(97)00008-5.

[85] I. T. Jolliffe and J. Cadima, "Principal component analysis: a review and recent developments," *Philos. Trans. R. Soc. Math. Phys. Eng. Sci.*, vol. 374, no. 2065, p. 20150202, Apr. 2016, doi: 10.1098/rsta.2015.0202.

[86] Md. A. M. Joadder, J. J. Myszewski, M. H. Rahman, and I. Wang, "A performance based feature selection technique for subject independent MI based BCI," *Health Inf. Sci. Syst.*, vol. 7, no. 1, p. 15, Dec. 2019, doi: 10.1007/s13755-019-0076-2.

[87] R. Corralejo, R. Hornero, and D. Alvarez, "Feature selection using a genetic algorithm in a motor imagery-based Brain Computer Interface," in *2011 Annual International Conference of the IEEE Engineering in Medicine and Biology Society*, Boston, MA: IEEE, Aug. 2011, pp. 7703–7706. doi: 10.1109/IEMBS.2011.6091898.

[88] J. H. Holland, *Adaptation in natural and artificial systems: an introductory analysis with applications to biology, control, and artificial intelligence*. Ann Arbor: Univ. of Michigan Press, 1975.

[89] D. E. Goldberg, *Genetic algorithms in search, optimization, and machine learning*, 30. print. Boston: Addison-Wesley, 1989.

[90] B. Wutzl, K. Leibnitz, F. Rattay, M. Kronbichler, M. Murata, and S. M. Golaszewski, "Genetic

algorithms for feature selection when classifying severe chronic disorders of consciousness," *PLOS ONE*, vol. 14, no. 7, p. e0219683, Jul. 2019, doi: 10.1371/journal.pone.0219683.

[91] Y. Jung, "Multiple predicting *K* -fold cross-validation for model selection," *J. Nonparametric Stat.*, vol. 30, no. 1, pp. 197–215, Jan. 2018, doi: 10.1080/10485252.2017.1404598.

[92] B. G. Marcot and A. M. Hanea, "What is an optimal value of k in k-fold cross-validation in discrete Bayesian network analysis?," *Comput. Stat.*, vol. 36, no. 3, pp. 2009–2031, Sep. 2021, doi: 10.1007/s00180-020-00999-9.

[93] A. Subasi and S. Mian Qaisar, "The Ensemble Machine Learning-Based Classification of Motor Imagery Tasks in Brain-Computer Interface," *J. Healthc. Eng.*, vol. 2021, pp. 1–12, Nov. 2021, doi: 10.1155/2021/1970769.

[94] B. Blankertz *et al.*, "The BCI competition III: validating alternative approaches to actual BCI problems," *IEEE Trans. Neural Syst. Rehabil. Eng.*, vol. 14, no. 2, pp. 153–159, Jun. 2006, doi: 10.1109/TNSRE.2006.875642.

[95] B. Blankertz *et al.*, "The BCI competition 2003: progress and perspectives in detection and discrimination of EEG single trials," *IEEE Trans. Biomed. Eng.*, vol. 51, no. 6, pp. 1044–1051, Jun. 2004, doi: 10.1109/TBME.2004.826692.

[96] R. Leeb, C. Brunner, G. Müller-Putz, A. Schlögl, and G. Pfurtscheller, "BCI Competition 2008–Graz data set B," *Graz Univ. Technol. Austria*, vol. 16, pp. 1–6, Jan. 2008.

[97] M.-H. Lee *et al.*, "EEG dataset and OpenBMI toolbox for three BCI paradigms: an investigation into BCI illiteracy," *GigaScience*, vol. 8, no. 5, p. giz002, May 2019, doi: 10.1093/gigascience/giz002.

[98] C. Brunner, R. Leeb, G. Müller-Putz, A. Schlögl, and G. Pfurtscheller, "BCI Competition 2008–Graz data set A," *Graz Univ. Technol. Austria*, vol. 16, pp. 1–6, Jan. 2008.

[99] C. Neuper, R. Scherer, M. Reiner, and G. Pfurtscheller, "Imagery of motor actions: Differential effects of kinesthetic and visual–motor mode of imagery in single-trial EEG," *Cogn. Brain Res.*, vol. 25, no. 3, pp. 668–677, Dec. 2005, doi: 10.1016/j.cogbrainres.2005.08.014.

[100] P. Dreyer, A. Roc, L. Pillette, S. Rimbert, and F. Lotte, "A large EEG database with users' profile information for motor imagery brain-computer interface research," *Sci. Data*, vol. 10, no. 1, p. 580, Sep. 2023, doi: 10.1038/s41597-023-02445-z.

[101] T. Ono, A. Kimura, and J. Ushiba, "Daily training with realistic visual feedback improves reproducibility of event-related desynchronisation following hand motor imagery," *Clin. Neurophysiol.*, vol. 124, no. 9, pp. 1779–1786, Sep. 2013, doi: 10.1016/j.clinph.2013.03.006.

[102] J. Too, A. Rahim, and N. Mohd, "Classification of Hand Movements based on Discrete Wavelet Transform and Enhanced Feature Extraction," *Int. J. Adv. Comput. Sci. Appl.*, vol. 10, no. 6, 2019, doi: 10.14569/IJACSA.2019.0100612.

[103] L. Fabien, L. Anatole, L. Fabrice, and A. Bruno, "Studying the Use of Fuzzy Inference Systems for Motor Imagery Classification," *IEEE Trans. Neural Syst. Rehabil. Eng.*, vol. 15, no. 2, pp. 322–324, Jun. 2007, doi: 10.1109/TNSRE.2007.897032.

[104] M. Zhong, F. Lotte, M. Girolami, and A. Lécuyer, "Classifying EEG for brain computer interfaces using Gaussian processes," *Pattern Recognit. Lett.*, vol. 29, no. 3, pp. 354–359, Feb. 2008, doi: 10.1016/j.patrec.2007.10.009.

[105] N. Brodu, F. Lotte, and A. Lecuyer, "Comparative study of band-power extraction techniques for Motor Imagery classification," in *2011 IEEE Symposium on Computational Intelligence, Cognitive Algorithms, Mind, and Brain (CCMB)*, Paris, France: IEEE, Apr. 2011, pp. 1–6. doi: 10.1109/CCMB.2011.5952105.

[106] N. Brodu, F. Lotte, and A. Lécuyer, "Exploring two novel features for EEG-based brain–computer interfaces: Multifractal cumulants and predictive complexity," *Neurocomputing*, vol. 79, pp. 87–94, Mar. 2012, doi: 10.1016/j.neucom.2011.10.010.

[107] H. Bashashati, R. K. Ward, G. E. Birch, and A. Bashashati, "Comparing Different Classifiers in Sensory Motor Brain Computer Interfaces," *PLOS ONE*, vol. 10, no. 6, p. e0129435, Jun. 2015, doi: 10.1371/journal.pone.0129435.

[108] W. CHEN, X. WANG, and T. ZHANG, "Research of Discrimination Between Left and Right

Hand Motor Imagery EEG Patterns Based on Tunable Q-Factor Wavelet Transform," *J. Electron. Inf. Technol.*, vol. 41, no. 3, pp. 530–536, 2019, doi: 10.11999/JEIT171191.

[109] Y. You, W. Chen, and T. Zhang, "Motor imagery EEG classification based on flexible analytic wavelet transform," *Biomed. Signal Process. Control*, vol. 62, p. 102069, Sep. 2020, doi: 10.1016/j.bspc.2020.102069.

[110] L. Chong, Z. Hai-Bin, L. Chun-Sheng, and W. Hong, "CSP/SVM-based EEG classification of imagined hand movements," *J. Northeast. Univ.*, vol. 31, no. 8, pp. 1098–1101, 2010.

[111] T. U. Jang, B. M. Kim, Y. M. Yang, W. Lim, and D. H. Oh, "Motor-imagery EEG signal classification using position matching and vector quantisation," *Int. J. Telemed. Clin. Pract.*, vol. 1, no. 4, pp. 306–313, 2016, doi: 10.1504/IJTMCP.2016.078426.

[112] A. Khasnobish, S. Bhattacharyya, A. Konar, and D. N. Tibarewala, "K-nearest neighbor classification of left-right limb movement using EEG data," in *In oral presentation in International conference on Biomedical Engineering and assistive technologies*, NIT Jalandhar, 2010.

[113] Y. R. Tabar and U. Halici, "A novel deep learning approach for classification of EEG motor imagery signals," *J. Neural Eng.*, vol. 14, no. 1, p. 016003, Feb. 2017, doi: 10.1088/1741-2560/14/1/016003.

[114] S. Salimpour, H. Kalbkhani, S. Seyyedi, and V. Solouk, "Stockwell transform and semi-supervised feature selection from deep features for classification of BCI signals," *Sci. Rep.*, vol. 12, no. 1, p. 11773, Jul. 2022, doi: 10.1038/s41598-022-15813-3.

[115] E. Dagdevir and M. Tokmakci, "Optimization of preprocessing stage in EEG based BCI systems in terms of accuracy and timing cost," *Biomed. Signal Process. Control*, vol. 67, p. 102548, May 2021, doi: 10.1016/j.bspc.2021.102548.

[116] Y. Han, B. Wang, J. Luo, L. Li, and X. Li, "A classification method for EEG motor imagery signals based on parallel convolutional neural network," *Biomed. Signal Process. Control*, vol. 71, p. 103190, Jan. 2022, doi: 10.1016/j.bspc.2021.103190.

[117] N. S. Malan and S. Sharma, "Motor Imagery EEG Spectral-Spatial Feature Optimization Using Dual-Tree Complex Wavelet and Neighbourhood Component Analysis," *IRBM*, vol. 43, no. 3, pp. 198–209, Jun. 2022, doi: 10.1016/j.irbm.2021.01.002.

[118] N. Lu, T. Li, X. Ren, and H. Miao, "A Deep Learning Scheme for Motor Imagery Classification based on Restricted Boltzmann Machines," *IEEE Trans. Neural Syst. Rehabil. Eng.*, vol. 25, no. 6, pp. 566–576, Jun. 2017, doi: 10.1109/TNSRE.2016.2601240.

[119] X. Liu, S. Xiong, X. Wang, T. Liang, H. Wang, and X. Liu, "A compact multi-branch 1D convolutional neural network for EEG-based motor imagery classification," *Biomed. Signal Process. Control*, vol. 81, p. 104456, Mar. 2023, doi: 10.1016/j.bspc.2022.104456.

[120] K. K. Ang, Z. Y. Chin, C. Wang, C. Guan, and H. Zhang, "Filter Bank Common Spatial Pattern Algorithm on BCI Competition IV Datasets 2a and 2b," *Front. Neurosci.*, vol. 6, 2012, doi: 10.3389/fnins.2012.00039.

[121] E. Dong, K. Zhou, J. Tong, and S. Du, "A novel hybrid kernel function relevance vector machine for multi-task motor imagery EEG classification," *Biomed. Signal Process. Control*, vol. 60, p. 101991, Jul. 2020, doi: 10.1016/j.bspc.2020.101991.

[122] S. U. Amin, M. Alsulaiman, G. Muhammad, M. A. Mekhtiche, and M. Shamim Hossain, "Deep Learning for EEG motor imagery classification based on multi-layer CNNs feature fusion," *Future Gener. Comput. Syst.*, vol. 101, pp. 542–554, Dec. 2019, doi: 10.1016/j.future.2019.06.027.

[123] H.-J. Ahn, D.-H. Lee, J.-H. Jeong, and S.-W. Lee, "Multiscale Convolutional Transformer for EEG Classification of Mental Imagery in Different Modalities," *IEEE Trans. Neural Syst. Rehabil. Eng.*, vol. 31, pp. 646–656, 2023, doi: 10.1109/TNSRE.2022.3229330.

ملخص:
تُمثل واجهات الدماغ والحاسوب **(BCI)** التي يُشار إليها أيضًا باسم واجهات الدماغ والآلة **(BMI)** قناة اتصال مباشرة بين الدماغ والأجهزة الخارجية دون الحاجة إلى الأعصاب المحيطية أو العضلات. وقد حظي هذا المجال باهتمام بحثي مستمر لعقود عديدة. ومن بين مختلف نماذج واجهات الدماغ والحاسوب، تبرز الأنظمة القائمة على التخيل الحركي (**MI**) بسبب سهولة استخدامها وتشغيلها البديهي. فمن خلال فك تشفير الأنماط الكهربائية الدماغية (**EEG**) المرتبطة بحركات متخيلة، تقدم واجهات التخيل الحركي أسلوب تحكم غير جراحي ذا إمكانات كبيرة في الهندسة العصبية وتكنولوجيا المساعدة. تُعد هذه الأنظمة واعدة لتحسين جودة الحياة للأفراد ذوي الإعاقات الحركية، بينما تفتح آفاقًا تطبيقية أوسع للمستخدمين الأصحاء. ومع ذلك، ورغم هذه الإمكانات، لا يزال الانتشار الواسع لواجهات التخيل الحركي مقيدًا بعدة تحديات مستمرة. فالإشارات الكهربائية الدماغية تكون بطبيعتها مشوشة وغير مستقرة ومتغيرة للغاية بين الأفراد. علاوة على ذلك، وعلى الرغم من أن أساليب التعلم العميق قد عززت أداء التصنيف، إلا أنها غالبًا ما تعاني من ضعف القابلية للتفسير، ومتطلبات حاسوبية عالية، واعتمادها على مجموعات بيانات كبيرة موسومة، مما يحد من ملاءمتها للتطبيقات الموجهة للمستخدم والتي تعمل في الزمن الحقيقي. وهذا يؤكد الحاجة إلى أطر عمل متكيفة وشفافة وفعالة لفك التشفير، قادرة على تقديم أداء قوي لمستخدمين متنوعين مع الحفاظ على قابلية الاستخدام والموثوقية السريرية.
تتناول هذه الأطروحة هذه الفجوات من خلال مساهمتين منهجيتين متكاملتين، تركز كلتاهما على هندسة الخصائص القابلة للتفسير والتحسين المخصص لكل فرد. تقدم المساهمة الأولى مجموعة شاملة من الخصائص المستمدة من المجالات الزمنية والترددية والزمنية-الترددية. ومن خلال تحسين مدة المعالجة الزمنية الخاصة بكل فرد، واختيار الخصائص، ووظيفة ترجيح الخصائص المقترحة (**WFF**)، يحقق هذا الإطار دقة تصنيف عالية عبر أربع مجموعات بيانات معيارية للتخيل الحركي تشمل 25 فردًا. وتركز المساهمة الثانية على مجموعة البيانات الأكثر تحدياً التي تحتوي على تخيل حركي رباعي الفئات، حيث حقق خط معالجة مخصص يجمع بين طريقة الفروق المزدوجة المعيارية (**NDD**)، والتقسيم الزمني المُحسّن، واختيار الخصائص عالية دقة بلغت 78.30%، مع تقديم رؤى قابلة للتفسير حول اختلاف نشاط القشرة الدماغية بين الأفراد. وبشكل جماعي، يثبت هذا العمل أن المنهجيات الهجينة، التي تدمج معالجة الإشارات، وهندسة الخصائص واختيارها، والتعلم الآلي خفيف الوزن، يمكن أن تنتج أنظمة تخيل حركي قوية وفعالة وشفافة دون الاعتماد على هياكل التعلم العميق المعقدة وغير الواضحة. ومن خلال تطوير المعايرة المخصصة والفك التشفيري القابل للتفسير، تساهم هذه الأبحاث في تطوير واجهات دماغية أكثر موثوقية وتركز على المستخدم، مما يدعم نقلها نحو التطبيقات العملية في العالم الحقيقي.
كلمات مفتاحيـــة: مخطط كهربية الدماغ، واجهة الكمبيوتر الدماغي، الصور الحركية ، استخراج الميزات ، التعلم الآلي ، التعلم العميق، الخوارزمية الجينية.

Résumé :
Les interfaces cerveau–ordinateur (BCI), également appelées interfaces cerveau–machine (ICM), établissent une voie de communication directe entre le cerveau et des dispositifs externes sans faire appel aux nerfs périphériques ni aux muscles. Ce domaine attire une attention soutenue de la recherche depuis plusieurs décennies. Parmi les différents paradigmes de BCI, les systèmes basés sur l'imagerie motrice (MI) se distinguent par leur convivialité et leur fonctionnement intuitif. En décodant les motifs électroencéphalographiques (EEG) associés aux mouvements imaginés, les MI-BCI offrent une modalité de contrôle non invasive au potentiel significatif en ingénierie neuronale et en technologie d'assistance. Ces systèmes sont prometteurs pour améliorer la qualité de vie des personnes à mobilité réduite tout en ouvrant des applications plus larges pour les utilisateurs sains. Cependant, malgré ce potentiel, le déploiement à grande échelle des MI-BCI reste limité par plusieurs défis persistants. Les signaux EEG sont intrinsèquement bruyants, non stationnaires et très variables d'un individu à l'autre. Par ailleurs, si les méthodes d'apprentissage profond ont amélioré les performances de classification, elles souffrent souvent d'une faible interprétabilité, de besoins computationnels élevés et d'une dépendance à de grands ensembles de données étiquetées, ce qui limite leur adéquation aux applications en temps réel et centrées sur l'utilisateur. Cela souligne le besoin de cadres de décodage adaptatifs, transparents et efficaces, capables d'offrir des performances robustes pour des utilisateurs variés tout en préservant l'utilisabilité et la fiabilité clinique. Cette thèse aborde ces lacunes à travers deux contributions méthodologiquement complémentaires, toutes deux axées sur l'ingénierie de caractéristiques interprétables et l'optimisation spécifique au sujet. La première contribution introduit un ensemble exhaustif de caractéristiques multi-domaines issues des représentations temporelles, fréquentielles et temps-fréquence. Grâce à l'optimisation de la durée temporelle spécifique au sujet, la sélection de caractéristiques et la fonction de pondération des caractéristiques (WFF) proposée, le cadre obtenu atteint une haute précision de classification sur quatre bases de données de référence MI-EEG regroupant 25 sujets. La seconde contribution se concentre sur la base de données plus exigeant contenant une imagerie motrice à quatre classes, pour lequel une pipeline adaptée combinant la différence double normalisée (NDD), la segmentation temporelle optimisée et la sélection de caractéristiques atteint une précision élevée de 78,30 %, tout en fournissant des insights interprétables sur la variabilité de l'activation corticale entre sujets. Collectivement, ce travail démontre que les méthodologies hybrides, qui intègrent le traitement du signal, l'ingénierie et la sélection de caractéristiques, ainsi que l'apprentissage automatique léger, peuvent produire des systèmes MI-BCI robustes, efficaces et transparents sans recourir à des architectures d'apprentissage profond opaques. En faisant progresser l'étalonnage personnalisé et le

décodage interprétable, cette recherche contribue au développement de BCI plus fiables et centrées sur l'utilisateur, favorisant ainsi leur passage vers des applications concrètes.

Mots Clés : Électroencéphalographie (EEG), Interface cerveau-machine (ICM), Imagerie motrice, Extraction de caractéristiques, Apprentissage automatique, Apprentissage profond, Algorithme génétique.

Abstract:

Brain–computer interfaces (BCIs), also referred to as brain–machine interfaces (BMIs), establish a direct communication pathway between the brain and external devices without engaging peripheral nerves or muscles. This field has attracted sustained research attention for decades. Among various BCI paradigms, motor imagery (MI)-based BCI systems stand out due to their user-friendliness and intuitive operation. By decoding electroencephalographic (EEG) patterns associated with imagined movements, MI-BCIs offer a non-invasive control modality with significant potential in neural engineering and assistive technology. These systems hold promise for enhancing the quality of life for individuals with mobility impairments while opening broader applications for healthy users. However, despite this promise, the widespread deployment of MI-BCIs remains constrained by several persistent challenges. EEG signals are inherently noisy, non-stationary, and highly variable across individuals. Moreover, although Deep learning methods have boosted classification performance, they often suffer from poor interpretability, high computational demands, and reliance on large labeled datasets, limiting their suitability for real-time, user-focused applications. This underscores the need for adaptive, transparent, and efficient decoding frameworks that deliver robust performance across diverse users while preserving usability and clinical reliability. This thesis addresses these gaps through two methodologically complementary contributions, both centered on interpretable feature engineering and subject-specific optimization. The first contribution introduces a comprehensive multi-domain features set derived from time, frequency, and time–frequency representations. Through Subject-specific time duration optimization, feature selection, and the proposed Weight Features Function (WFF), the framework yields high classification accuracy across four benchmark MI-EEG datasets that contain 25 subjects. The second contribution focuses on the more challenging dataset that contains four-class motor imagery, for which a tailored pipeline combining Normal Double Difference (NDD), optimized temporal segmentation, and feature selection achieves a high accuracy of 78.30%, and also provides interpretable insights into inter-subject cortical activation variability. Collectively, this work has demonstrated that hybrid methodologies, which merge signal processing, feature engineering, feature selection, and lightweight machine learning, can yield robust, efficient, and transparent MI-BCI systems without reliance on opaque deep learning architectures. By advancing personalized calibration and interpretable decoding, this research contributes to more reliable and user-centered BCIs, supporting their translation toward real-world applications.

Key Words: EEG, BCI, Motor Imagery, Feature Extraction, Machine Learning, Deep Learning, Genetic Algorithm.